Comparison of the Inverse Scattering Series (ISS) Free-Surface Multiple-Elimination (FSME) algorithm, and the industry-standard SRME: Defining the circumstances where each method is the appropriate tool-box choice

Chao Ma*, **Qiang Fu*** **and Arthur B. Weglein***

**M-OSRP, Physics Department, University of Houston*

617 Science and Research Building 1

Houston, TX, 77204

(June 9, 2019)

GEO-2018-0411

Running head: **ISS free-surface multiple elimination**

ABSTRACT

The industry standard Surface-Related Multiple Elimination (SRME) provides an approximate predictor of the amplitude and phase of free-surface multiples. That approximate predictor then calls upon an energy-minimization adaptive-subtraction step to bridge the difference between the SRME prediction and the actual free-surface multiple. For free-surface multiples that are proximal to other events, the criteria behind energy-minimization adaptive-subtraction can be invalid. When applied under those circumstances, a proximal primary can often be damaged. To reduce the dependence on the adaptive process requires a more accurate free-surface-multiple prediction. The Inverse Scattering Series (ISS) Free-

Surface Multiple Elimination (FSME) predicts free surface multiples with both the accurate time and accurate amplitude of free surface multiples for a multi-dimensional earth, directly and without any subsurface information.. To quantify these differences a comparison with analytic data is carried out, confirming that when a free surface multiple interferes with a primary, applying SRME with adaptive subtraction can and will damage the primary, whereas the ISS free surface elimination will surgically remove the free surface multiple without damaging the interfering primary. On the other hand if the free surface multiple is isolated then SRME with adaptive subtraction can be a cost effective tool box choice. SRME and ISS free surface multiple elimination each have an important and distinct role to play in the seismic toolbox, and each method is the indicated choice under different circumstances.

INTRODUCTION

In the beginning of the paper, it is useful to remind ourselves of the definitions of seismic events based on their travel histories (Weglein et al., 2003). For instance, figure 1 shows different types of seismic events in marine seismic exploration. In marine seismic exploration, reference waves are *first* defined as waves that travel directly from source to receiver and waves that first travel up to the air-water boundary and then to the receiver. These two types of waves did not experience the subsurface. All other events have experienced the subsurface. *Then*, among the waves that did experience the subsurface, ghost events are defined as the seismic events that begin their propagation histories by traveling up from the source to the air-water boundary (source ghosts) or end their histories by traveling down from the air-water boundary to the receiver (receiver ghosts) or both (source-and-receiver ghosts). *After that*, events that begin their history going downward from the source and end their history upward at the receiver are divided into primary events and multiple events. Primary events are defined as the events that experience only one upward reflection during their propagation history, whereas multiple events are defined as the events that experience multiple reflections during their propagation history. Multiple events are further divided into free-surface multiples and internal multiples depending on the location of downward reflection between two consecutive upward reflections.

Multiples that have at least one downward reflection at the air-water (for offshore exploration) or air-land (for onshore exploration) surface are called free surface multiples, whereas multiples that have all of their downward reflections below the air-water or air-land surface are called internal multiples (Weglein et al., 1997). The order of a free-surface multiple is defined as the number of reflections it has experienced only at the air-water

or air-land surface. In contrast, the order of an internal multiple is defined by the total number of downward reflections below the air-water or air-land surface. Notice that, these definitions of different event types define a sequence of processing steps.

In principle, only primaries are called upon to determine structure and to identify subsurface properties (Weglein, 2016, 2018b). To obtain a data set consisting of primaries, all other events need to be predicted and removed. Hence, multiples, along with the reference waves, source ghosts, receiver ghosts and source-and-receiver ghosts, all need to be predicted and removed from the seismic data in order to obtain the primary-only input to imaging and inversion methods (Weglein, 2018a). There are two types of primaries and multiples: recorded primaries and multiples, and unrecorded primaries and multiples. Recorded multiples can be used to provide an approximate image of an unrecorded primary. Unrecorded multiples must be removed in order to use a recorded multiple to find an approximate image of an unrecorded primary. Currently in the petroleum industry, smooth velocity models are used to locate structure and perform amplitude analysis. For a smooth velocity model, multiples will always produce imaging artifacts. Therefore, multiples (both recorded and unrecorded) need to be removed first from the reflection data before imaging primaries for processing goals that seek to effectively locate and invert reflections. This paper will confine itself to removing recorded free surface multiples.

Both removing and using multiples are seeking the images of primaries: recorded primaries and unrecorded primaries, respectively. As pointed out in Weglein (2018b), the relationship between 'removing multiples' and 'using multiples' is not adversarial but complementary. This paper belongs to the study of the methods in 'removing multiples'.

The methods for removing multiples have advanced and have become more effective.

However, the concomitant industry trend towards ever more complex exploration areas and difficult plays has at times outpaced advances in multiple-attenuation capability. For example, currently, the removal of multiples, especially those that are interfering with primaries, for an unknown and complex multidimensional subsurface, remains a key open issue, and high priority pressing challenge for offshore and on-shore conventional and unconventional plays. We advocate a tool-box approach, in general, and seek to understand the place and role that each method within the toolbox plays within the spectrum of different capabilities and responses, and how to choose the method that's a best match for the user's specific application and objective. We also advocate adding new options to the toolbox to increase the collection of circumstances that can be addressed.

In this particular paper, we examine and compare two methods (i.e., the Inverse Scattering Series Free-Surface Multiple Elimination (ISS FSME) (Carvalho et al., 1991; Weglein et al., 1997, 2003) and the Surface-Related Multiple Elimination (SRME)) (Berkhout, 1985; Verschuur, 1991; Verschuur et al., 1992) for the removal of *free-surface* multiples. We suggest a guide to when each can be the appropriate choice within the free-surface-multiple-removal toolbox. The SRME method has been widely used and has become (and we expect will remain) the workhorse and industry-standard for removing free-surface multiples. Similarly, the effectiveness of the ISS FSME has been demonstrated in many complicated synthetic and field data tests (e.g., Carvalho and Weglein (1994); Maston et al. (1999); Weglein and Dragoset (2005); Zhang (2007); Ferreira (2011)).

These free-surface multiple removal methods share a property that both methods do not require subsurface information. However, there are significant and well-documented difference between these two methods as discussed in Weglein, Matson and Berkhout (2000); Weglein et al. (2000); Weglein and Dragoset (2005). For example, one difference is the

SRME method predicts the approximate amplitude and time of free-surface multiples. In contrast, the ISS FSME method predicts free-surface multiples with both the accurate amplitude and accurate time. There are circumstances where that difference will be significant and important for removing free-surface multiples without damaging interfering or proximal primaries. The ISS free surface multiple elimination method is both more effective and more compute demanding compared to SRME. There are circumstances where the added cost is indicated, and other cases where the lower cost SRME will be the cost-effective choice.

Our aim and single objective is to use examples in 1D with analytic input data to provide a quantitative analysis between two methods in terms of predicting free-surface multiples and removing interfering free-surface multiples without damaging primaries. The outline of the paper is as follows: we first describe the ISS free-surface multiple prediction and SRME free-surface multiple prediction. We examine the difference in physics theory that resides behind the different ISS FSME and the SRME predictions. After that, we use 1D prestack examples for a quantitative comparison of the free-surface multiple prediction between the ISS FSME and SRME methods. We conclude with a discussion and guide for indicated tool box choices.

THE INVERSE SCATTERING SERIES (ISS) FREE-SURFACE MULTIPLE ELIMINATION (FSME) ALGORITHM

In this section, we describe the ISS FSME algorithm (Carvalho et al., 1991; Weglein et al., 1997, 2003). We start by first describing the pre-processing steps before the ISS FSME and then describing the ISS free-surface multiple prediction.

We provide a 2D marine development as an example to illustrate the steps. Given the

recorded seismic data (see figure 1), $D(x_g, x_s, t)$ where x_g, x_s and t represent receiver and source locations, and time, respectively. **(1)** The first step is to remove the reference waves. **(2)** After the removal of the reference wave (producing reflection data), the second step is to remove source ghosts and receiver ghosts and source-and-receiver ghosts, that produces deghosted reflection data.

(3) After the removal of reference waves and all ghosts (i.e., source ghosts, receiver ghosts and source-and-receiver ghosts), deghosted seismic reflection data (represented by $D_1'(x_g, x_s, t)$) enters the ISS FSME to predict and remove free-surface multiples as follows:

- $D_1'(x_g, x_s, t)$ is first Fourier transformed over x_g, x_s, t (i.e., $D_1'(x_g, x_s, t) \rightarrow D_1'(k_g, k_s, \omega)$, see A-22 for the Fourier transform convention).

- The Fourier transformed data, $D_1'(k_g, k_s, \omega)$ enters the ISS free-surface-multiple-prediction equations (i.e., equation 1) to predict free-surface multiples (represented by $D_n'(k_g, k_s, \omega)$, where $n = 2, 3, 4, \cdots$) with both accurate time and accurate amplitude (in opposite polarity compared with actual free-surface multiples), of order $n-1$,

$$D_n'(k_g, k_s, \omega) = -\frac{1}{2\pi A(\omega)} \int dk \; e^{iq(z_g+z_s)} D_1'(k_g, k, \omega) \; (2iq) \; D_{n-1}'(k, k_s, \omega),$$
$$n = 2, 3, 4, \ldots \; . \tag{1}$$

  The quantities $A(\omega)$, z_g and z_s in Equ. 1 are the source signature, receiver depth and source depth, respectively. $q = \sqrt{\frac{\omega^2}{c_0} - k^2}$.

- Then, these predicted $(n-1)$th order free-surface multiples ($D_n'(k_g, k_s, \omega)$, where $n = 2, 3, 4, \cdots$) are Inverse Fourier transformed back to x_g, x_s and t, and added to the

input data $D_1'(x_g, x_s, t)$ to obtain data without free-surface multiples, see equation 2.

$$\begin{aligned} D'(x_g, x_s, t) = & \ D_1'(x_g, x_s, t) + D_2'(x_g, x_s, t) + D_3'(x_g, x_s, t) + \cdots , \\ & = \sum_{n=1}^{\infty} D_n'(x_g, x_s, t). \end{aligned} \tag{2}$$

It should be mentioned that the subsequent prediction terms in the series (equation 2), represented by $D_2', D_3', ...$, provide predictions of free-surface multiples of different orders. Specifically, each term in D_n' (where $n = 2, 3, 4...$) when added to the earlier terms in the series (including the data D_1') performs two functions: (1) it eliminates the nth order free-surface multiple. and (2) it alters all higher order free-surface multiples to be prepared for their removal by higher-order D_j' terms, where $j = n + 1, n + 2, ...$ (Weglein et al., 2003; Zhang and Shaw, 2010; Ma and Weglein, 2016). The output of the ISS FSME, $D'(x_g, x_s, t)$, represents the data without reference waves, without all ghosts, and without free-surface multiples.

SRME

The 2D SRME free-surface-multiple prediction, denoted by M, (Berkhout, 1985; Verschuur, 1991; Verschuur et al., 1992) is calculated by using seismic data without reference waves and without receiver-side ghosts, but retaining source-side ghosts, denoted by P, as follows,

$$M(x_g, x_s; \omega) = \int P(x_g, x; \omega) P(x, x_s; \omega) dx. \tag{3}$$

In the above equation 3, x_g, x_s, ω are receiver and source location and temporal frequency, respectively. To obtain equation 3, one would have to assume in the physics derivation that the data was generated by a vertically-separated dipole source in the water column

[with the reference wave and source and receiver ghosts removed (see details in Appendix B)]. Notice that, the actual monopole source itself together with its source ghost (corresponding to a mirror image [in the air above the sea surface] of the actual monopole source in the water) is assumed in the SRME prediction step to be an approximation to the dipole source in the water column (see figure B-1).

The physics theory differences between these two free-surface-multiple-prediction algorithms is studied in Appendix A and Appendix B. In the next section, we focus on a quantitative comparison between the ISS and SRME free-surface multiple predictions.

A QUANTITATIVE COMPARISON BETWEEN THE ISS AND SRME FREE-SURFACE MULTIPLE PREDICTIONS

In this section, we aim to provide a quantitative comparison between the ISS free-surface multiple prediction and SRME free-surface multiple prediction.

From the last section, we know that the called-for input data to the two free-surface multiple-prediction algorithms is different. The input seismic data for the ISS FSME algorithm is generated by a monopole source and with the reference wave and all ghosts removed (see figure 2, I). For SRME the input is seismic data generated by a dipole source and with the reference wave and ghosts removed. However, in practice, since a data due to a vertically-separated dipole source is not realizable, the assumption made within SRME is to approximate what a dipole source in the water would produce by a monopole source and its source-side ghost (in the air) (see figure B-1 and figure 2, II (a)).

Following that, in the first set of comparisons (see the first bullet in figure 3), we provide the different called-for inputs to these two free-surface multiple-prediction algorithms. For ISS free-surface multiple-prediction algorithm, we use data due to a monopole source with

the reference wave and all ghosts removed. For SRME free-surface multiple-prediction algorithm, we use data due to a monopole source the reference wave and the receiver-side ghosts removed (source-side ghosts are retained in the data).

In practice, source and receiver ghosts are often removed early in the processing chain (for interest in band-width and resolution benefit) and prior to multiple removal processing taking place. Hence, we carry out a second set of comparisons with input data with the reference wave and all ghosts removed for both algorithms. The latter tests are carried out with and without noise (see the second and third bullet in figure 3).

In the third set of comparisons, we repeat the previous comparison, with input data generated by an absorptive medium (see the fourth bullet in figure 3). We aim to examine whether for input data generated by an absorptive medium, the two free-surface multiple-prediction algorithms retain their relative and different levels of effectiveness, i.e., the ISS predicts free-surface multiples with both accurate amplitude and time, and the SRME predicts free-surface multiples with approximate amplitude and approximate time in the presence of *an* absorptive medium.

In Weglein et al. (2003) page R52-55 provides a proof that the ISS free surface multiple elimination method predicts the precise time and amplitude of all free surface multiples, without any subsurface information, and independent of earth model type. Similarly, on p R55-62 of Weglein et al. (2003) it is shown that the ISS internal multiple attenuator predicts the precise time and approximate amplitude of all internal multiples, without subsurface information, and independent of earth model type.

A first set of comparisons

In this first set of comparisons, given the required input of these two free-surface multiples algorithms, we provide a quantitative comparison of the predicted free-surface multiples by the ISS FS and the SRME methods. In other words, for ISS free-surface multiple prediction, the input data is without reference waves and without all ghosts; for SRME free-surface multiple prediction, the input data is without the reference wave and receiver ghosts (the source ghosts are retained in its input data).

Figure 4 shows the model with one horizontal reflector and a free-surface. Based on this model, we use the Cagniard-de Hoop (the CdH) method (Cagniard (1939); de Hoop (1959)) to generate the date. For a model with one horizontal reflector and a free-surface, CdH method is able to obtain the analytical solutions of different events separately. This allows us to (1) generate data according to each algorithm's required input and (2) to attribute any difference in the comparison to the two prediction algorithms rather than to numerical or other issues with the data. Figures 5 and 6 show the input to the ISS and SRME free-surface multiple predictions, respectively. Figures 7 and 8 show the prediction results from the ISS and SRME. Notice that, for the ISS free-surface multiple prediction, we use equation 1 for $n = 2$ [for first order free surface multiples]. Figures 9 and 10 show the trace comparison at 500m offset between the input data and free-surface multiple predictions from ISS and SRME, respectively. The result show that the ISS FSME predicts free-surface multiples with accurate time and accurate amplitude, whereas the SRME predicts free-surface multiples with approximate time and amplitude.

A second set of comparisons

Figure 11 shows the model we used to generate analytic input data in the (k_x, ω) domain for a 1D subsurface [using the reflectivity method]. For example, a primary due to a horizontal reflector has an analytic form shown below (see e.g., Stolt and Weglein (1985)):

$$-R(k_x,\omega)\frac{e^{iq(2a-z_g-z_s)}}{2iq}, \tag{4}$$

where $R(k_x,\omega), a, z_g$ and z_s are plane wave reflection coefficient, depths of the reflector, receiver and source, respectively; $q=\sqrt{\frac{\omega^2}{c_0^2}-k_x^2}$, c_0 is the velocity above the reflector. For this model, the above expression for a primary can be generalized to generate other events analytically. A Ricker wavelet with peak frequency at 30Hz is convolved with the analytic form to generate the data.

Notice that, in our example, (1) only three events (two primaries and one free-surface multiple) are generated, (2) the depths of the reflectors and velocities are chosen such that the second primary destructively interferes with the free-surface multiple. We examine two cases using input data with and without random noise. Notice that, the only difference between these two tests is the input data, the input data for test 1 contains no noise whereas the input data for test 2 contains random noise.

For test 1, Figures 12 to 16 show the synthetic input data, ISS free-surface multiple prediction, SRME free-surface multiple prediction, results after the ISS FSME and SRME+adaptive, and the actual primary, respectively. Please notice that for the predictions of free-surface multiples in figure 13 and figure 14, higher-order free-surface multiples (as we know) are also predicted. Please also note that the result from ISS FSME was obtained by directly subtracting the ISS prediction result from the data without an adaptive procedure, whereas the result from SRME was obtained by combining the SRME free-

surface multiple prediction and the adaptive procedure.

Comparing the primary in the data (figure 17) with the multiple-removal result after ISS FSME (figure 15), we find that, with the accurate multiple prediction, the ISS FSME has surgically removed the free-surface multiple and recovered the primary.

Comparing the original data (figure 12) with the result after SRME + adaptive (figure 16), we notice the SRME can successfully remove the isolated multiple. The isolated free-surface multiple in figure 12 is removed in figure 16. In figure 16 the arrows point to the removed free-surface multiple. But the adaptive procedure can easily damage the primary which interferes with the multiple (red circle in figure 16). It is worth mentioning that, we employed least-square (L2-norm) energy minimization adaptive subtraction, which is a current standard practice in the industry, to remove the predicted free surface multiple event from the data in figure 16.

Figures 18 to 22 provide trace plots to examine the results in detail at different offsets. In these trace plots, red, blue and green lines represent actual data, ISS FSME multiple prediction and SRME multiple prediction, respectively. In the 100m, 500m, 1000m and 1250m offset trace plots, primaries and multiples are separately from each other. These plots show that the ISS free-surface multiple prediction has the accurate time and amplitude, hence it overlaps with the actual multiple in the data. Whereas the SRME prediction has approximate amplitude and time and it shows a disagreement with the actual multiple in the data.

Notice that, at offset 750m, the primary and multiple overlap. Figure 23 shows the comparison between the actual primary (blue line) with the multiple-removal result after ISS FSME (red line) and the multiple-removal result after SRME+adaptive (green line) at

offset 750m. This figure shows the primary can be recovered by ISS FSME whereas the SRME combined with the adaptive damages the primary.

For test 2 in which the input data have random noise, figures 24 to 29 show the synthetic input data, multiple prediction results from ISS FSME, SRME, results after the ISS FSME and SRME+adaptive, and the actual primary, respectively. Similarly, figures 30 to 35 provide trace plots. Examining these comparisons, we can draw the similar conclusion as in the case without noise.

A third set of comparisons

Weglein et al. (2003) showed the model-type independent properties of both the ISS free-surface multiple elimination algorithm and the internal multiple attenuation algorithm. The meaning of model-type independent is that the removal of free-surface multiples and the attenuation of internal multiples is each achievable with precisely the same algorithm for an entire class of earth model types. The members of the models type class include acoustic, elastic and anelastic media. Matson (1997) studied and demonstrated the effectiveness of ISS elastic multiple removal from multicomponent land and ocean bottom seismic data. Here, we provide a numerical example to demonstrate and confirm the effectiveness of the ISS FSME algorithm for an absorptive medium.

The input data is generated based on model shown in figure 11, with Q values 200,100, and 100 for the three layers from top to bottom. The analytic input data is generated using the analytic forms of different events (see e.g., equation 4 for a primary) and a constant Q model (known as frequency independent Q model), see Kolsky (1953). Figures 36, 37 and 38 show the input data, ISS free-surface multiple prediction and SRME free-surface

multiple prediction, respectively. Figures 39 and 40 show the result after the ISS FSME and SRME +adaptive, respectively. Figures 42 to 46 show the trace comparison between the input data, ISS free-surface multiple prediction and SRME free-surface multiple prediction at offset 100m, 500m, 750m, 1000m, 1250m. Figure 47 shows the trace comparison at offset 750m between the actual primary, the result after the ISS FSME and result after the SRME +adaptive. Examining the result of this test, we can conclude that, for data generated by an acoustic medium that's absorptive, the same ISS FSME algorithm remains effective to accurately predict the free-surface multiple and can surgically remove free-surface multiples that interfere with primaries, without damaging primaries. We have numerically confirmed that the ISS FSME algorithm remains effective with data from an absorptive medium. That is consistent with the model type independent nature of the algorithm.

The ISS FSME is more computational costly than the SRME. The ISS free-surface multiple prediction equation is in the wavenumber-frequency domain, the obliquity factor in it ($2iq$) precludes a simple transform from wavenumber-frequency domain to space-frequency to obtain a convolutional equation (which is cheaper) as in SRME free-surface multiple prediction.

DISCUSSION

Providing pre-requisites of the ISS FSME algorithm

The ISS FSME has well understood pre-requisites: source signature estimation and removal, removal of the reference wave, and source and receiver-side deghosting. Providing these pre-requisites is relatively mature for marine application. Advances in acquisition (e.g. over/under cable and dual-sensor towed streamer), have provided the data requirements of

more effective wave theoretic methods, for those pre-requisites. For example, Weglein and Secrest (1990), Osen et al. (1998), and Tan (1999) provide effective methods to estimate the source signature and radiation pattern using Green's theorem. For the prediction (and use or removal) of the reference waves, the distinct advantages (e.g., (1) no need for Fourier transforms over receivers and sources, and (2) can accommodate a horizontal or non-horizontal measurement surface). Applying Green's theorem wave separation methods on marine data have been advanced by Weglein et al. (2002b); Zhang (2007); Mayhan and Weglein (2013). For deghosting, the industry widely used $P - V_z$ method (e.g., Amundsen (1993)) can be effective when the measurement surface is horizontal. The Green's theorem based deghosting method (Weglein et al. (2002a); Zhang (2007); Mayhan (2013)) is the natural Green's theorem wave theoretic generalization of $P - V_z$ and has been extended to accommodate a depth-variable cable by the recent work of Wu and Weglein (2017), Zhang (2017) and Shen (2017). To provide the pre-requisites for on-shore application, the recent work of Wu and Weglein (2014, 2015, 2016a,b) has contributed to extending off-shore Green's theorem preprocessing for wavelet estimation, reference waves (including ground roll) prediction and removal, and deghosting to the on-shore elastic case, in preparation for on-shore processing.

A new adaptive criteria that aligned with the algorithm itself

We have shown that, given its pre-requisites, the ISS FSME will predict free-surface multiples with an accurate time and an accurate amplitude. These predicted multiples can be used to surgically remove free-surface multiples that interfere with primaries, without damaging the primaries. In practice, an adaptive step could still be needed. The energy-minimization criteria is viewed (by some thoughtful individuals) as the biggest current impediment to effective multiple removal under complex circumstances. New adaptive cri-

teria need to be developed. We are developing a new adaptive criteria derived as a property of the multiple removal algorithm. One candidate criteria is proposed in Weglein (2012).

CONCLUSION

We examined the origin of the missing obliquity factor in the SRME prediction step. We then used 1D prestack examples for a quantitative comparison of the free-surface-multiple prediction between the ISS FSME and SRME methods. The ISS FSME method provides a toolbox capability and option for a more accurate prediction of free-surface multiples. There are circumstances where this new and more effective capability might not be needed. For example, to remove isolated free-surface multiples, an approximate free-surface multiple prediction plus an adaptive subtraction by the SRME method might be sufficient and indicated as a cost-effective approach. However, there are many circumstances that this new ISS FS multiple elimination capability is called-for and needed. For example, (1) to remove a free-surface multiple that is interfering with a primary without damaging the primary, by providing a more accurate free-surface multiple prediction and relying less on the adaptive step. (2) And when it is unclear if a free-surface multiple is (or is not) interfering with a primary, the ISS FSME would be a prudent choice. When this capability is needed, the ISS FSME method provides an important and valuable, option in the toolbox. It goes without saying that for SRME and ISS free surface multiple elimination methods to deliver their promise they must be applied in their 2D and 3D versions, where the subsurface has 2D and 3D variability.

ISS methods for attenuating or eliminating internal multiples, place a high bar, on not having residual free surface multiples or damaged primaries in the data. If ISS internal multiple removal is the goal, we suggest a serious consideration of the most effective method

for removing free surface multiples, the ISS FS multiple elimination.

ACKNOWLEDGMENT

We would like to thank M-OSRP sponsors for their support and encouragement. The reviewers of this paper are thanked for their constructive and worthwhile comments and suggestions. We thank Dr. Mayhan for his help in editing this paper.

APPENDIX A

THE ISS AND ITS SUBSERIES FOR FREE-SURFACE MULTIPLE ELIMINATION

In this section we provide a derivation of the Inverse Scattering Series (ISS) Free-Surface Multiple Elimination (FSME) method. Towards that end, we begin with (following Weglein et al. (2003)) a very brief introduction and background on scattering theory and the distinct forward and inverse scattering series. A fuller development of the concepts and methods in this Appendix can be found in Weglein et al. (2003) and `http://www.mosrp.uh.edu/events/annual-meetings/meeting-18`.

The seismic forward problem

The seismic forward modeling problem is to predict the wavefield in a medium when the medium properties that govern wave propagation in the medium and the source that generates the wavefield are prescribed. For example, for an acoustic, one parameter (variable velocity, constant density) medium, the single frequency wave equation for the pressure field due to a localized Dirac delta function source at $\vec{r_s}$

$$[\nabla^2 + k^2]G(\vec{r}, \vec{r_s}, \omega) = -\delta(\vec{r} - \vec{r_s}), \tag{A-1}$$

where $k = \omega/c(\vec{r})$, ω is the temporal frequency and $c(\vec{r})$ is the velocity configuration. The wavefield $G(\vec{r}, \vec{r_s}, \omega)$ at $\vec{r}$ due to source at $\vec{r_s}$ can be modeled directly in terms of the actual velocity configuration, $c(\vec{r})$ using e.g., a finite difference, finite element, Lattice Boltzmann method given the medium properties $c(\vec{r})$ and the source function.

In scattering theory, the forward problem is described differently. Scattering theory is a

form of perturbation theory. That is, in scattering theory the actual medium is separated into two parts, one part is called the reference medium, the other part is called the perturbation (the difference between the actual medium and the reference medium). In general, we can express the differential equations governing wave propagation in the actual medium and reference medium as

$$LG = -\delta(\vec{r} - \vec{r}_s), \tag{A-2}$$

and

$$L_0 G_0 = -\delta(\vec{r} - \vec{r}_s), \tag{A-3}$$

respectively. $L$and L_0 here are general differential operators in the actual and reference medium, and $G$and G_0 are the actual and reference wavefields, respectively. δ is a Dirac delta source function, and $\vec{r}$, $\vec{r}_s$ are the field and source locations, respectively. The perturbation differential operator is defined as $V \equiv L - L_0$. Notice that the differential operators L and L_0 contain the properties in the actual and the reference media that govern wave propagation in those medium. Different Earth model-types are described by different forms of operators L and L_0. These operators contain the (spatially variant) parameters of the specific earth model type (e.g., acoustic, elastic, anisotropic and anelastic). For example, for an acoustic, variable velocity constant density model type, $L = \nabla^2 + k^2$, where $k = \omega/c(\vec{r})$ as illustrated in equation A-1. $L_0 = \nabla^2 + k^2$, where $k_0 = \omega/c_0(\vec{r})$ as in $[\nabla^2 + k_0^2]G_0(\vec{r}, \vec{r_s}, \omega) = -\delta(\vec{r} - \vec{r_s})$.

We can express the actual medium differential operator L in terms of a reference medium differential operator L_0 and a perturbation operator V as $L = L_0 + V$. The perturbation operator is defined as $V = L - L_0$. Thus, equation A-2 can be written as

$$(L_0 + V)G = -\delta, \tag{A-4}$$

Rearranging the above expression as follows,

$$L_0 G = -\delta - VG,$$

$$G = -L_0^{-1}\delta - L_0^{-1}VG \tag{A-5}$$

Now substituting $\delta = -L_0 G_0$ (equation A-3) and considering $L_0^{-1} = -G_0$, we have,

$$G = L_0^{-1}L_0 G_0 - L_0^{-1}VG,$$

$$G = G_0 + G_0 VG. \tag{A-6}$$

The last equation A-6 is called the Lippmann-Schwinger equation (e.g., Taylor, 1972). The Lippmann-Schwinger equation is an operator relationship between G (the wavefield in the actual medium), G_0 (the wavefield in the reference medium) and V (the perturbation). G appears on both sides of equation A-6. To solve A-6 for G we can treat $G = G_0$ (the first term on the right hand side of A-6) as a first approximation for G. Then substituting $G = G_0$ on the right hand side of A-6, we find an approximation for G as $G_0 + G_0 V G_0$, and then once again substitute this next approximation for G on the right hand side of A-6 we find an updated approximation for G as

$$G_0 + G_0 V G_0 + G_0 V G_0 V G_0. \tag{A-7}$$

Then, continuing this successive substitution process for G on the right hand side of A-6, we find,

$$G = G_0 + G_0 V G_0 + G_0 V G_0 V G_0 + G_0 V G_0 V G_0 V G_0 + \cdots . \tag{A-8}$$

The difference between the actual wavefield G and reference wavefield G_0 is defined as scattered wavefield, $\psi_s = G - G_0$.

The seismic *forward* problem is solved in scattering theory by equation A-8, i.e., given the reference wavefield G_0 and perturbation V (the right hand side of A-8), equation A-8

can be used as a forward modeling tool to obtain the actual wavefield G (the left hand of A-8). The forward problem determines G from L. In scattering theory, L is given by L_0 and V and therefore G_0 and V enters the forward or seismic modeling series A-8. In common with all modeling methods, modeling (or the forward problem) within scattering theory depends on first specifying the earth model type and then all the precise earth properties within that model type. The recorded seismic data corresponds to the wavefield (G or ψ_s) recorded on the measurement surface.

The seismic inverse problem

The seismic *inverse* problem is to solve for the medium properties L in terms of recorded values of the wavefield on the measurement surface outside V and the source.

The seismic inverse problem is solved in scattering theory by first solving for V. Then V is added to the reference medium operator L_0 to obtain the actual medium operator L. To know L is to know all the physical properties that govern wave propagation in the actual medium. To derive the inverse scattering method to solve for V, let's first return to the forward series A-8. We note that equation A-8 has the form of a generalized geometric series (Weglein, 2017)

$$G - G_0 = S = ar + ar^2 + ar^3 + ... = \frac{ar}{1-r}, \tag{A-9}$$

for $|r| < 1$, where we have identified in our simple algebraic geometric series analog $a = G_0$ and $r = VG_0$. If we label the terms on the right hand side of (A-9) as $S_1 = ar, S_2 = ar^2$, ..., where S_n is the part of S that is n-th order in r, then, equation A-9 becomes

$$S = S_1 + S_2 + S_3 + \cdots = \frac{ar}{1-r}. \tag{A-10}$$

Solving A-10 for r, in terms of S/a produces an inverse geometric series

$$r = \frac{S/a}{1+S/a} = S/a - (S/a)^2 + (S/a)^3 + \cdots, = r_1 + r_2 + r_3 + \cdots, \tag{A-11}$$

when $|S/a| < 1$, where r_n is the portion of r that is nth order in S/a.

For the seismic inverse problem, we evaluate A-8 for sources and receivers on the measurement surface, and associate S with the recorded values of the scattered wavefield $S = (\psi_s)_{ms} = (G - G_0)_{ms}$, and the forward series follow from treating the forward solution as S in terms of V, and the inverse series as V in terms of S. The inverse series is the analog of equation A-11, where $r_1, r_2, \cdots$ are replaced with $V_1, V_2, \cdots$:

$$V = V_1 + V_2 + V_3 + \cdots, \tag{A-12}$$

where V_n is the portion of V that is nth order in the data, D. The data, D, are the recorded values of ψ_s, that is $(\psi_s)_{MS}$. Substituting equation A-12 into equation A-8 and evaluating both sides of equation A-8 on the measurement surface, and setting terms of equal order in the data equal, produces the following set of equations (see, e.g., Weglein et al., 2003)

$$(\psi_s)_{ms} = (G_0 V_1 G_0)_{ms}, \tag{A-13}$$

$$0 = (G_0 V_2 G_0)_{ms} + (G_0 V_1 G_0 V_1 G_0)_{ms}, \tag{A-14}$$

$$0 = (G_0 V_3 G_0)_{ms} + (G_0 V_2 G_0 V_1 G_0)_{ms} + (G_0 V_1 G_0 V_2 G_0)_{ms} + (G_0 V_1 G_0 V_1 G_0 V_1 G_0)_{ms}, \tag{A-15}$$

$$0 = (G_0 V_n G_0)_{ms} + (G_0 V_1 G_0 V_{n-1} G_0)_{ms} + \cdots + (G_0 V_1 G_0 V_1 G_0 V_1 \cdots G_0 V_1 G_0)_{ms}. \tag{A-16}$$

V_1 can be solved in equation A-13 using the measured scattered wavefield $(\psi_s)_{ms}$ and the reference wavefield G_0. Then, substitute V_1 into equation A-14, solve for V_2 as in equation A-13. In this manner, we can compute any V_n only using the measured scattered wavefield $(\psi_s)_{ms}$ and the reference wavefield G_0. Hence $V = \sum_{n=1}^{\infty} V_n$ is an explicit direct inversion

solution, and doesn't require any subsurface information. The inverse step in A-13 - A-16 when solving for $V_1, V_2, V_3, ...$ involves inverting the same unchanged operator G_0 and when the reference medium is homogeneous that inverse step is analytic (Weglein et al., 2003).

The inverse scattering series methods were first developed by Moses (1956), Prosser (1969) and Razavy (1975). Weglein et al. (1981) and Stolt and Jacobs (1980) applied the inverse scattering series methods to extract multidimensional earth information from seismic data. Carvalho (1992) performed empirical tests of the ISS method for a normal incident plane wave on a 1D acoustic medium. The result indicated the full series only converges when the difference between the actual Earth's acoustic velocity and reference velocity (water velocity) is less than 11%. In response, the idea of isolated task-specific subseries was developed as a way to extract useful information from the only direct inversion method for a multi-dimensional subsurface. The isolated task ISS subseries are: (1) free-surface multiple elimination; (2) internal multiple attenuation/elimination; (3) Q compensation without knowing or estimating Q; (4) depth imaging; and (5) inversion (parameter estimation). The identification of the terms in the ISS to be included in a given task-specific subseries used several different types of analysis with testing of new concepts to evaluate, refine and develop embryonic thinking based on forward series processes and analogues and a large dose of physical intuition (Weglein et al., 2003). For example, for free-surface multiples, understanding how the forward scattering series produces or generates a free-surface multiple event provides a "hint" where the inverse process that removes that event might be located. That "hint", due to a symmetry between event creation and event removal, turns out to be useful. For internal multiples location of terms that perform attenuation and elimination is described in (Weglein et al., 2003) page R55-R62. For the purpose of this paper, it is useful to review the thinking behind locating the ISS subseries for removing free-surface multiples.

In the absence of a free surface [and choosing an infinite whole space of water as the reference medium], a forward series equation (A-8) describing the data is constructed from the direct propagating Green's function, G_0^d, and the perturbation operator, V. V represents the difference between the actual material properties of the world and the reference medium. V has non-zero values starting at the water bottom. In the presence of a free surface, let G_0^{fs} correspond to the extra part of the Green's function due to a Dirac delta point source in the water column that propagates up and reflects off the free-surface and has a field point below the free-surface.

With the free surface present, the forward series is constructed from $G_0 = G_0^d + G_0^{fs}$ and the same perturbation operator, V. Hence, G_0 with or without G_0^{FS} is the only difference between the forward series with and without the free surface. Therefore, G_0^{fs} is responsible for generating those events in the forward or modeling series that owe their existence to the presence of the free surface, i.e., ghosts and free-surface multiples. In the inverse series, equations (A-13) to (A-16), it is reasonable to infer that G_0^{fs} will be responsible for all the extra tasks that inversion needs to perform when starting with data containing ghosts and free-surface multiples rather than data without those events. Those extra inverse tasks include deghosting and the removal of free-surface multiples.

The inverse series expansions, equations (A-13) to (A-16), consist of terms $(G_0 V_n G_0)_m$ with $G_0 = G_0^d + G_0^{fs}$. Source and receiver deghosting is realized by removing the two outside $G_0 = G_0^d + G_0^{fs}$ functions and replacing them with G_0^d.

Data is considered the measured values of scattered wavefield, equation A-13. The source and receiver deghosted data (represented by $\tilde{D}$), is related to V_1 as $\tilde{D} = (G_0^d V_1 G_0^d)_m$. After the deghosting operation, the objective is to remove the free-surface multiples from

the deghosted data, $\tilde{D}$.

The terms in the inverse series expansions, (A-13) to (A-16), replacing D with input $\tilde{D}$, contain both G_0^d and G_0^{fs} between the operators V_i. The outer G_0^d's (rather than $G_0 = G_0^d + G_0^{fs}$) indicate that the data have been source and receiver deghosted. The inner G_0^d and G_0^{fs} are where the five inversion tasks (free surface multiple removal, internal multiple removal, depth imaging, Q compensation without knowing or estimating Q, inversion/parameter estimation) reside. If we consider the inverse scattering series and $G_0 = G_0^d + G_0^{fs}$, and if we assume that the data has been source and receiver deghosted (i.e., G_0^d replaces $(G_0^{fs} + G_0^d)$ on the outside of all terms), then the terms in the series are of three types:

$$\begin{aligned} Type1 &: \left(G_0^d V_i G_0^{fs} V_j G_0^{fs} V_k G_0^d\right)_{ms} \\ Type2 &: \left(G_0^d V_i G_0^{fs} V_j G_0^d V_k G_0^d\right)_{ms} \\ Type3 &: \left(G_0^d V_i G_0^d V_j G_0^d V_k G_0^d\right)_{ms}. \end{aligned}$$

We interpret these types of terms from a task isolation point of view. Type 1 terms have only G_0^{fs} between two V_i,V_j contributions; these terms when added to $\tilde{D}$ remove free-surface multiples and perform no other task. Type 2 terms have both G_0^d and G_0^{fs} between two V_i,V_j contributions; these terms perform free-surface multiple removal *plus* a task associated with G_0^d. (Tasks that G_0^d will achieve are: internal multiple removal, Q compensation, depth imaging, and non-linear direct parameter estimation) Type 3 have only G_0^d between two V_i,V_j contributions; these terms do not remove any free-surface multiples. Type 2 terms are coupled tasks with both a free surface and a G_0^d tasks. The idea behind task separated subseries is two fold: 1) isolate the terms in the overall series that perform a given task *as if no other tasks exist* (e.g., Type 1 above) and after performing that task on the data 2) not to return to the original inverse series with its coupled tasks involving G_0^{fs} and G_0^d, but

rather restart the problem with an input data free of free-surface multiples, D'.

With the idea of isolated task separated subseries, the subseries for removing free-surface multiples resides in Type 1 terms. Collecting all Type 1 terms, we have

$$D'_1 \equiv \widetilde{D} = (G_0^d V_1 G_0^d)_{ms}, \tag{A-17}$$

$$D'_2 = (G_0^d V_2 G_0^d)_m = -(G_0^d V_1 G_0^{fs} V_1 G_0^d)_{ms}. \tag{A-18}$$

$$\begin{aligned} D'_3 = &- (G_0^d V_1 G_0^{fs} V_1 G_0^{fs} V_1 G_0^d)_{ms} \\ &- (G_0^d V_2 G_0^{fs} V_1 G_0^d)_{ms} \\ &- (G_0^d V_1 G_0^{fs} V_2 G_0^d)_{ms} \\ &\dots \end{aligned} \tag{A-19}$$

$D'_1 \equiv \widetilde{D}$ is the first term; it is the seismic data after the removal of the reference wave $G_0 = G_0^d + G_0^{FS}$ and then source and receiver deghosting the scattered wavefield.

D'_3 can be simplified as (see e.g., Weglein et al. (2003))

$$D'_3 = (D_0^d V_1 G_0^{fs} V_1 G_0^{fs} V_1 G_0^d)_{ms}. \tag{A-20}$$

Equation A-17 can be expressed as follows,

$$D'_1(x_g, z_g, x_s, z_s, \omega) = \int dx_1 dz_1 dx_2 dz_2 G_0^d(x_g, z_g, x_1, z_1, \omega) V_1(x_1, z_1, x_2, z_2, \omega) G_0^d(x_2, z_2, x_s, z_s, \omega). \tag{A-21}$$

Following the Fourier transform convention defined in e.g., Clayton and Stolt (1981); Weglein et al. (2003),

$$D(k_g, k_s, \omega) = \int\int\int D(x_g, x_s, t) e^{ik_s x_s - ik_g x_g + i\omega t} dt dx_g dx_s, \tag{A-22}$$

Fourier transforming over x_g, x_s on both sides of equation A-21,

$$D'_1(k_g, z_g, k_s, z_s, \omega) = \int dx_1 dz_1 dx_2 dz_2 G_0^d(k_g, z_g, x_1, z_1, \omega) V_1(x_1, z_1, x_2, z_2, \omega) G_0^d(x_2, z_2, k_s, z_s, \omega). \tag{A-23}$$

$G_0^d\left(k_g, z_g, x_1, z_1, \omega\right)$ and $G_0^d\left(x_2, z_2, k_s, z_s, \omega\right)$ are (see e.g., Clayton and Stolt (1981))

$$G_0^d\left(k_g, z_g, x_1, z_1, \omega\right) = -\frac{e^{-i(k_g x_1 - q_g|z_1 - z_g|)}}{2iq_g} = -\frac{e^{-i(k_g x_1 - q_g(z_1 - z_g))}}{2iq_g}, \tag{A-24}$$

and

$$G_0^d\left(x_2, z_2, k_s, z_s, \omega\right) = -\frac{e^{i(k_s x_2 + q_s|z_2 - z_s|)}}{2iq_s} = -\frac{e^{i(k_s x_2 + q_s(z_2 - z_s))}}{2iq_s}, \tag{A-25}$$

respectively. Notice that, in equations A-24 and A-25, we have assumed $z_1 > z_g$ and $z_2 > z_s$ to remove the absolute value ($|z_1 - z_g| \to (z_1 - z_g)$, $|z_2 - z_s| \to (z_2 - z_s)$) in the Green's functions. That assumption corresponds to the assumption that the perturbation $V_1(x_1, z_1, x_2, z_2)$ is *below* (and larger than) the source z_s and receiver depth z_g (i.e., measurement surface). The positive direction for z is pointing downward, hence, the perturbation being non-zero below the measurement surface means $z_1 > z_g$ and $z_2 > z_s$ for a non-zero V_1 contribution.

Substituting equations A-24 and A-25 into equation A-23, we have

$$\begin{aligned} D_1'\left(k_g, z_g, k_s, z_s, \omega\right) &= \int dx_1 dz_1 dx_2 dz_2 \frac{e^{-i(k_g x_1 - q_g(z_1 - z_g))}}{2iq_g} V_1\left(x_1, z_1, x_2, z_2, \omega\right) \frac{e^{i(k_s x_2 + q_s(z_2 - z_s))}}{2iq_s} \\ &= \frac{e^{-iq_g z_g} e^{-iq_s z_s}}{2iq_g 2iq_s} V_1\left(k_g, q_q, k_s, q_s, \omega\right), \end{aligned} \tag{A-26}$$

where we recognize the integrals over x_1, z_1, x_2, z_2 as Fourier transforms.

Similarly, in Equation A-18,

$$D_2'(x_g, z_g, x_s, z_s, \omega) = \left(G_0^d(x_g, z_g, x_1, z_1) V_2(x_1, z_1, x_2, z_2, \omega) G_0^d(x_2, z_2, x_s, z_s, \omega)\right)_{ms}$$

can be expressed as

$$D_2'\left(k_g, z_g, k_s, z_s, \omega\right) = \frac{e^{-iq_g z_g} e^{-iq_s z_s}}{2iq_g 2iq_s} V_2\left(k_g, q_q, k_s, q_s \omega\right). \tag{A-27}$$

And for

$$\begin{aligned}&\left(G_0^d(x_g,z_g,x_1,z_1,\omega)V_2(x_1,z_1,x_2,z_2,\omega)G_0^d(x_2,z_2,x_s,z_s,\omega)\right)_{ms}=\\&-\left(G_0^d(x_g,z_g,x_1,z_1,\omega)V_1(x_1,z_1,x_2,z_2,\omega)G_0^{fs}(x_2,z_2,x_3,z_3,\omega)V_1(x_3,z_3,x_4,z_4,\omega)\right.\\&\left.\times G_0^d(x_4,z_4,x_s,z_s,\omega)\right)_{ms},\end{aligned}\tag{A-28}$$

the left hand side can be expressed as

$$LHS=\frac{e^{-iq_gz_g}e^{-iq_sz_s}}{2iq_g2iq_s}V_2\left(k_g,q_q,k_s,q_s,\omega\right).\tag{A-29}$$

To solve for the right hand side of equation A-28, we have $G_0^d\left(k_g,z_g,x_1,z_1,\omega\right)$ and $G_0^d\left(x_2,z_2,k_s,z_s,\omega\right)$ expressed in equations A-24, A-25, respectively. $G_0^{fs}(x_2,z_2,x_3,z_3,\omega)$ can be expressed as follows (see figure A-1),

$$G_0^{fs}(x_2,z_2,x_3,z_3,\omega)=\frac{1}{2\pi}\int dk\frac{e^{ik(x_2-x_3)}e^{iq(z_2+z_3)}}{2iq},\tag{A-30}$$

Notice that, we have assumed the free-surface is at depth $z=0$ in this expression. The right hand side now can be expressed as follows,

$$\begin{aligned}RHS=-G_0^dV_1G_0^{fs}V_1G_0^d&=-\int dx_1dz_1dx_2dz_2dx_3dz_3dx_4dz_4\frac{e^{-i(k_gx_1-q_g(z_1-z_g))}}{2iq_g}\\&\times V_1\left(x_1,z_1,x_2,z_2,\omega\right)\frac{1}{2\pi}\int dk\frac{e^{ik(x_2-x_3)}e^{iq(z_2+z_3)}}{2iq}V_1\left(x_3,z_3,x_4,z_4,\omega\right)\frac{e^{i(k_sx_4+q_s(z_4-z_s))}}{2iq_s}\\&=-\frac{e^{-iq_gz_g}e^{-iq_sz_s}}{2iq_g2iq_s}\frac{1}{2\pi}\int dkV_1\left(k_g,q_q,k,q,\omega\right)\frac{1}{2iq}V_1\left(k,q,k_s,q_s,\omega\right).\end{aligned}\tag{A-31}$$

Canceling common factors on both sides (equations A-29 and A-31), we have

$$V_2(k_g,k_s,\omega)=-\frac{1}{2\pi}\int dkV_1(k_g,k,\omega)\frac{1}{2iq}V_1(k,k_s,\omega).\tag{A-32}$$

Substituting V_1 with D_1' using equation A-26 and V_2 with D_2' using equation A-27, we obtain the second term D_2' as follows,

$$D_2'(k_g,k_s,\omega)=-\frac{1}{2\pi}\int dkD_1(k_g,k,\omega)(2iq)e^{iq(z_g+z_s)}D_1(k,k_s,\omega).\tag{A-33}$$

In practice A-33 is the free surface elimination algorithm that directly inputs D_1 and outputs D_2'. Next, we show one example from Jingfeng Zhang (2007) to demonstrate that the ISS free-surface multiple-prediction algorithm predicts free-surface multiples with accurate time and amplitude.

Figure A-2 shows the model used to generate input data. The calculations are in the data domain: V_1, V_2, $\cdots$ are never solved for in ISS data driven algorithms. The data contains the reference waves (yellow line), source and receiver ghosts (dashed blue line), free-surface multiples (black line), and primaries (red line). This data is first pre-processed by distinct Green's theorem methods to remove the reference waves, and source and receiver ghosts. Then, the pre-processed data (consisting of primaries and free-surface multiples (for this example), see solid line in figure A-3) enter the ISS FSME algorithm. The result after the ISS FSME is shown in figure A-3 using a dashed line. Notice that the result after the ISS FSME is obtained by $D_2' + D_1'$. When D_2' is added to D_1', two things happen, first-order free-surface multiples are eliminated, and all higher-order free-surface multiples are altered, and prepared for their removal by higher order terms in the ISS FSME subseries, D_3', D_4', etc.

APPENDIX B

COMPARING THE ISS FSME WITH SRME

In appendix A, we have provided a brief derivation of the ISS FSME algorithm. The ISS FSME inputs seismic data that is generated by monopole sources (or source arrays) and that has the reference waves and source ghosts, receiver ghosts and source-and-receiver ghosts all removed.

This algorithm predicts the exact time and exact amplitude of all free-surface multiples at all offsets. That provides a good starting point and opportunity to understand under what set of approximations we can derive the SRME prediction with its approximate prediction of the amplitude and phase of the free-surface multiples. That then locates and identifies the origin of the missing physics in the SRME prediction. It turns out that the SRME prediction corresponds to a data with the reference waves removed and with source and receiver deghosted data, but where the source consists of a vertically separately dipole source in the water column. The vertically-separated dipole source is defined as the limit of two vertically separately (of opposite sign) Dirac delta sources as the distance between them approaches zero and the source amplitude goes to infinity, in such a way that the product of source amplitude and the distance between them remains constant. Since a data due to a vertically dipole source is not realizable in practice, the idea within SRME is to seek to approximate what a dipole source would produce by keeping the source side ghost (see figure B-1). That approximation and substitution is the origin of the missing or erroneous physics and results in an approximate prediction of both the amplitude and phase of the free-surface multiples. We examine the consequence of that approximation and substitution on the exact ISS FSME prediction in this Appendix B.

Below we follow the SRME prescription to input the data with only the reference wave and receiver-side ghosts removed (i.e., keeping the source-side ghost). Under that SRME assumption, equations A-17 to A-18 become

$$D_1'' = \left(G_0^d V_1 \left(G_0^d + G_0^{fs}\right)\right)_{ms}, \tag{B-1}$$

$$D_2'' = \left(G_0^d V_2 \left(G_0^d + G_0^{fs}\right)\right)_{ms} = -\left(G_0^d V_1 G_0^{fs} V_1 \left(G_0^d + G_0^{fs}\right)\right)_{ms}. \tag{B-2}$$

With

$$G_0^{fs}\left(x_2, z_2, k_s, z_s, \omega\right) = \frac{e^{i(k_s x_2 + q_s(z_2+z_s))}}{2iq_s},$$

Equation B-1 now becomes,

$$D_1''\left(k_g, z_g, k_s, z_s, \omega\right) = \frac{e^{-iq_g z_g}\left(e^{-iq_s z_s} - e^{iq_s z_s}\right)}{2iq_g 2iq_s} V_1\left(k_g, q_q, k_s, q_s, \omega\right) \tag{B-3}$$

The left part of Equation B-2 becomes,

$$D_2''\left(k_g, z_g, k_s, z_s, \omega\right) = \frac{e^{-iq_g z_g}\left(e^{-iq_s z_s} - e^{iq_s z_s}\right)}{2iq_g 2iq_s} V_2\left(k_g, q_q, k_s, q_s, \omega\right) \tag{B-4}$$

The right part of equation B-2 becomes,

$$-\frac{e^{-iq_g z_g}\left(e^{-iq_s z_s} - e^{iq_s z_s}\right)}{2iq_g 2iq_s}\frac{1}{2\pi}\int dk V_1\left(k_g, q_q, k, q, \omega\right)\frac{1}{2iq} V_1\left(k, q, k_s, q_s, \omega\right) \tag{B-5}$$

We have,

$$V_2(k_g, k_s, \omega) = -\frac{1}{2\pi}\int dk V_1(k_g, k, \omega)\frac{1}{2iq} V_1(k, k_s, \omega) \tag{B-6}$$

Now, substituting V_1, V_2 with D_1'', D_2'' in equations B-3 and B-4, respectively, we have

$$D_2''\left(k_g, z_g, k_s, z_s, \omega\right) = \frac{1}{2\pi}\int dk D_1''\left(k_g, z_g, k, z_s, \omega\right)\frac{2iqe^{iqz_g}}{\left(e^{iqz_s} - e^{-iqz_s}\right)} D_1''\left(k, z_g, k_s, z_s, \omega\right). \tag{B-7}$$

Let's take a look at the factor $(e^{iqz_s} - e^{-iqz_s})$ in the denominator. For a source that is close to the free-surface (which means z_s is small, since the free-surface is assumed to be at depth $z = 0$ in this case), the factor $(e^{iqz_s} - e^{-iqz_s})$ can be approximated by

$$e^{iqz_s} - e^{-iqz_s} \approx iqe^{-iqz_s} 2z_s.$$

Under this approximation, equation B-7 becomes

$$\begin{aligned} D_2''\left(k_g, z_g, k_s, z_s, \omega\right) &= \frac{1}{2\pi}\int dk D_1''\left(k_g, z_g, k, z_s, \omega\right)\frac{2iqe^{iqz_g}}{\left(e^{iqz_s} - e^{-iqz_s}\right)} D_1''\left(k, z_g, k_s, z_s, \omega\right) \\ &\approx \frac{1}{2\pi}\int dk D_1''\left(k_g, z_g, k, z_s, \omega\right)\left(e^{iq(z_g+z_s)}\right) D_1''\left(k, z_g, k_s, z_s, \omega\right)\frac{1}{z_s} \end{aligned} \tag{B-8}$$

Now, if the receiver in the actual experiment is close to the free-surface (z_g is small), then equation B-8 will be proportional to

$$\frac{1}{2\pi}\int dk D_1''\left(k_g, z_g, k, z_s, \omega\right) D_1''\left(k, z_g, k_s, z_s, \omega\right). \tag{B-9}$$

Inverse Fourier transform on k_g and k_s, we have

$$\frac{1}{2\pi}\int dk D_1''(x_g, k, \omega) D_1''(k, x_s; \omega).$$

Expressing $D_1''(x_g, k, \omega)$ and $D_1''(k, x_s; \omega)$ using their Fourier Transforms,

$$\frac{1}{2\pi}\int dk \underline{\int dx' D_1''(x_g, x'; \omega) e^{ikx'}} \underline{\int dx'' D_1''(x'', x_s; \omega) e^{-ikx''}}.$$

Rearrange the above equation,

$$\frac{1}{2\pi}\int dx' \int dx'' D_1''(x_g, x'; \omega) D_1''(x'', x_s; \omega) \int dk e^{ik(x'-x'')}.$$

We have

$$\begin{aligned}
&\frac{1}{2\pi}\int dx' \int dx'' D_1''(x_g, x'; \omega) D_1''(x'', x_s; \omega) \int dk e^{ik(x'-x'')} \\
=&\frac{1}{2\pi}\int dx' \int dx'' D_1''(x_g, x'; \omega) D_1''(x'', x_s; \omega) \Big(2\pi\delta(x'-x'')\Big) \\
=&\int dx D_1''(x_g, x; \omega) D_1''(x, x_s; \omega).
\end{aligned} \tag{B-10}$$

We obtain the convolutional SRME free-surface-multiple-prediction equation. Hence, the industry standard free-surface algorithm, SRME, can be derived as an approximation to the ISS FSME algorithm. The ISS FSME predicts the exact time and amplitude of all free-surface multiples of different orders at all offsets. SRME predicts the approximate amplitude and phase of free surface multiples at all offsets.

REFERENCES

Amundsen, L., 1993, Wavenumber-based filtering of marine point-source data: Geophysics, **58**, 1335–1348.

Berkhout, A. J., 1985, Seismic migration: Theoretical aspects: Elsevier Publishing Co.

Cagniard, L., 1939, Reflexion et refraction des ondes sismiques progressive: Gauthier-Villar.

Carvalho, P. M., and Weglein, A. B., 1994, Wavelet estimation for surface multiple attenuation using a simulated annealing algorithm: SEG Technical Program Expanded Abstracts.

Carvalho, P. M., Weglein, A. B., and Stolt, R. H., 1991, Examples of a nonlinear inversion method based on the T-matrix of scattering theory: Application to multiple suppression: SEG Expanded Abstracts, pages 1319–1322.

Carvalho, P. M., 1992, Free-surface multiple reflection elimination method based on nonlinear inversion of seismic data: Ph.D. thesis, Universidade Federal da Bahia.

Clayton, R. W., and Stolt, R. H., 1981, A Born-WKBJ inversion method for acoustic reflection data: Geophysics, **46**, no. 11, 1559–1567.

de Hoop, A. T., 1959, The surface line source problem: Appl. Sci. Res. B., **8**, 349–356.

Ferreira, A., 2011, Internal multiple removal in offshore brrazil seismic data using the inverse scattering series: Ph.D. thesis, University of Houston.

Kolsky, H., 1953, The propagation of stress waves in viscoelastic solids: Philosophical Magazine, **1**, no. 8, 693–710.

Ma, C., and Weglein, A., 2016, Examining the interdependence and cooperation of the terms in the distinct inverse-scattering subseries for free-surface multiple and internal multiple removal: SEG Technical Program Expanded Abstract, pages 4561–4565.

Maston, K., Corrigan, D., Weglein, A., Yong, C. Y., and Carvalho, P., 1999, Inverse scattering internal multiple attenuation: Results from complex synthetic and field data examples: SEG Expaned Abstract.

Matson, K. H., 1997, An inverse-scattering series method for attenuating elastic multiples from multicomponent land and ocean bottom seismic data: Ph.D. thesis, University of British Columbia.

Mayhan, J., and Weglein, A., 2013, First application of green's theorem-derived source and receiver deghosting on deep-water gulf of mexico synthetic (seam) and field data: Geophysics, **78**, no. 2, WA77–WA89.

Mayhan, J. D., 2013, Wave-theoretic preprocessing to allow the inverse scattering series methods for multiple removal and depth imaging to realize their potential and impact: Methods, examples, and added value: Ph.D. thesis, University of Houston.

Moses, H., 1956, Calculation of scattering potential from reflection coefficients: Phys. Rev., **102**, no. 2, 559–567.

Osen, A., Secrest, B. G., Amundsen, L., and Reitan, A., 1998, Wavelet estimation from marine pressure measurements: Geophysics, **63**, 2108–2119.

Prosser, R. T., 1969, Formal solutions of inverse scattering problems: Journal of Mathematical Physics, **10**, no. 10, 1819–1822.

Razavy, M., 1975, Determination of the wave velocity in an inhomogeneous medium from reflection data: J. Acoust. Soc. Am., **58**, 956–963.

Shen, Y., 2017, Wave-theory-based seismic data preprocessing: An extension of the current deghosting method to allow for a variable measurement surface topography and its impact on the inverse scattering series multiple removal: Ph.D. thesis, University of Houston.

Stolt, R. H., and Jacobs, B., 1980, Inversion of seismic data in a laterally heterogeneous medium: Stanford Exploration Project, **24**.

Stolt, R. H., and Weglein, A. B., 1985, Migration and inversion of seismic data: Geophysics, **50**, no. 12, 2458–2472.

Tan, T. H., 1999, Wavelet spectrum estimation: Geophysics, **64**, 1836–1846.

Taylor, J. R., 1972, Scattering theory: the quantum theory of nonrelativistic collisions: John Wiley & Sons, Inc.

Verschuur, D. J., Berkhout, A. J., and Wapenaar, C. P. A., 1992, Adaptive surface-related multiple elimination: Geophysics, **57**, 1166–1177.

Verschuur, D. J., 1991, Surface-related multiple elimination, an inversion approach: Ph.D. thesis, Delft University of Technology.

Weglein, A., and Dragoset, W., 2005, Multiple attenuation.:, Geophysics reprint series Soc. Expl. Geophys.

Weglein, A. B., and Secrest, B. G., July 1990, Wavelet estimation for a multidimensional acoustic earth model: Geophysics, **55**, no. 7, 902–913.

Weglein, A. B., Boyce, W. E., and Anderson, J. E., 1981, Obtaining three-dimensional velocity information directly from reflection seismic data: An inverse scattering formalism: Geophysics, **46**, no. 8, 1116–1120.

Weglein, A. B., Gasparotto, F. A., Carvalho, P. M., and Stolt, R. H., November-December 1997, An inverse-scattering series method for attenuating multiples in seismic reflection data: Geophysics, **62**, no. 6, 1975–1989.

Weglein, A. B., Matson, K. H., and Berkhout, A. J., 2000, Wave theoretic approaches to multiple attenuation: Concepts, status, open issues, and plans: Part ii: Offshore Technology Conference.

Weglein, A. B., Shaw, S. A., Matson, K. H., Sheiman, J. L., Stolt, R. H., Tan, T. H., Osen, A., Correa, G. P., Innanen, K. A., Guo, Z., , and Zhang, J., 2002a, New approaches to deghosting towed-streamer and ocean-bottom pressure measurements: SEG Expanded Abstracts, pages 2114–2117.

——— 2002b, New approaches to deghosting towed-streamer and ocean-bottem pressure measurements: 72nd Annual International Meeting, SEG, Expanded Abstracts, pages 1016–1019.

Weglein, A. B., Araujo, F. V., Carvalho, P. M., Stolt, R. H., Matson, K. H., Coates, R. T., Corrigan, D., Foster, D. J., Shaw, S. A., and Zhang, H., 2003, Inverse scattering series and seismic exploration: Inverse Problems, **19**, no. 6, R27–R83.

Weglein, A., 2012, Short note: an alternative subtraction criteria (to energy minimization) for free-surface multiple removal: Mission-Oriented Seismic Research Program (M-OSRP) Annual Report.

Weglein, A. B., 2016, Multiple:signal or noise?: Geophysics, **81**, no. 4, v283–v302.

Weglein, A. B., 2017, A direct inverse method for subsurface properties: The conceptual and practical benefit and added value in comparison with all current indirect methods, for example, amplitude-variation-with-offset and full-waveform inversion: Interpretation, **5**, no. 3, SL89–SL107.

Weglein, A., 2018a, A new and comprehensive perspective on the role of primaries and multiples in seismic-data processing for structure determination and amplitude analysish: SEG Technical Program Expanded Abstract, pages 4548–4552.

——— 2018b, A new and comprehensive perspective on the role of primaries and multiples in seismic data processing structure determination and amplitude analysis: Journal of Seismic Exploration, page Submitted.

Wu, J., and Weglein, A., 2014, Elastic green's theorem preprocessing for on-shore internal multiple attenuation: Theory and initial synthetic data tests: SEG Technical Program Expanded Abstract, pages 4299–4304.

Wu, J., and Weglein, A., 2015, Preprocessing in displacement space for on-shore seismic processing: removing ground roll and ghosts without damaging the reflection data: SEG Technical Program Expanded Abstract, pages 4626–4630.

Wu, J., and Weglein, A., 2016a, Green's theorem-based onshore preprocessing: A reduced data requirement assuming a vacuum/earth model for the air/earth interface and the evaluation of the usefulness of that assumption: SEG Technical Program Expanded Abstract, pages 4685–4689.

——— 2016b, Predicting deghosted reflection data for both pressure and multicomponent

displacements at the ocean bottom: SEG Technical Program Expanded Abstract, pages 4751–4755.

Wu, J., and Weglein, A., 2017, A new method for deghosting data collected on a depth-variable acquisition surface by combining green's theorem wave separation followed by a stolt extended claerbout iii wave prediction for one-way propagating waves.: SEG Expanded Abstracts, pages 4859–4864.

Zhang, H., and Shaw, S., 2010, 1-D analytical analysis of higher order internal multiples predicted via the inverse scattering series based algorithm: SEG Technical Program Expanded Abstracts, **29**, 3493–3498.

Zhang, J., 2007, Wave theory based data preparation for inverse scattering multiple removal, depth imaging and parameter estimation: Analysis and numerical tests of green's theorem deghosting theory: Ph.D. thesis, University of Houston.

Zhang, Z., 2017, Impact of the topography of the acquisition surface on preprocessing and subsequent free surface multiple elimination and depth migration: Examining the issue and providing a preprocessing response that accommodates a variable topography - thereby allowing subsequent multiple removal and imaging methods to deliver their promise and potential: Ph.D. thesis, University of Houston.

LIST OF FIGURES

free-surface multiples, respectively. We can see from this trace comparison, the SRME provides an approximate free-surface multiple prediction.

11 A 1D subsurface model with two primary events and one free-surface multiple event.

12 Input data generated based on the model shown in figure 11.

13 Prediction of free-surface multiple by the ISS FSME (D_2' in equation 1) using the input data shown in figure 12.

14 Prediction of free-surface multiple by the SRME using the input data shown in figure 12.

15 Free-surface multiple removal result after directly subtracting the ISS prediction result (figure 13) from the data (figure 12).

16 Free-surface multiple removal result by combing the SRME prediction (figure 14) and adaptive subtraction.

17 Actual primaries in the data shown in figure 12.

18 Trace comparison at Offset 100m. Red, blue and green line represent actual data, ISS free-surface multiple prediction and SRME prediction, respectively.

19 Trace comparison at Offset 500m. Red, blue and green line represent actual data, ISS free-surface multiple prediction and SRME prediction, respectively.

20 Trace comparison at Offset 750m. Red, blue and green line represent actual data, ISS free-surface multiple prediction and SRME prediction, respectively.

21 Trace comparison at Offset 1000m. Red, blue and green line represent actual data, ISS free-surface multiple prediction and SRME prediction, respectively.

22 Trace comparison at Offset 1250m. Red, blue and green line represent actual data, ISS free-surface multiple prediction and SRME prediction, respectively.

23 Trace comparison at Offset 750m. Red, blue and green represent the actual primary, result after ISS FSME and result after the SRME + adaptive, respectively.

24 Input data with random noise added on the analytic data.

25 Prediction of free-surface multiple by the ISS FSME (D_2' in equation 1) using the input data shown in figure 24.

26 Prediction of free-surface multiple by the SRME using the input data shown in figure 24.

27 Free-surface multiple removal result after directly subtracting the ISS prediction result (figure 25) from the data (figure 24).

28 Free-surface multiple removal result by combing the SRME prediction (figure 26) and adaptive subtraction.

29 Actual primaries in the data shown in figure 24.

30 Trace comparison at Offset 100m. Red, blue and green line represent actual data, ISS free-surface multiple prediction and SRME prediction, respectively.

31 Trace comparison at Offset 500m. Red, blue and green line represent actual data, ISS free-surface multiple prediction and SRME prediction, respectively.

32 Trace comparison at Offset 750m. Red, blue and green line represent actual data, ISS free-surface multiple prediction and SRME prediction, respectively.

33 Trace comparison at Offset 1000m. Red, blue and green line represent actual data, ISS free-surface multiple prediction and SRME prediction, respectively.

34 Trace comparison at Offset 1250m. Red, blue and green line represent actual data, ISS free-surface multiple prediction and SRME prediction, respectively.

35 Trace comparison at Offset 750m. Red, blue and green represent the actual primary, result after ISS FSME and result after the SRME + adaptive, respectively.

36 Input data generated from an absorptive medium.

37 Prediction of free-surface multiple by the ISS FSME (D_2' in equation 1) using the input data generated by an absorptive medium shown in figure 36.

38 Prediction of free-surface multiple by the SRME using the input data generated by an absorptive medium shown in figure 36.

39 Free-surface multiple removal result after directly subtracting the ISS prediction result (figure 37) from the data (figure 36).

40 Free-surface multiple removal result by combing the SRME prediction (figure 38) and adaptive subtraction.

41 Actual primaries in the input data shown in figure 36.

42 Trace comparison at Offset 100m. Red, blue and green line represent actual data, ISS free-surface multiple prediction and SRME prediction, respectively.

43 Trace comparison at Offset 500m. Red, blue and green line represent actual data, ISS free-surface multiple prediction and SRME prediction, respectively.

44 Trace comparison at Offset 750m. Red, blue and green line represent actual data, ISS free-surface multiple prediction and SRME prediction, respectively.

45 Trace comparison at Offset 1000m. Red, blue and green line represent actual data, ISS free-surface multiple prediction and SRME prediction, respectively.

46 Trace comparison at Offset 1250m. Red, blue and green line represent actual data, ISS free-surface multiple prediction and SRME prediction, respectively.

47 Trace comparison at Offset 750m. Red, blue and green represent the actual primary, result after ISS FSME and result after the SRME + adaptive, respectively.

A-1 Green's function G_0^{fs}, travels up from the source to the free-surface and then down to the receiver.

A-2 Model used to generated data in Zhang (2007) to test the ISS FSME.

A-3 A trace comparison between the input data D_1' (solid line) to the ISS FSME and output data $D_1' + D_2'$ after the ISS FSME. When D_2' is added to D_1', two things happen, the first-order free-surface multiple is eliminated, all higher-order free-surface multiples are altered, and prepared for their removal by D_3', D_4', etc.

B-1 (a) Monopole source and its 2D Green's function in k_x, ω domain. (b) Dipole source and its 2D Green's function. (c) Monopole source & its source ghosts and their 2D Green's functions. Free-surface is at depth $z = 0$. $q = \sqrt{\frac{\omega^2}{c_0} - k_x^2}$, where ω, k_x and c_0 are the temporal frequency, horizontal wavenumber, and medium velocity.

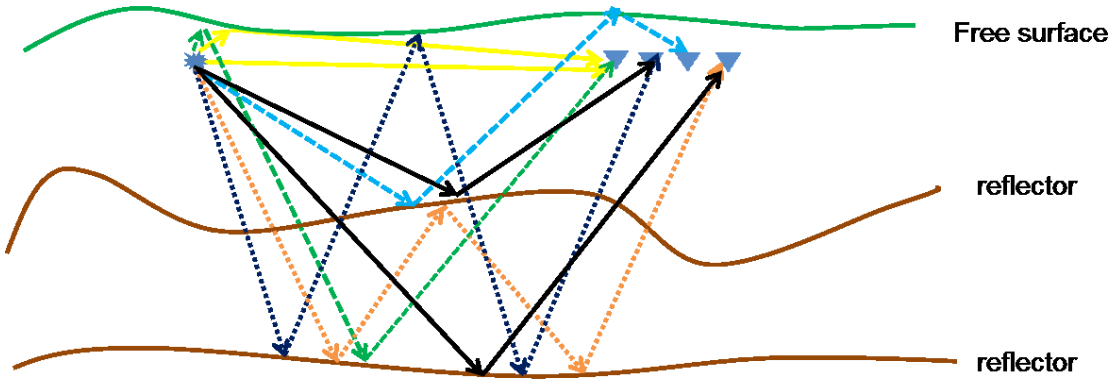

Figure 1: Illustration of different seismic events in marine environment. Yellow solid line: reference waves; Green and light blue dashed: source ghost and receiver ghost, respectively; Dark blue dashed line: free surface multiple; Orange dashed line: internal multiple; solid black line: primary.

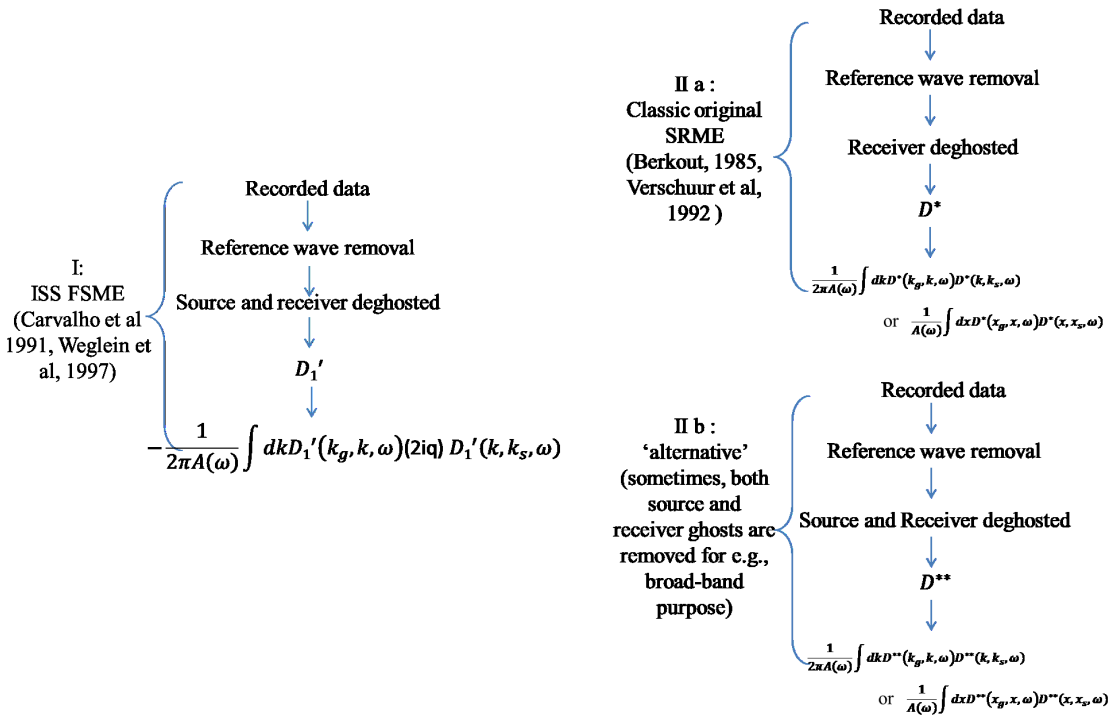

Figure 2: ISS free-surface multiple prediction algorithm and SRME free-surface multiple prediction algorithm

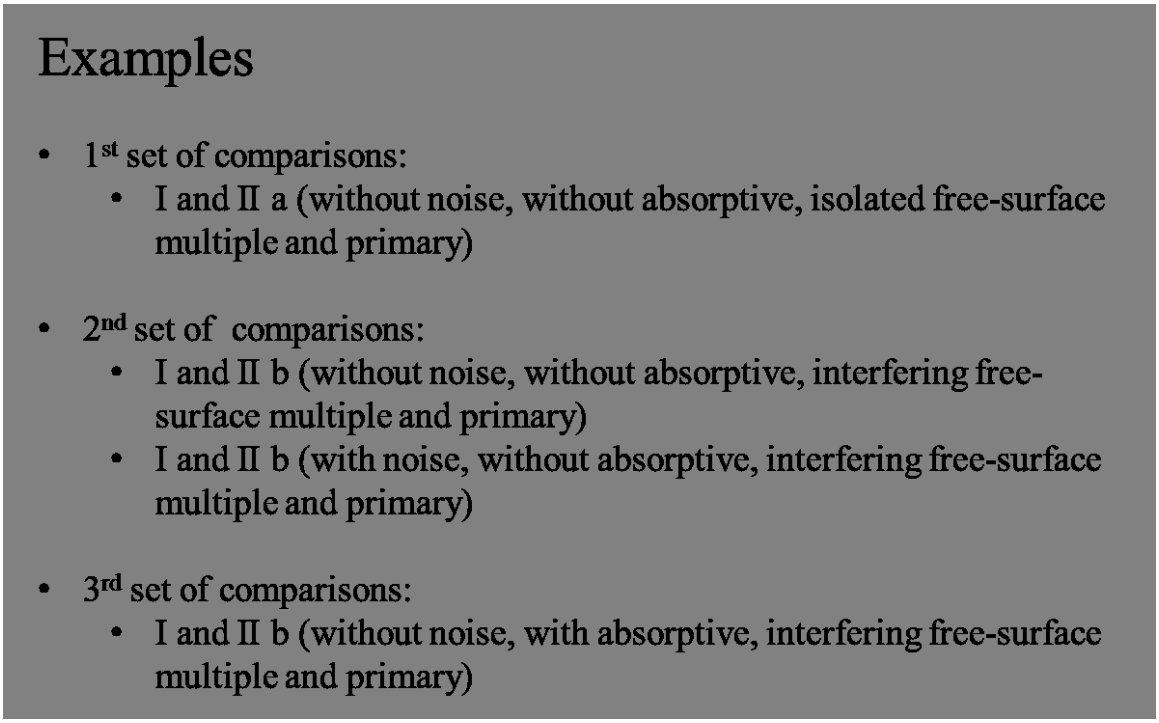

Figure 3: Three sets of comparisons between the ISS free-surface multiple prediction and SRME free-surface multiple prediction

Chao Ma, Qiang Fu, and Arthur B. Weglein – GEO-2018-0411

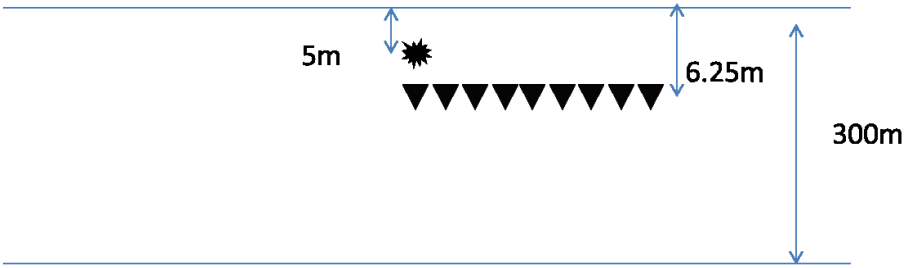

Figure 4: A 1D subsurface model with a horizontal reflector and a free-surface.

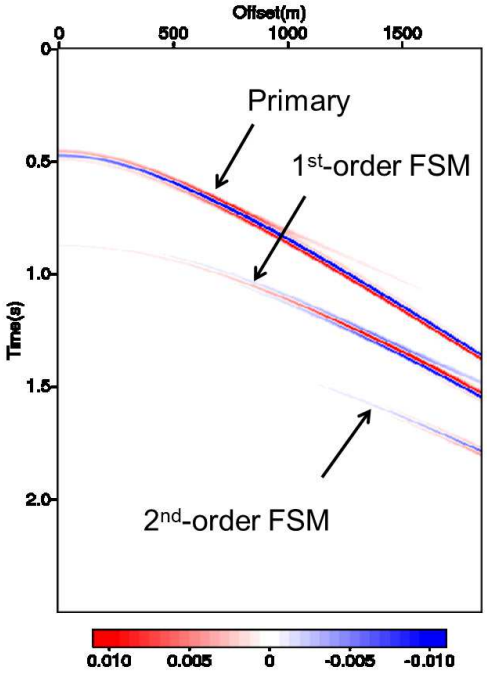

Figure 5: Input data for the ISS free-surface multiple prediction. Notice that, only primaries and free-surface multiples are generated for ISS FSME input.

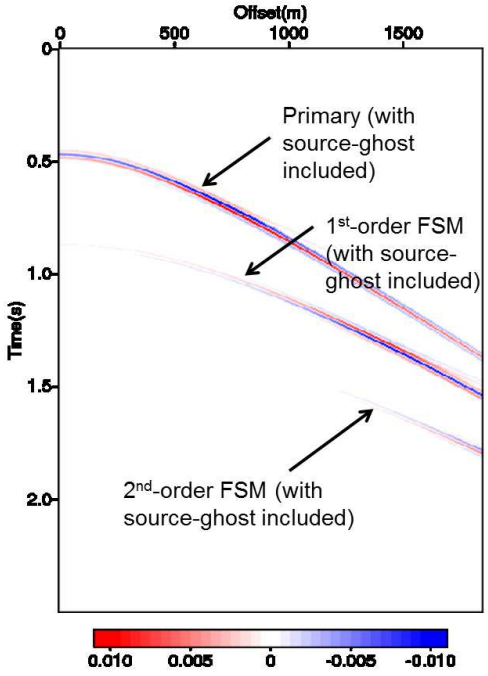

Figure 6: Input data for the SRME free-surface multiple prediction. Notice that, primaries and free-surface multiples and their source ghosts are generated for SRME input

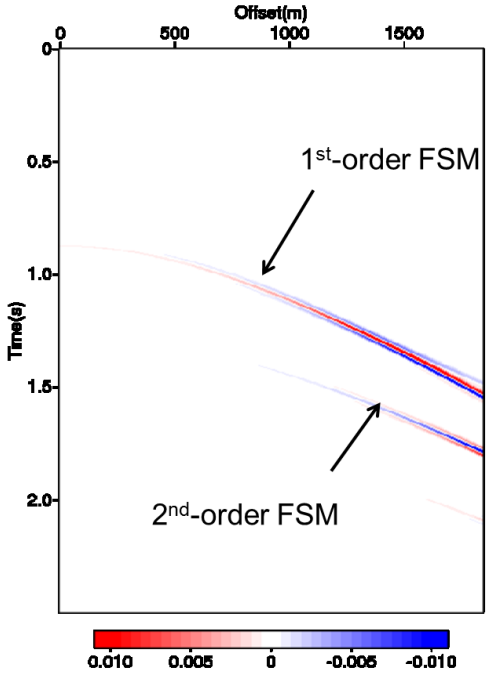

Figure 7: ISS free-surface multiple prediction (D_2' in equation 1) with the input in figure 5.

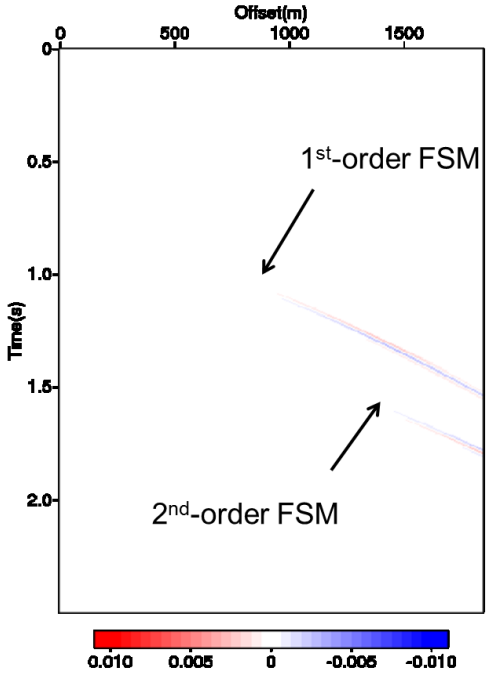

Figure 8: SRME free-surface multiple prediction (equation 3) with the input in figure 6.

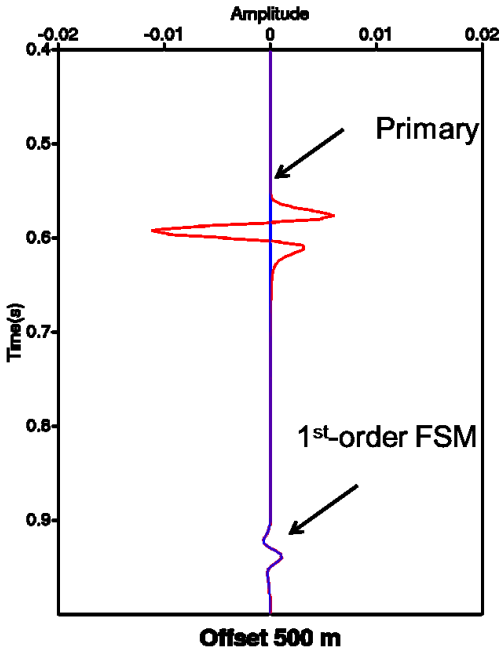

Figure 9: A trace comparison at 500m offset between the input of the ISS FSME and its prediction. The red and blue line represent input data to the ISS FSME and its prediction, respectively. We can see the ISS free-surface multiple prediction agrees with the actual free-surface multiple very well. Notice that, the predicted free-surface multiple has opposite sign compared with the actual free-surface multiple, we first flip the polarity of the prediction, then compare it with the actual data for easy comparison.

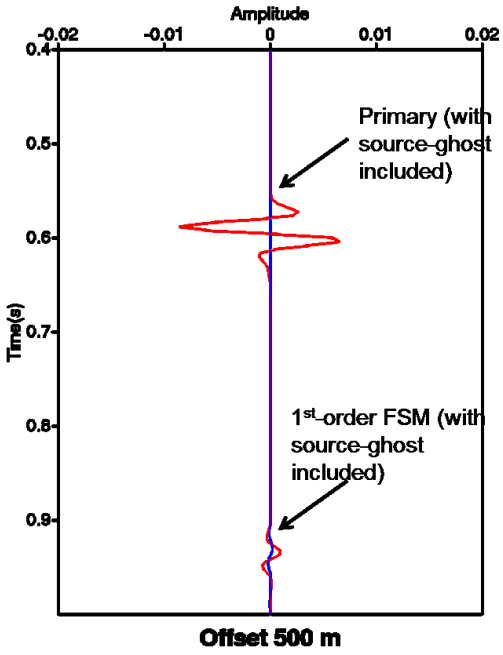

Figure 10: A trace comparison at 500m offset between the input of the SRME and its prediction. The red and blue represent the input data to the SRME and its prediction for free-surface multiples, respectively. We can see from this trace comparison, the SRME provides an approximate free-surface multiple prediction.

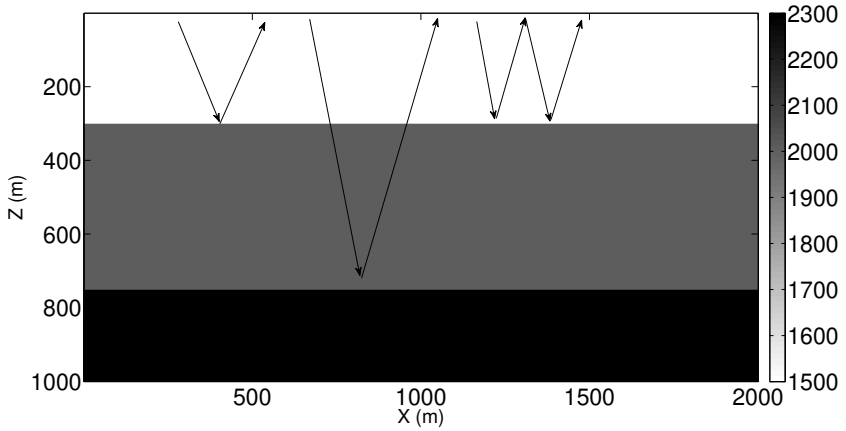

Figure 11: A 1D subsurface model with two primary events and one free-surface multiple event.

Chao Ma, Qiang Fu, and Arthur B. Weglein – GEO-2018-0411

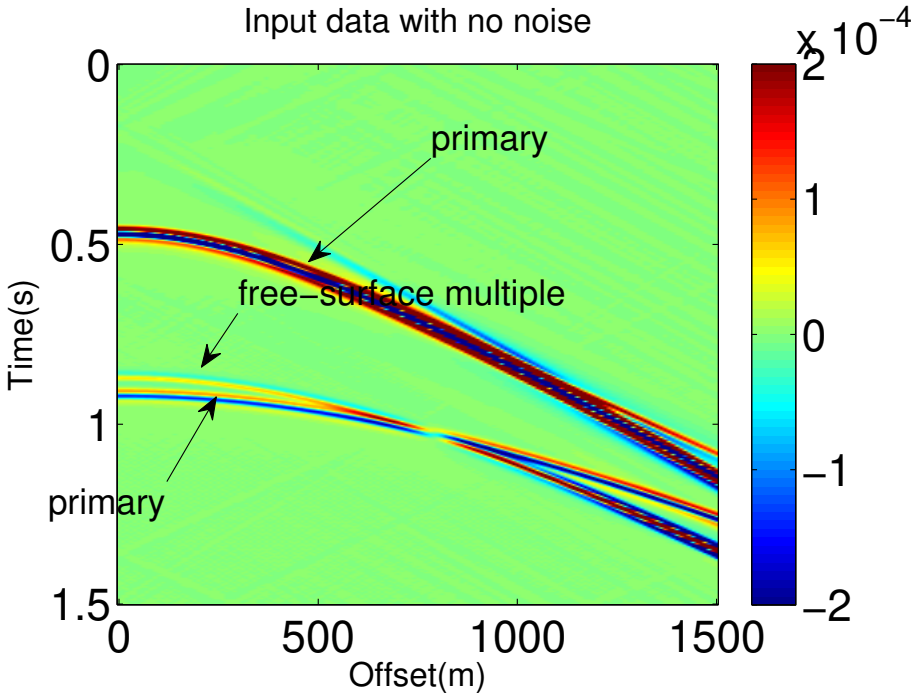

Figure 12: Input data generated based on the model shown in figure 11.

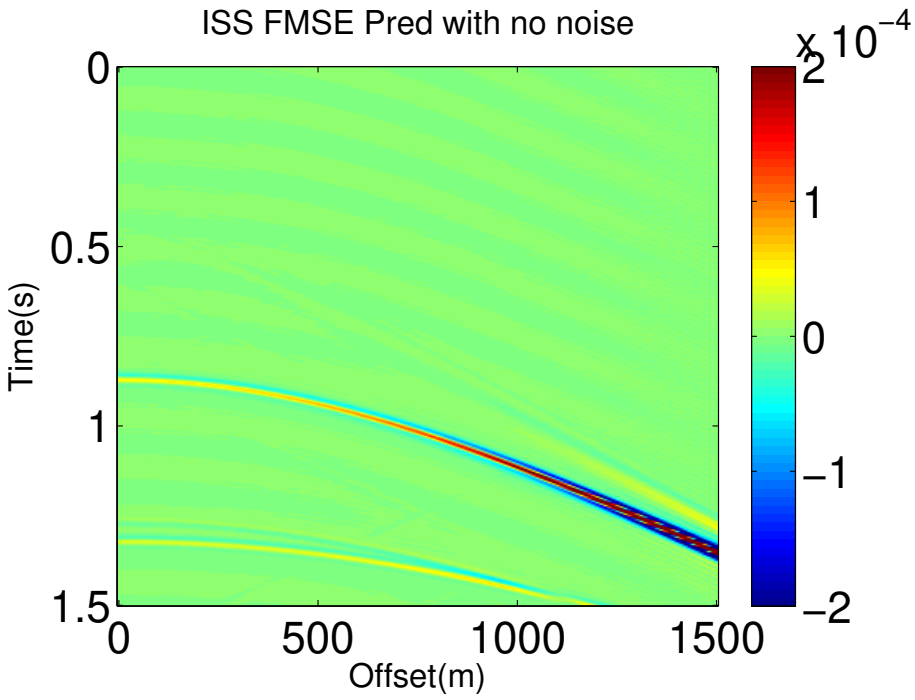

Figure 13: Prediction of free-surface multiple by the ISS FSME (D_2' in equation 1) using the input data shown in figure 12.

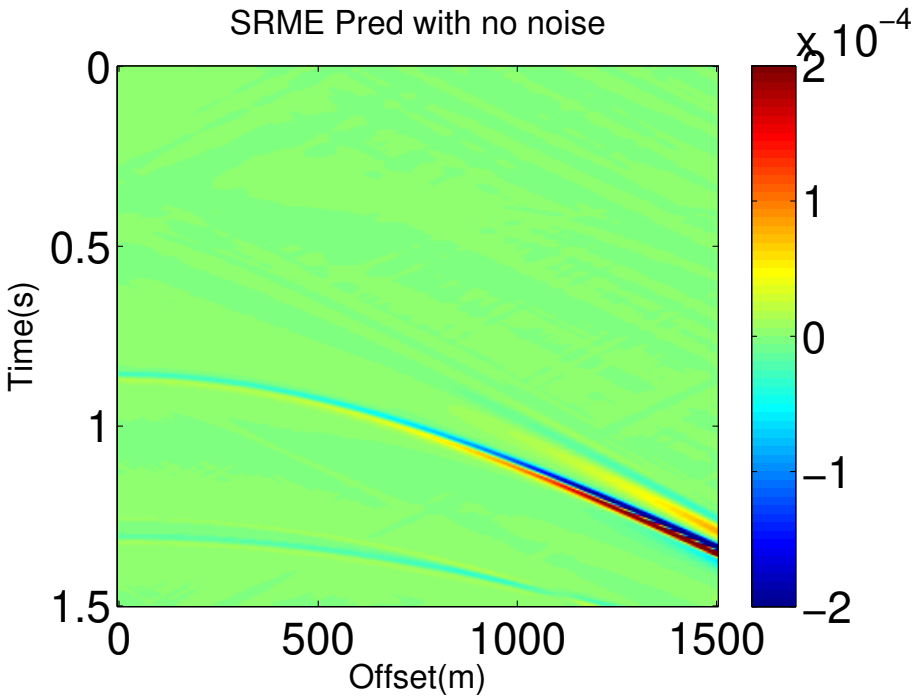

Figure 14: Prediction of free-surface multiple by the SRME using the input data shown in figure 12.

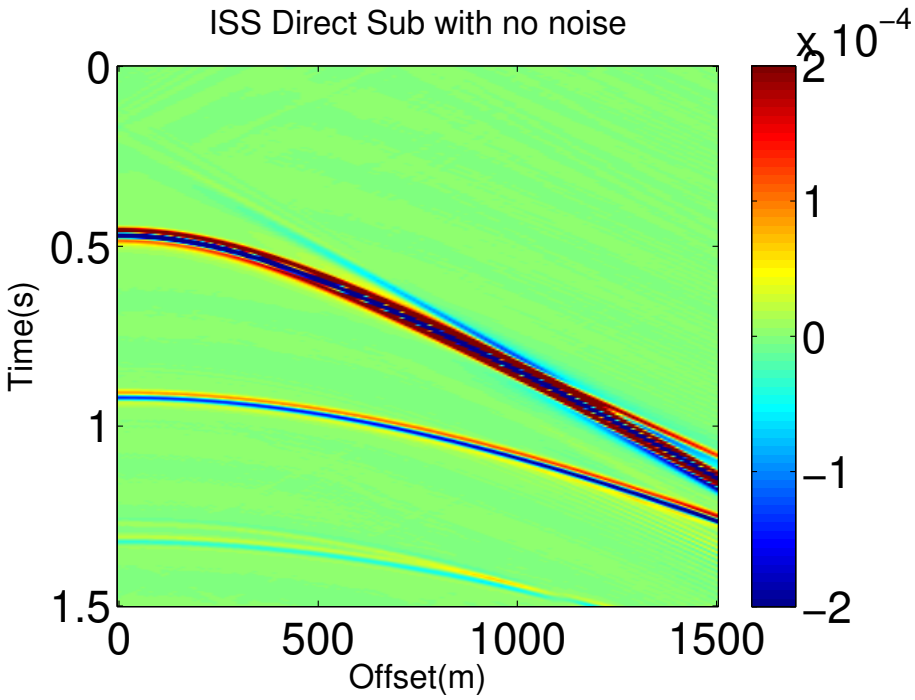

Figure 15: Free-surface multiple removal result after directly subtracting the ISS prediction result (figure 13) from the data (figure 12).

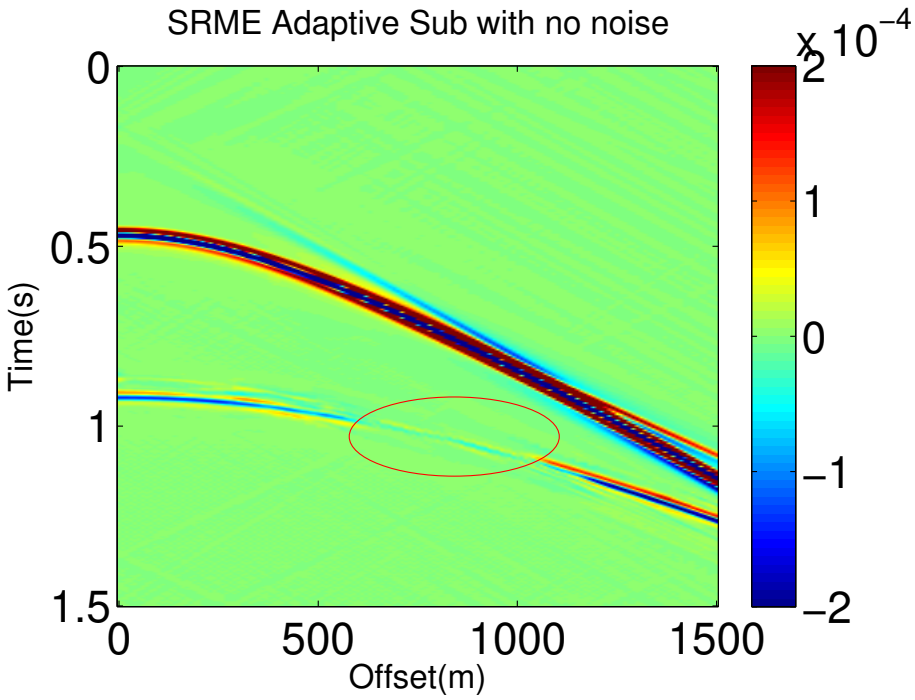

Figure 16: Free-surface multiple removal result by combing the SRME prediction (figure 14) and adaptive subtraction.

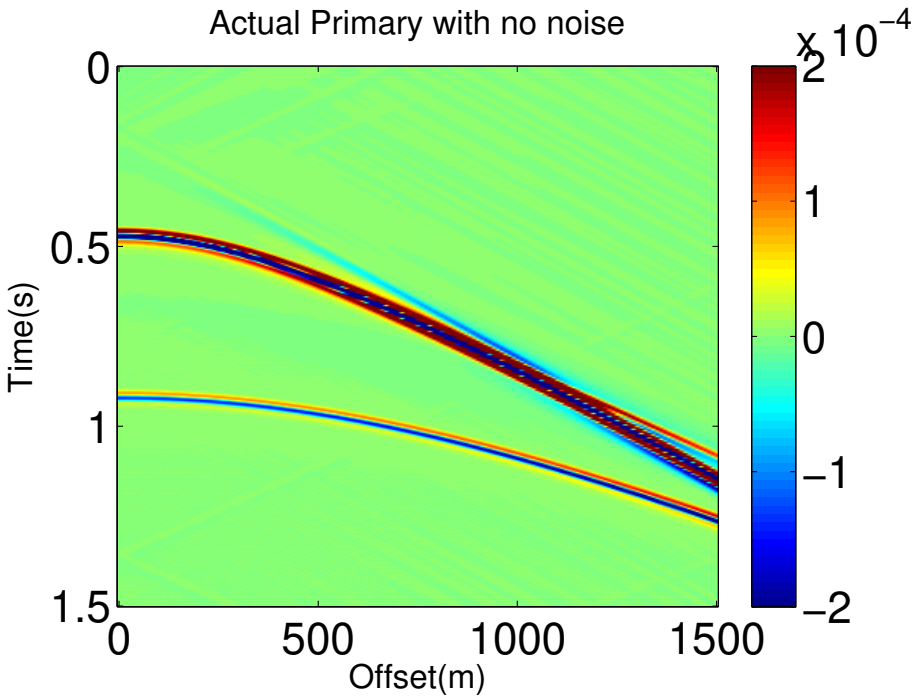

Figure 17: Actual primaries in the data shown in figure 12.

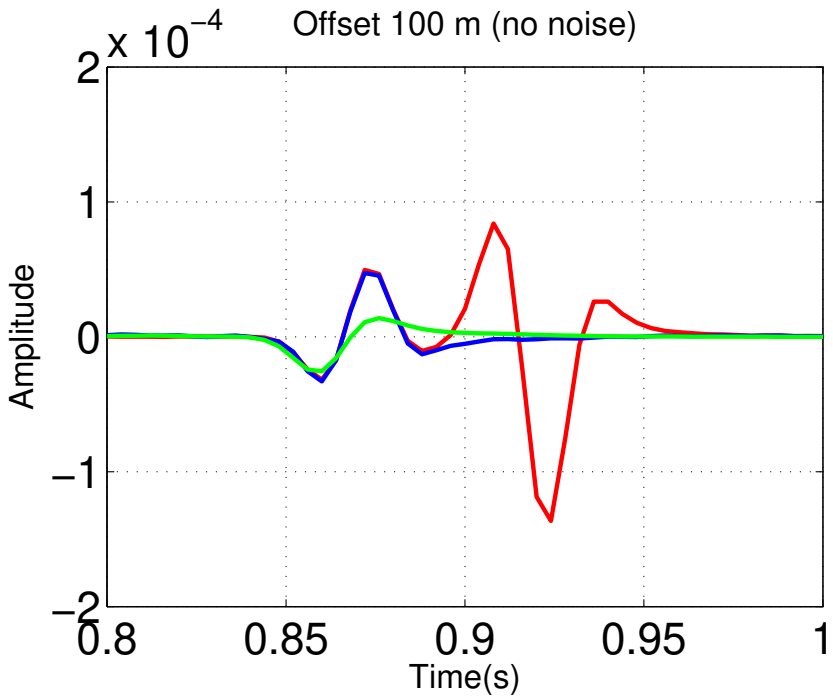

Figure 18: Trace comparison at Offset 100m. Red, blue and green line represent actual data, ISS free-surface multiple prediction and SRME prediction, respectively.

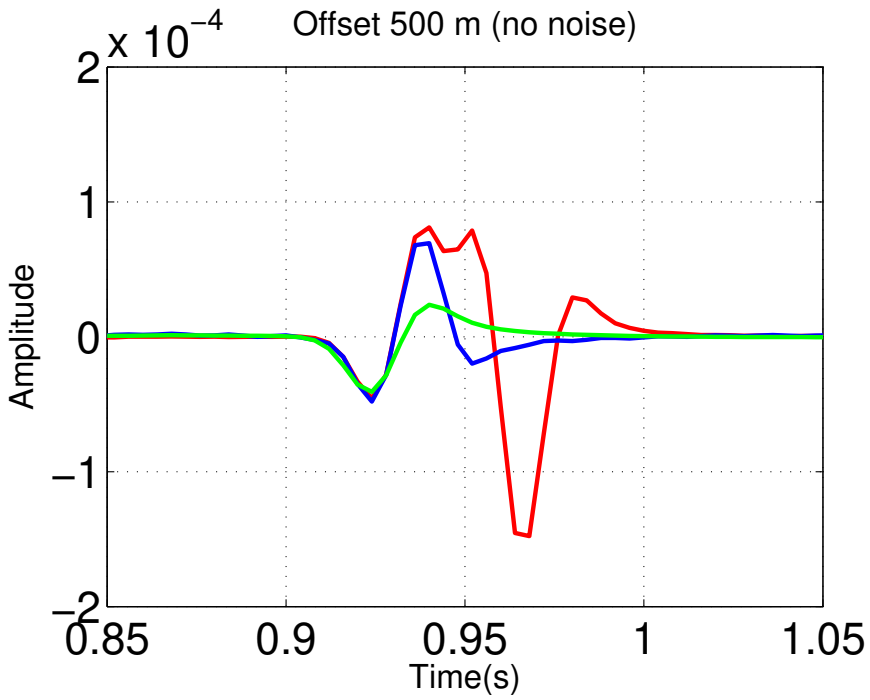

Figure 19: Trace comparison at Offset 500m. Red, blue and green line represent actual data, ISS free-surface multiple prediction and SRME prediction, respectively.

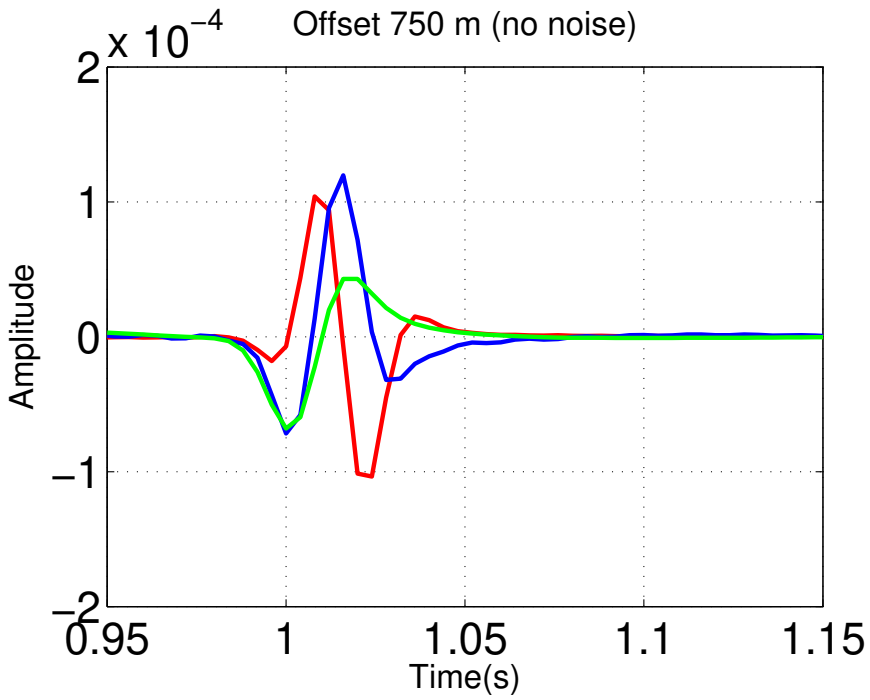

Figure 20: Trace comparison at Offset 750m. Red, blue and green line represent actual data, ISS free-surface multiple prediction and SRME prediction, respectively.

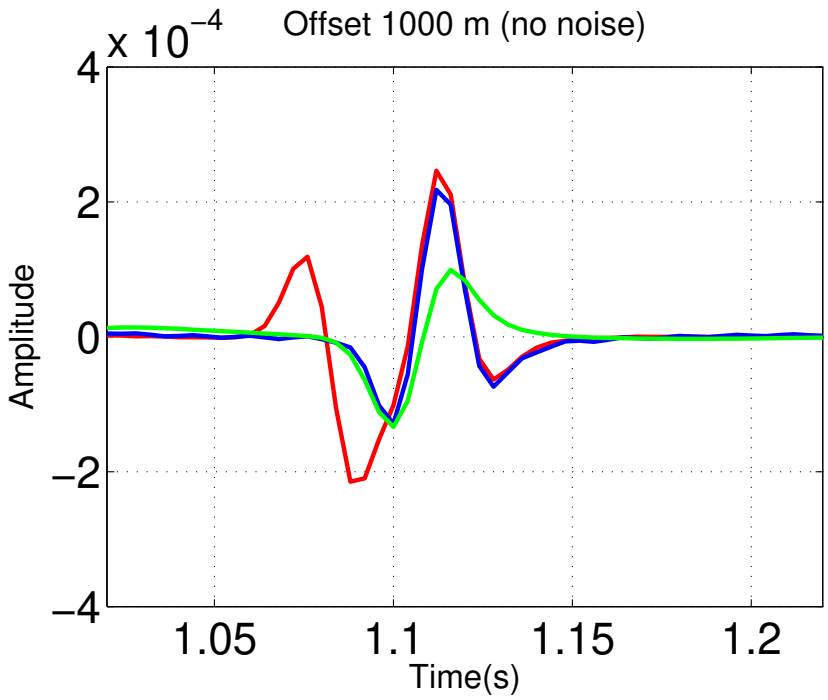

Figure 21: Trace comparison at Offset 1000m. Red, blue and green line represent actual data, ISS free-surface multiple prediction and SRME prediction, respectively.

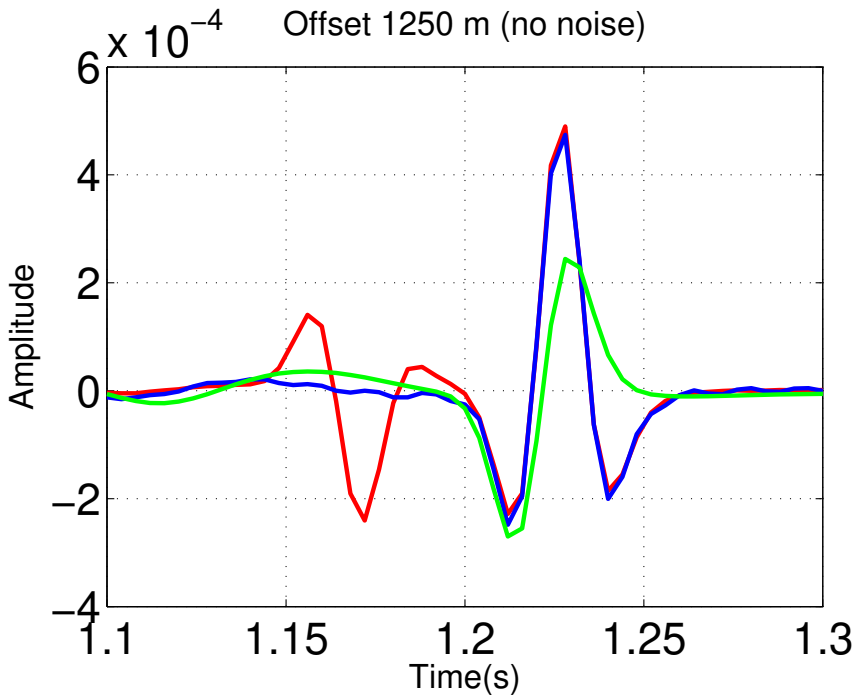

Figure 22: Trace comparison at Offset 1250m. Red, blue and green line represent actual data, ISS free-surface multiple prediction and SRME prediction, respectively.

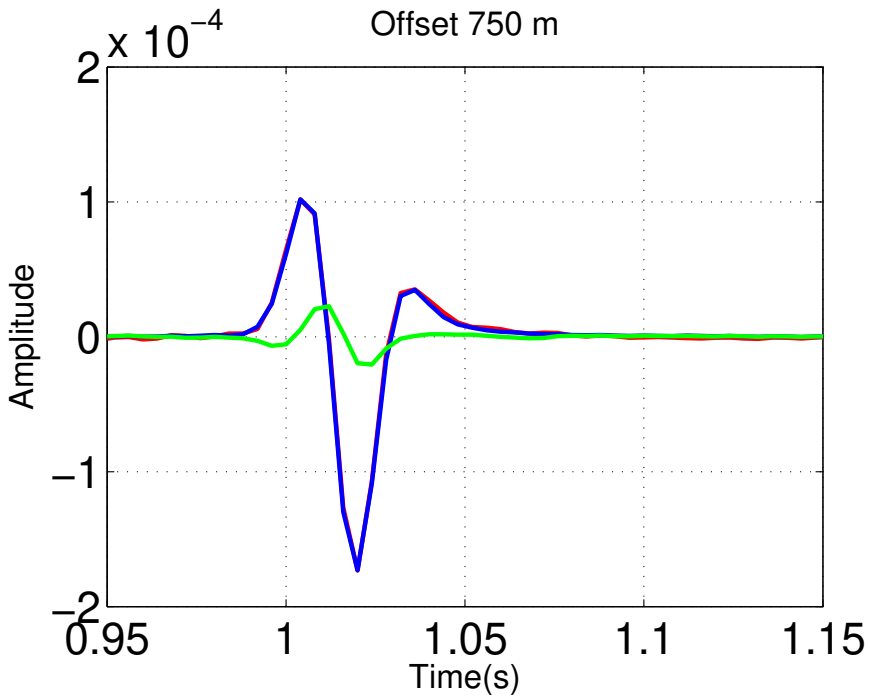

Figure 23: Trace comparison at Offset 750m. Red, blue and green represent the actual primary, result after ISS FSME and result after the SRME + adaptive, respectively.

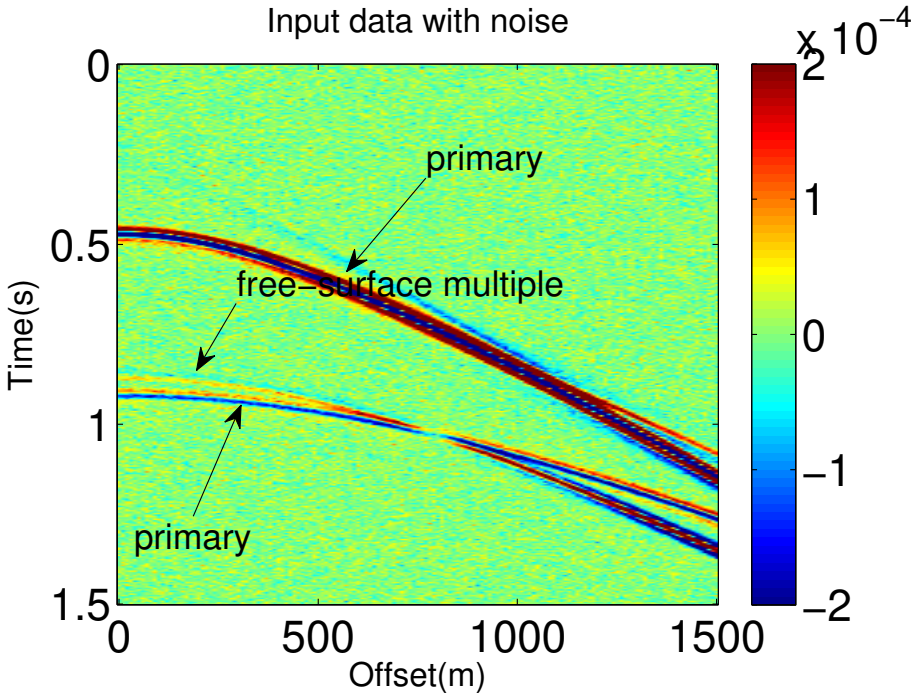

Figure 24: Input data with random noise added on the analytic data.

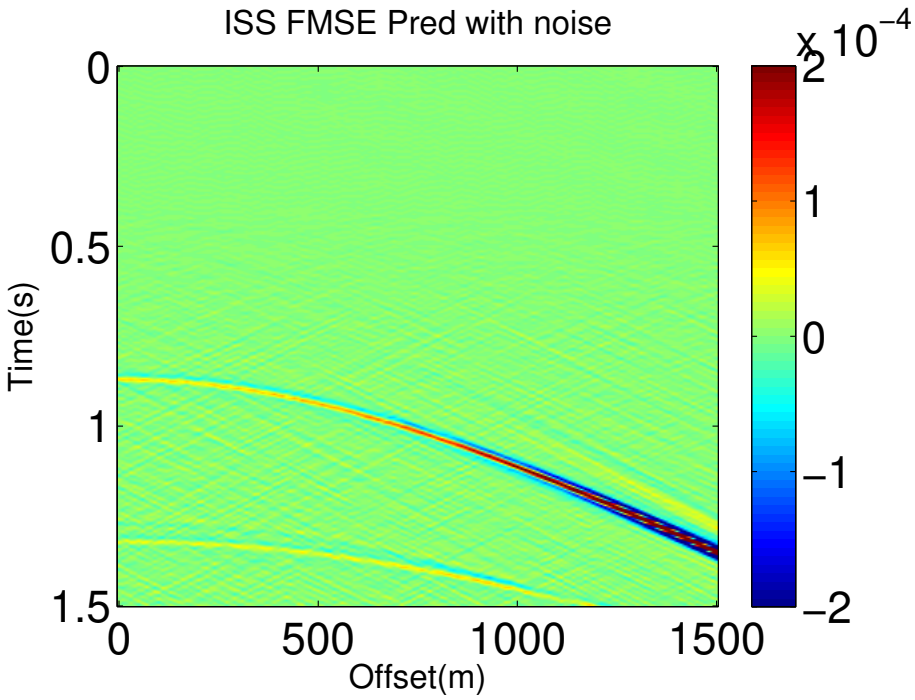

Figure 25: Prediction of free-surface multiple by the ISS FSME (D_2' in equation 1) using the input data shown in figure 24.

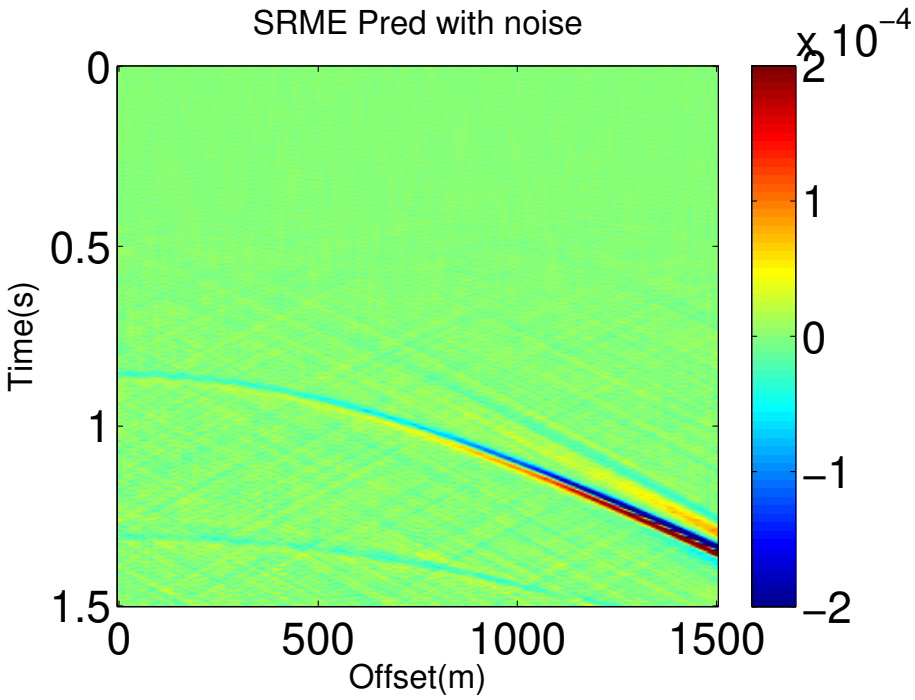

Figure 26: Prediction of free-surface multiple by the SRME using the input data shown in figure 24.

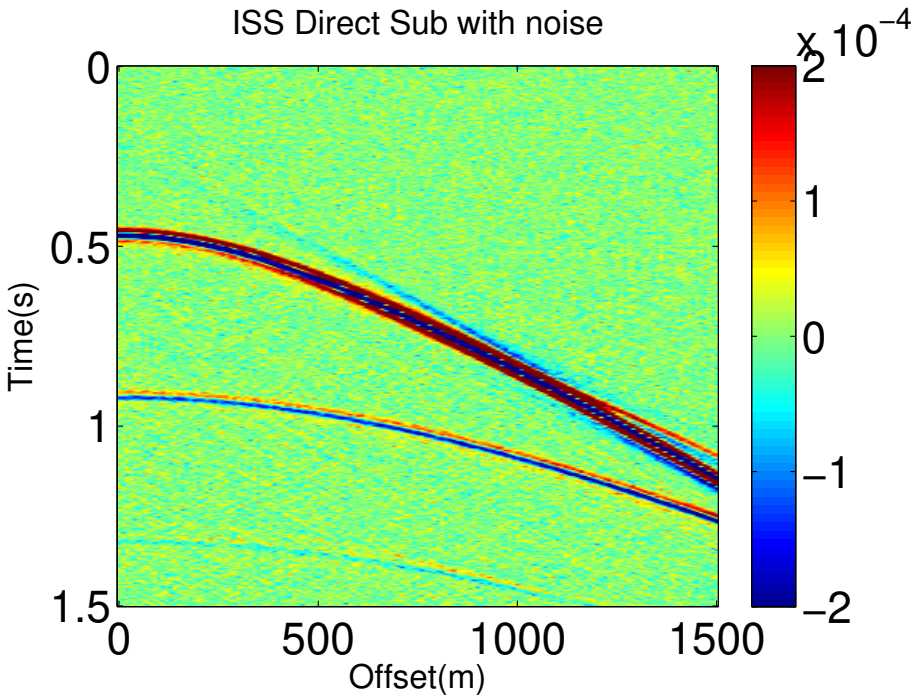

Figure 27: Free-surface multiple removal result after directly subtracting the ISS prediction result (figure 25) from the data (figure 24).

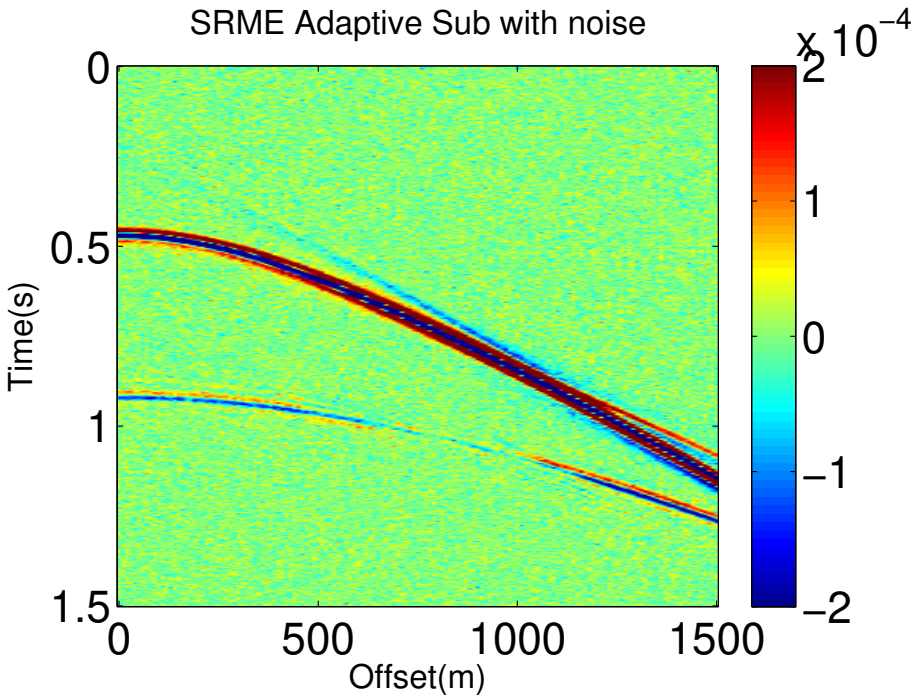

Figure 28: Free-surface multiple removal result by combing the SRME prediction (figure 26) and adaptive subtraction.

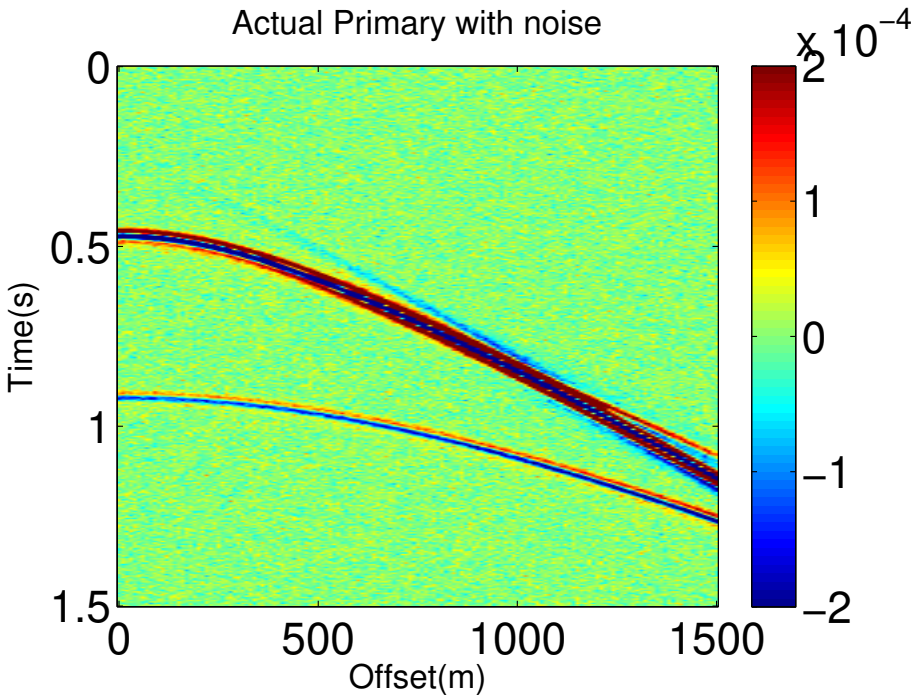

Figure 29: Actual primaries in the data shown in figure 24.

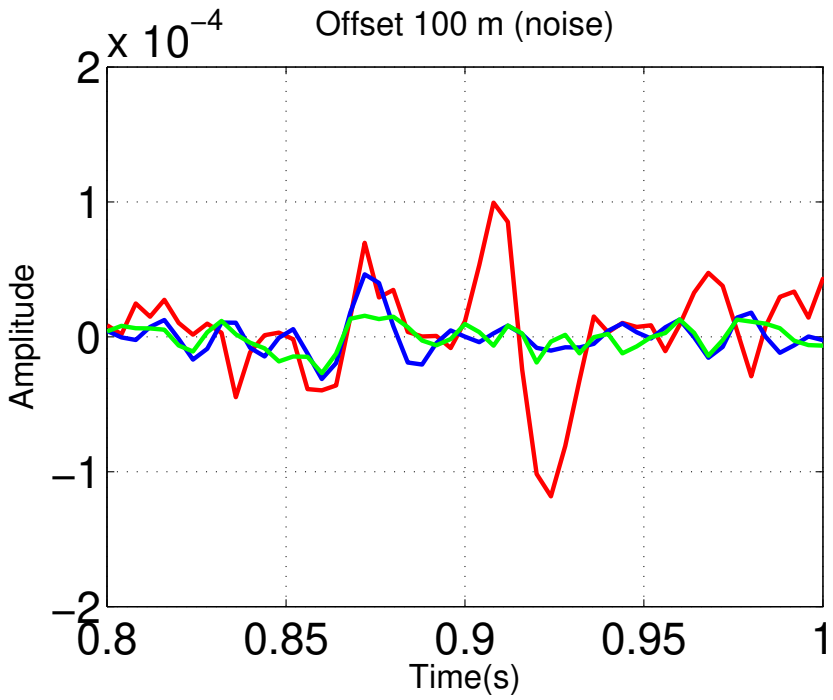

Figure 30: Trace comparison at Offset 100m. Red, blue and green line represent actual data, ISS free-surface multiple prediction and SRME prediction, respectively.

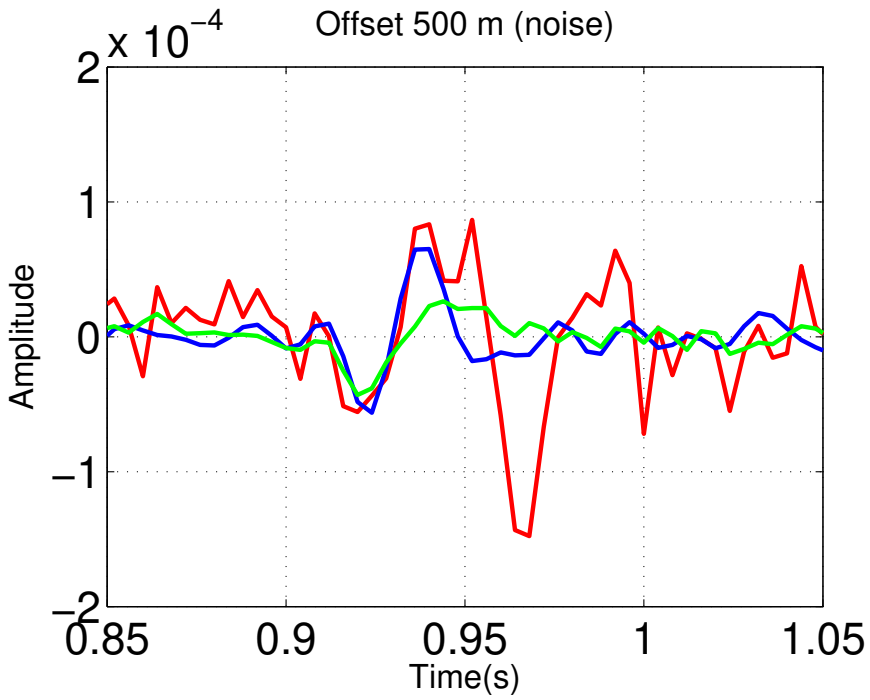

Figure 31: Trace comparison at Offset 500m. Red, blue and green line represent actual data, ISS free-surface multiple prediction and SRME prediction, respectively.

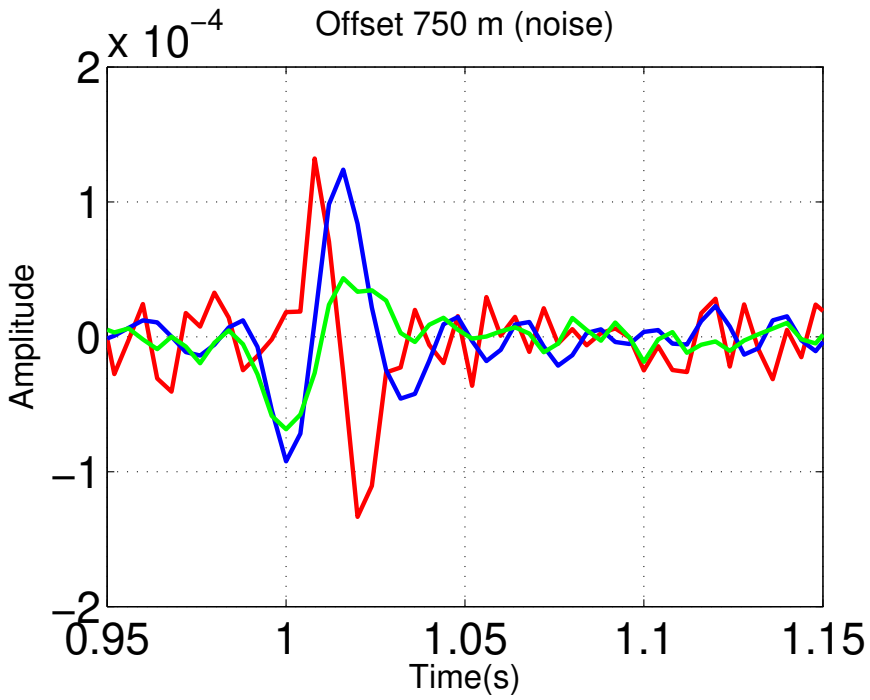

Figure 32: Trace comparison at Offset 750m. Red, blue and green line represent actual data, ISS free-surface multiple prediction and SRME prediction, respectively.

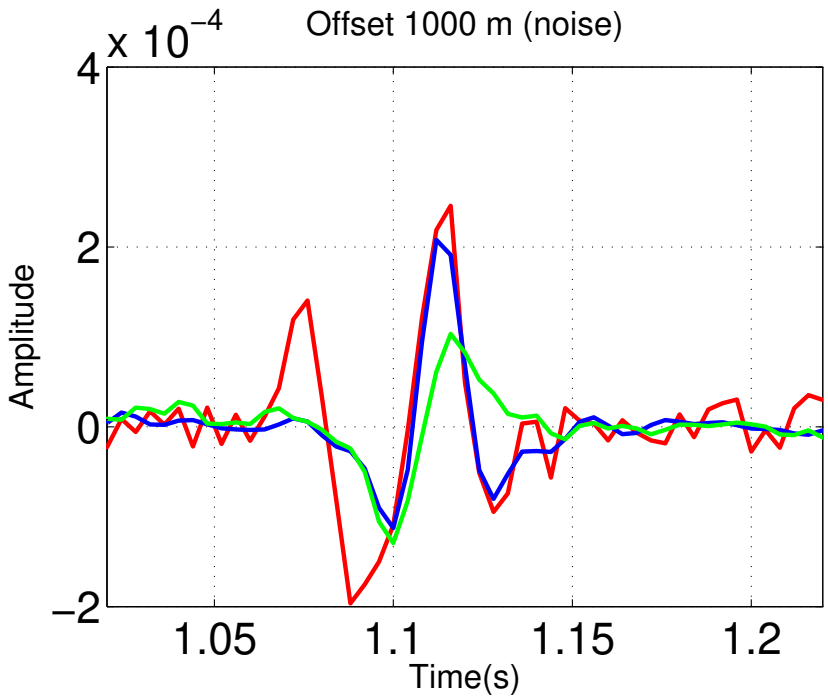

Figure 33: Trace comparison at Offset 1000m. Red, blue and green line represent actual data, ISS free-surface multiple prediction and SRME prediction, respectively.

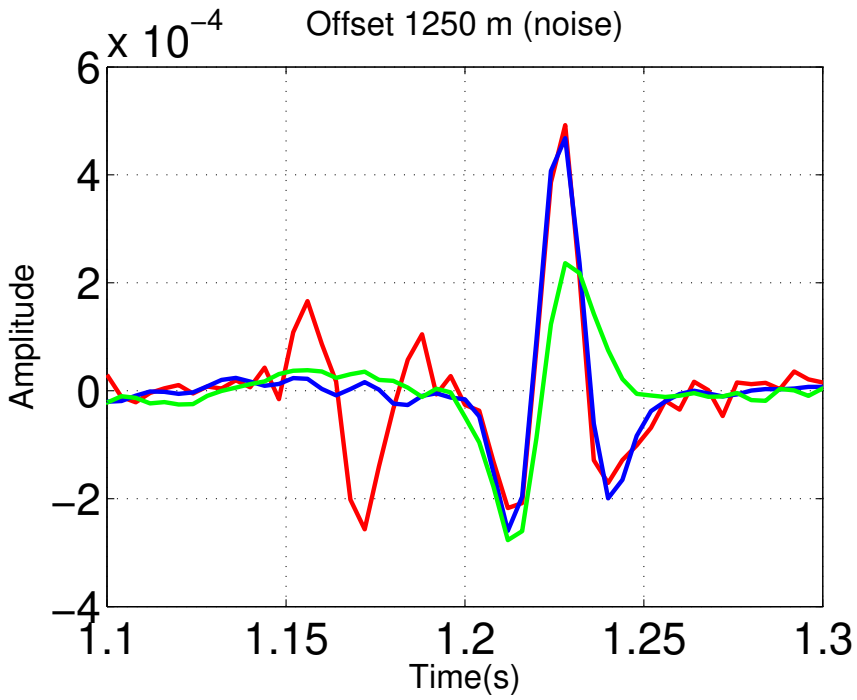

Figure 34: Trace comparison at Offset 1250m. Red, blue and green line represent actual data, ISS free-surface multiple prediction and SRME prediction, respectively.

Chao Ma, Qiang Fu, and Arthur B. Weglein – GEO-2018-0411

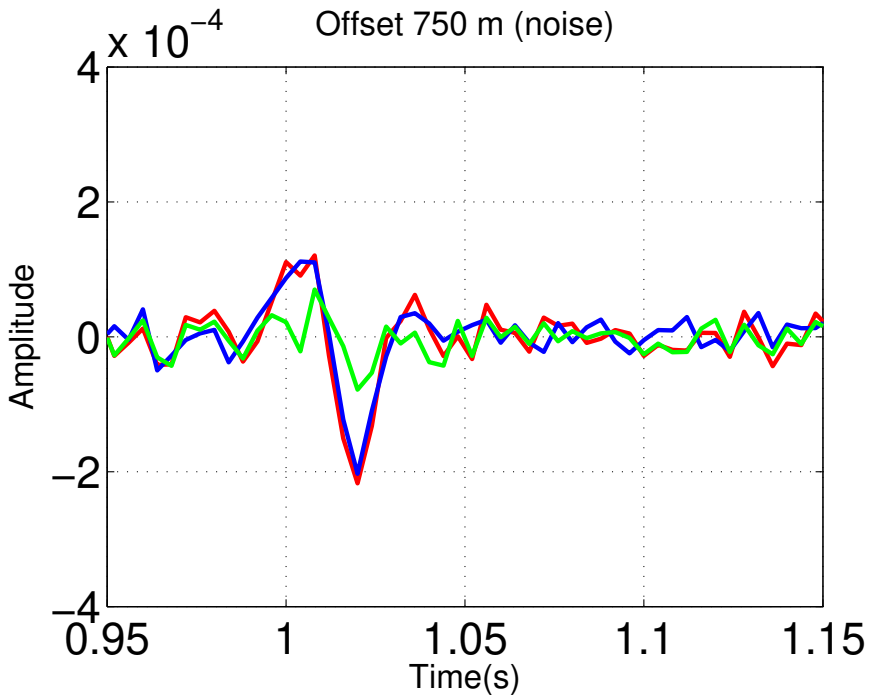

Figure 35: Trace comparison at Offset 750m. Red, blue and green represent the actual primary, result after ISS FSME and result after the SRME + adaptive, respectively.

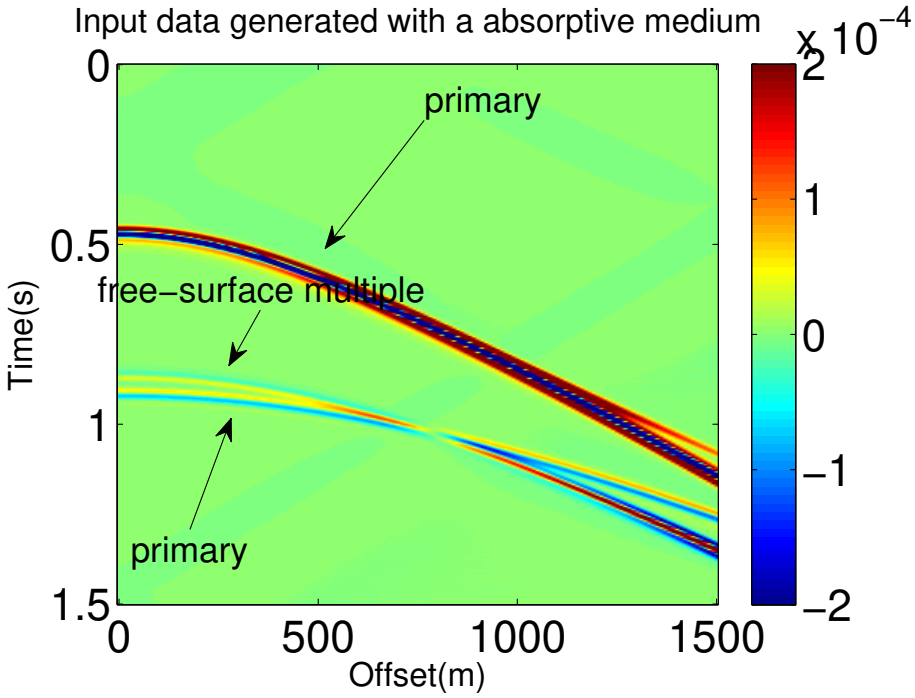

Figure 36: Input data generated from an absorptive medium.

Chao Ma, Qiang Fu, and Arthur B. Weglein – GEO-2018-0411

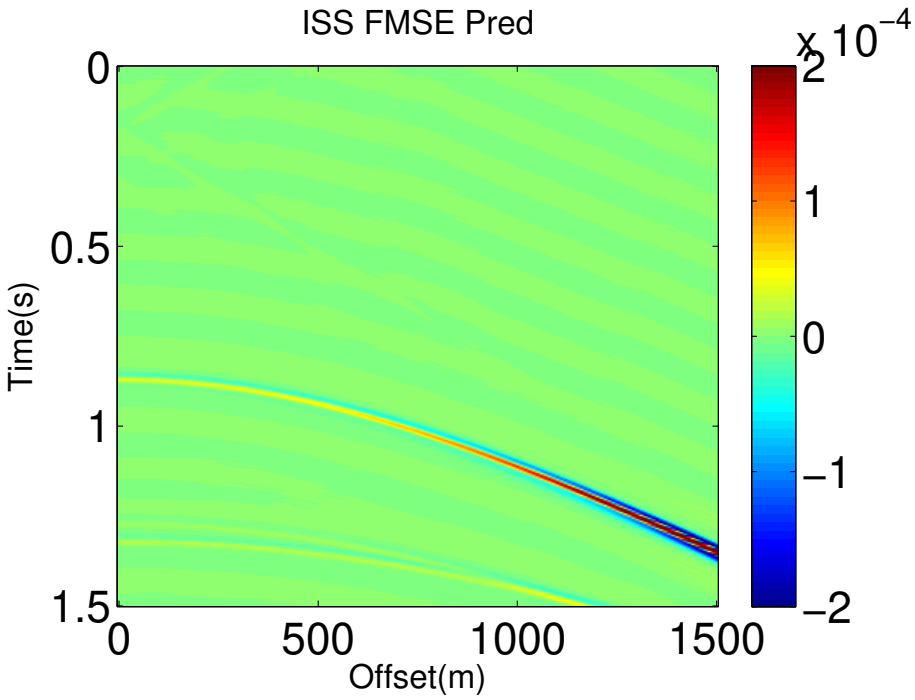

Figure 37: Prediction of free-surface multiple by the ISS FSME (D_2' in equation 1) using the input data generated by an absorptive medium shown in figure 36.

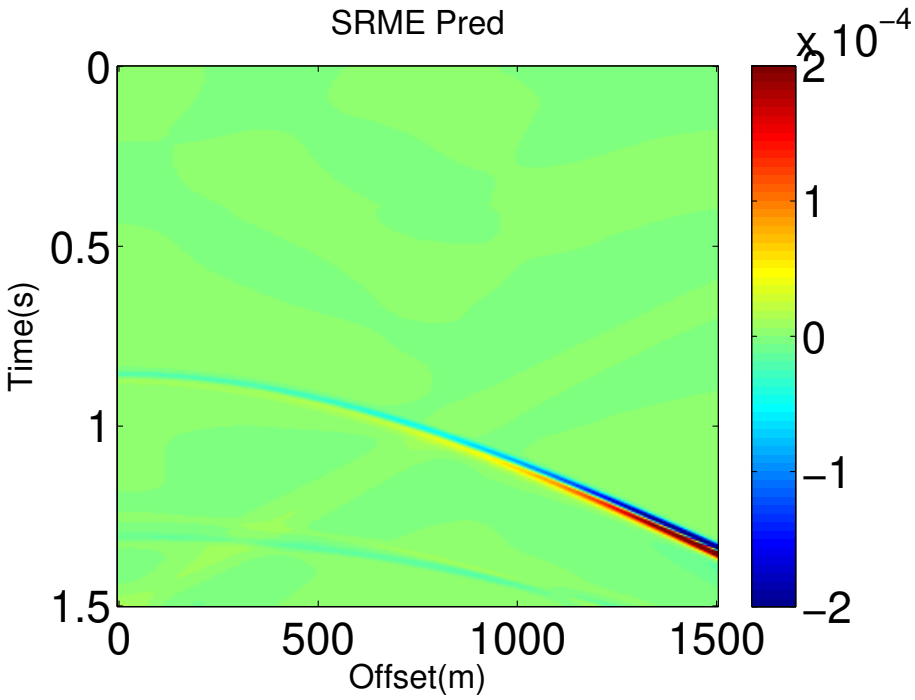

Figure 38: Prediction of free-surface multiple by the SRME using the input data generated by an absorptive medium shown in figure 36.

Chao Ma, Qiang Fu, and Arthur B. Weglein – GEO-2018-0411

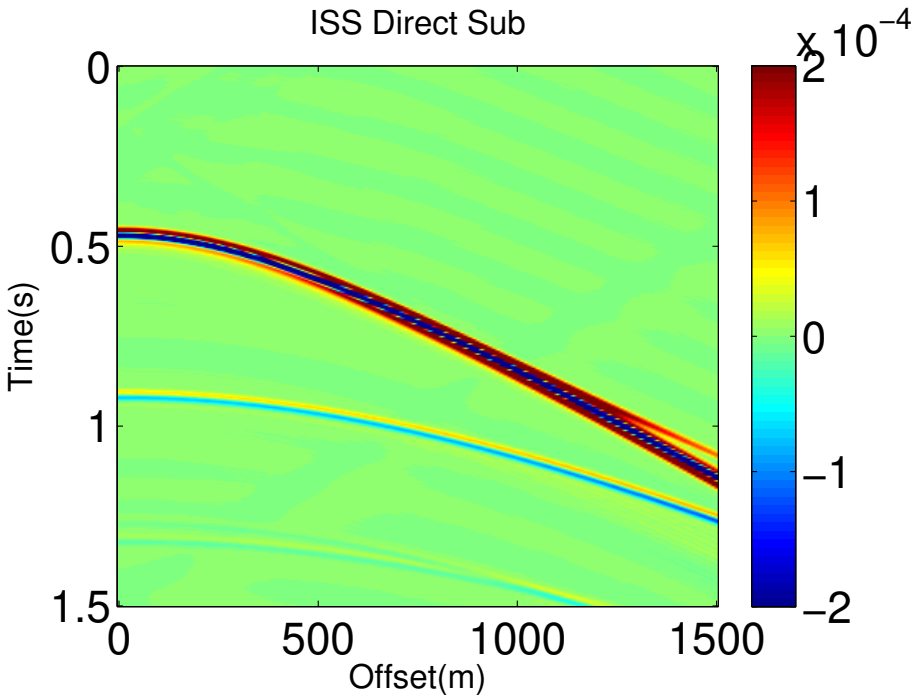

Figure 39: Free-surface multiple removal result after directly subtracting the ISS prediction result (figure 37) from the data (figure 36).

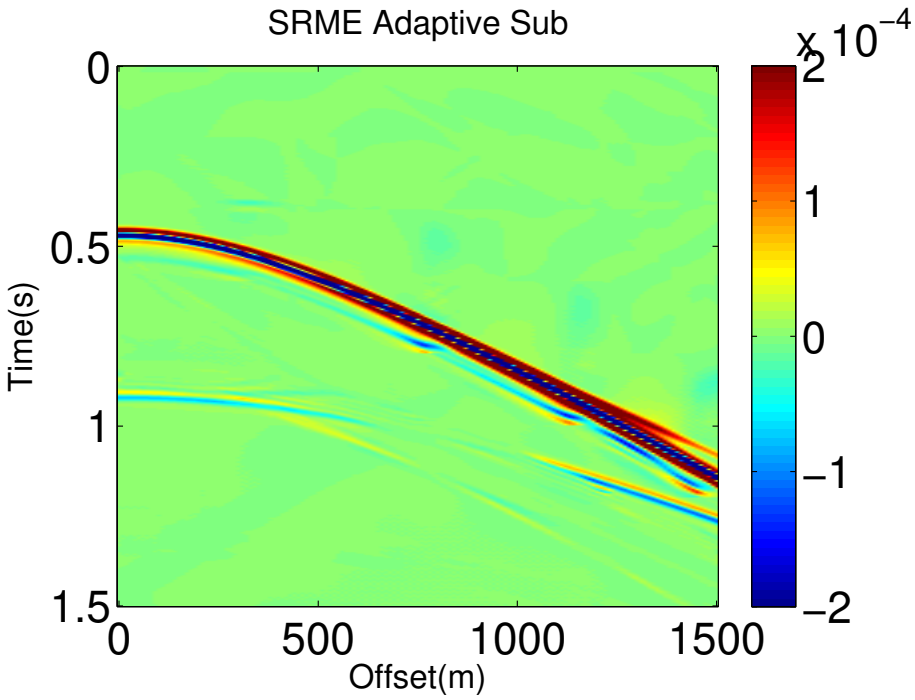

Figure 40: Free-surface multiple removal result by combing the SRME prediction (figure 38) and adaptive subtraction.

Chao Ma, Qiang Fu, and Arthur B. Weglein – GEO-2018-0411

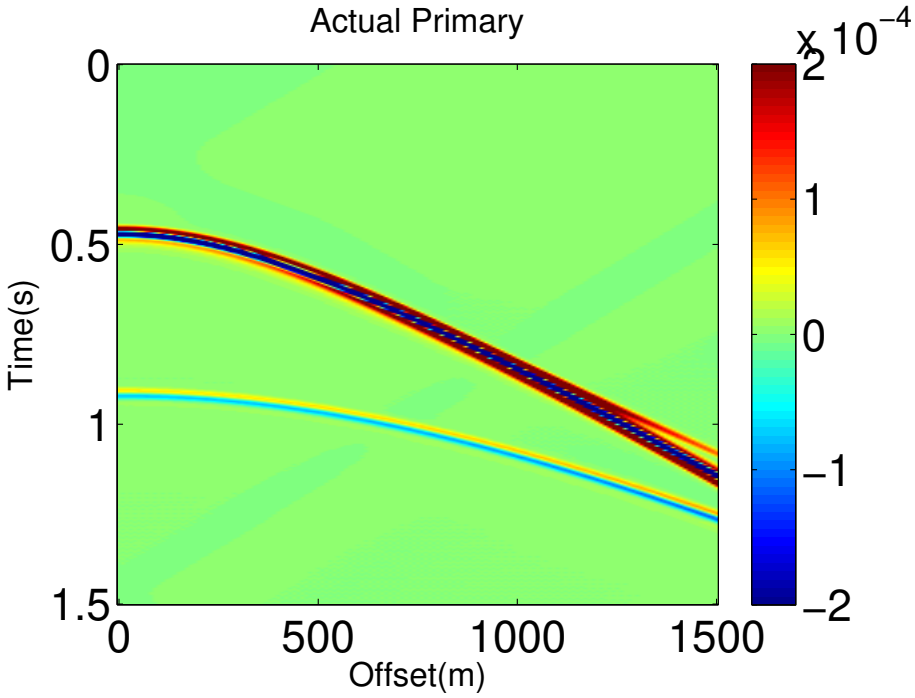

Figure 41: Actual primaries in the input data shown in figure 36.

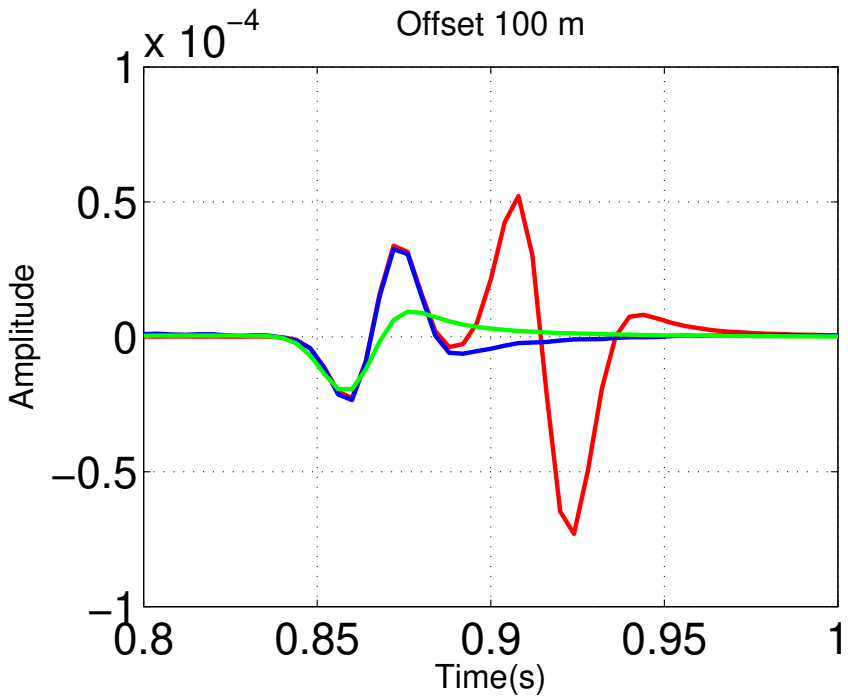

Figure 42: Trace comparison at Offset 100m. Red, blue and green line represent actual data, ISS free-surface multiple prediction and SRME prediction, respectively.

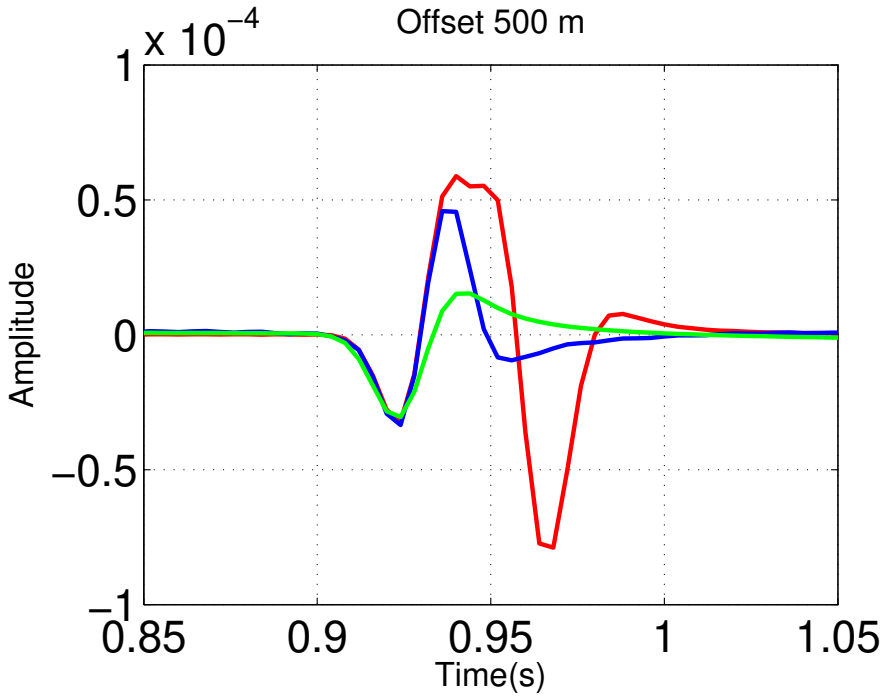

Figure 43: Trace comparison at Offset 500m. Red, blue and green line represent actual data, ISS free-surface multiple prediction and SRME prediction, respectively.

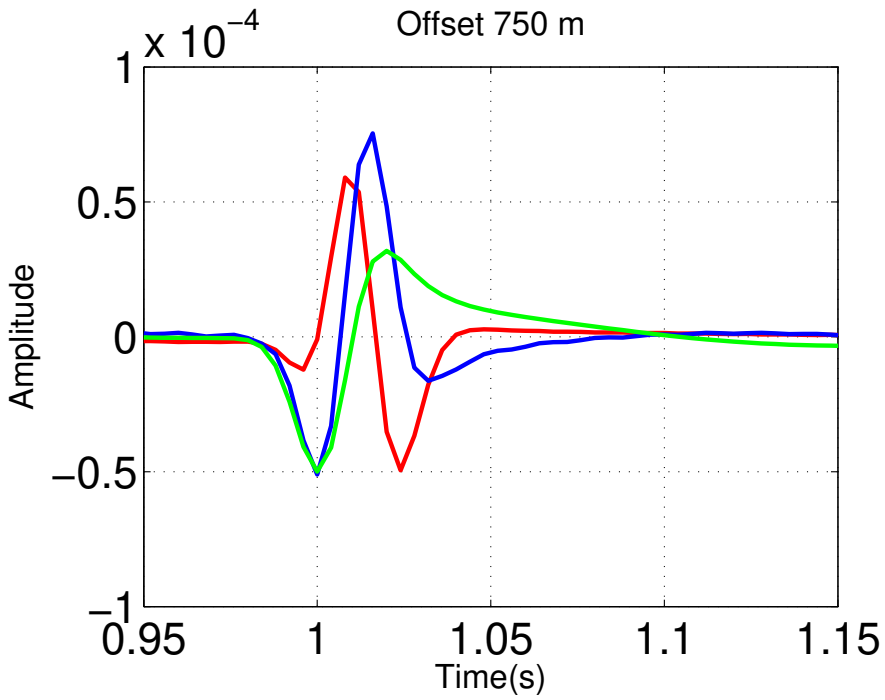

Figure 44: Trace comparison at Offset 750m. Red, blue and green line represent actual data, ISS free-surface multiple prediction and SRME prediction, respectively.

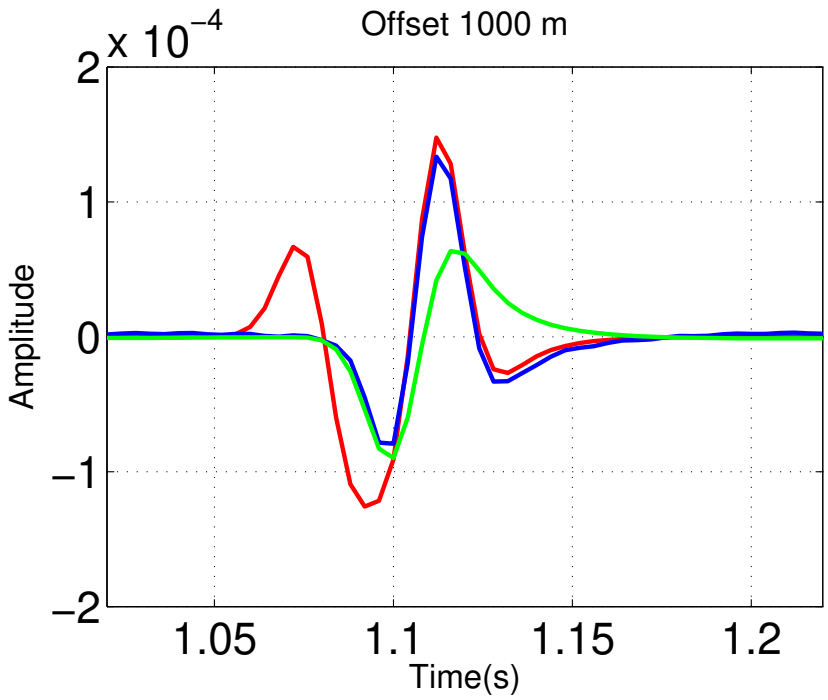

Figure 45: Trace comparison at Offset 1000m. Red, blue and green line represent actual data, ISS free-surface multiple prediction and SRME prediction, respectively.

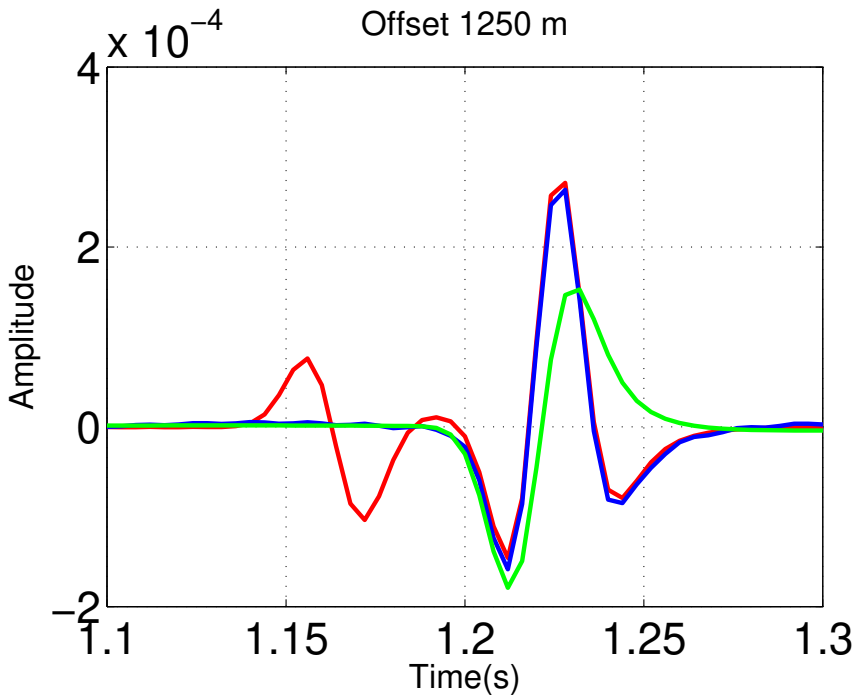

Figure 46: Trace comparison at Offset 1250m. Red, blue and green line represent actual data, ISS free-surface multiple prediction and SRME prediction, respectively.

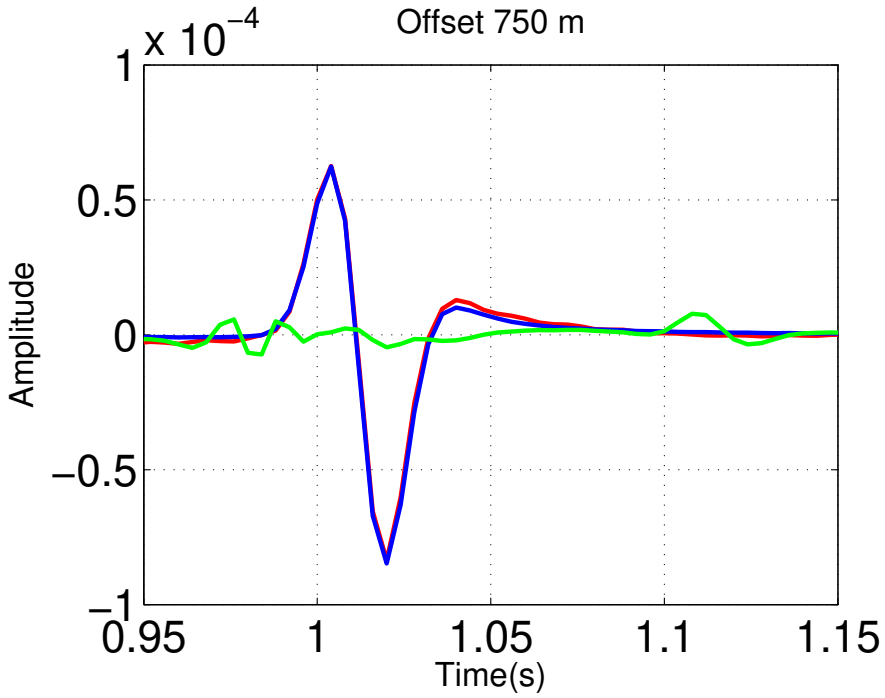

Figure 47: Trace comparison at Offset 750m. Red, blue and green represent the actual primary, result after ISS FSME and result after the SRME + adaptive, respectively.

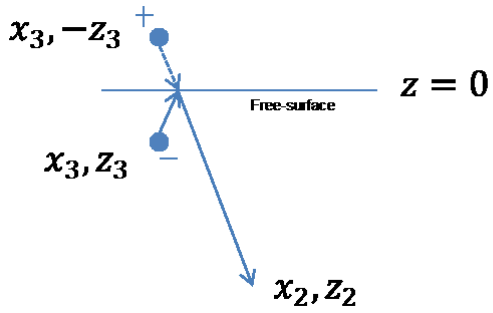

$$G_0^{fs}(x_2, z_2, x_3, z_3, \omega) = \frac{1}{2\pi}\int dk \frac{e^{ik(x_2-x_3)}e^{iq|z_2-(-z_3)|}}{2iq}$$
$$= \frac{1}{2\pi}\int dk \frac{e^{ik(x_2-x_3)}e^{iq(z_2+z_3)}}{2iq}$$

Figure A-1: Green's function G_0^{fs}, travels up from the source to the free-surface and then down to the receiver.

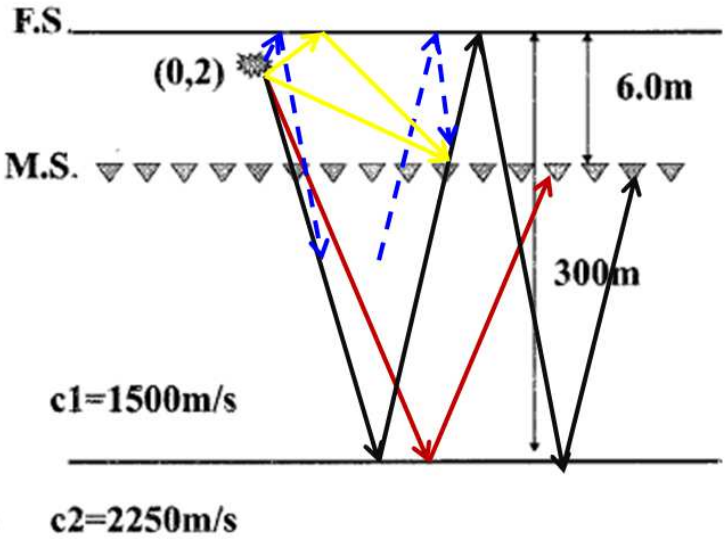

Figure A-2: Model used to generated data in Zhang (2007) to test the ISS FSME.

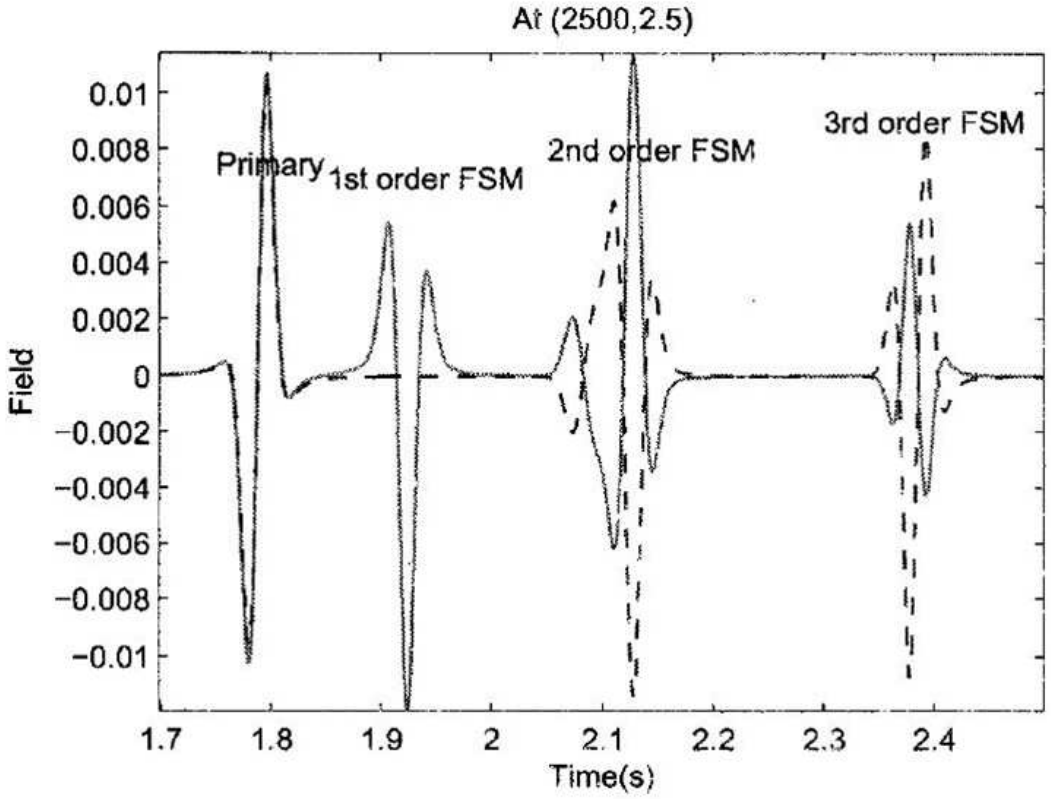

Figure A-3: A trace comparison between the input data D_1' (solid line) to the ISS FSME and output data $D_1' + D_2'$ after the ISS FSME. When D_2' is added to D_1', two things happen, the first-order free-surface multiple is eliminated, all higher-order free-surface multiples are altered, and prepared for their removal by D_3', D_4', etc.

Chao Ma, Qiang Fu, and Arthur B. Weglein – GEO-2018-0411

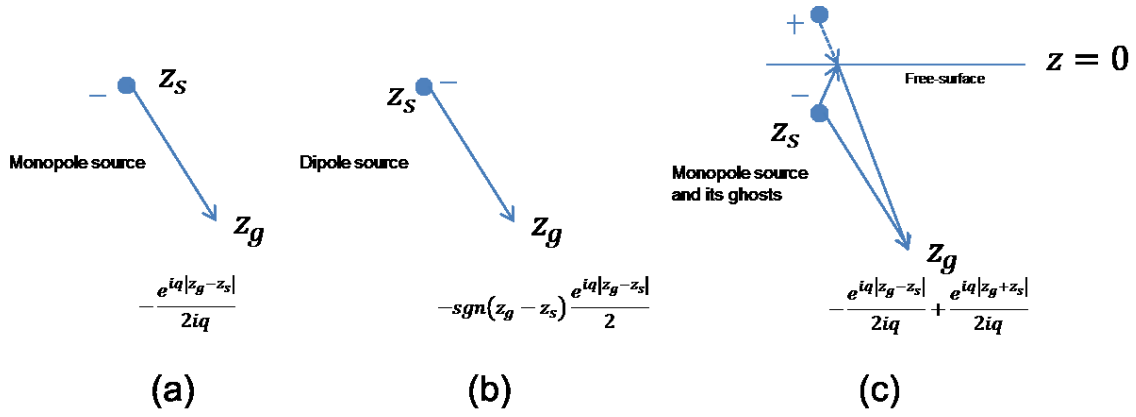

Figure B-1: (a) Monopole source and its 2D Green's function in k_x, ω domain. (b) Dipole source and its 2D Green's function. (c) Monopole source & its source ghosts and their 2D Green's functions. Free-surface is at depth $z = 0$. $q = \sqrt{\frac{\omega^2}{c_0} - k_x^2}$, where ω, k_x and c_0 are the temporal frequency, horizontal wavenumber, and medium velocity.

Chao Ma, Qiang Fu, and Arthur B. Weglein – GEO-2018-0411

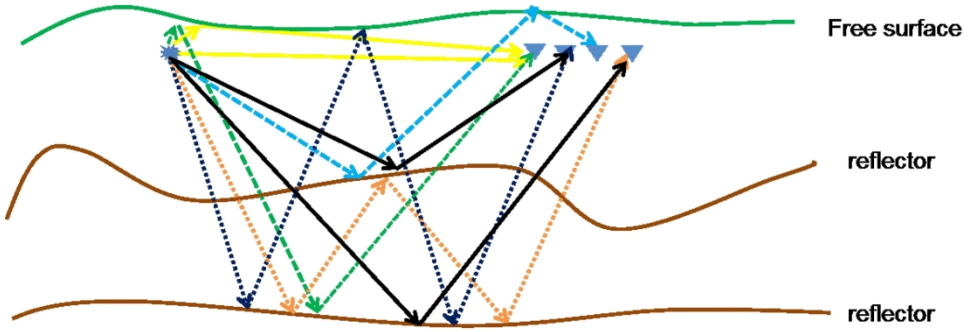

Illustration of different seismic events in marine environment. Yellow solid line: reference waves; Green and light blue dashed: source ghost and receiver ghost, respectively; Dark blue dashed line: free surface multiple; Orange dashed line: internal multiple; solid black line: primary.

206x72mm (300 x 300 DPI)

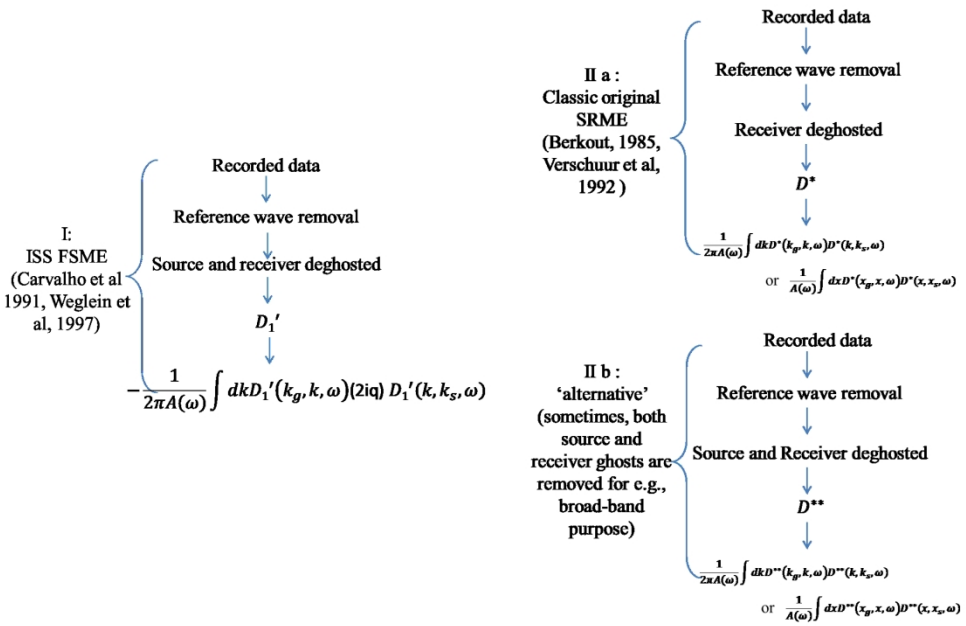

ISS free-surface multiple prediction algorithm and SRME free-surface multiple prediction algorithm

339x240mm (300 x 300 DPI)

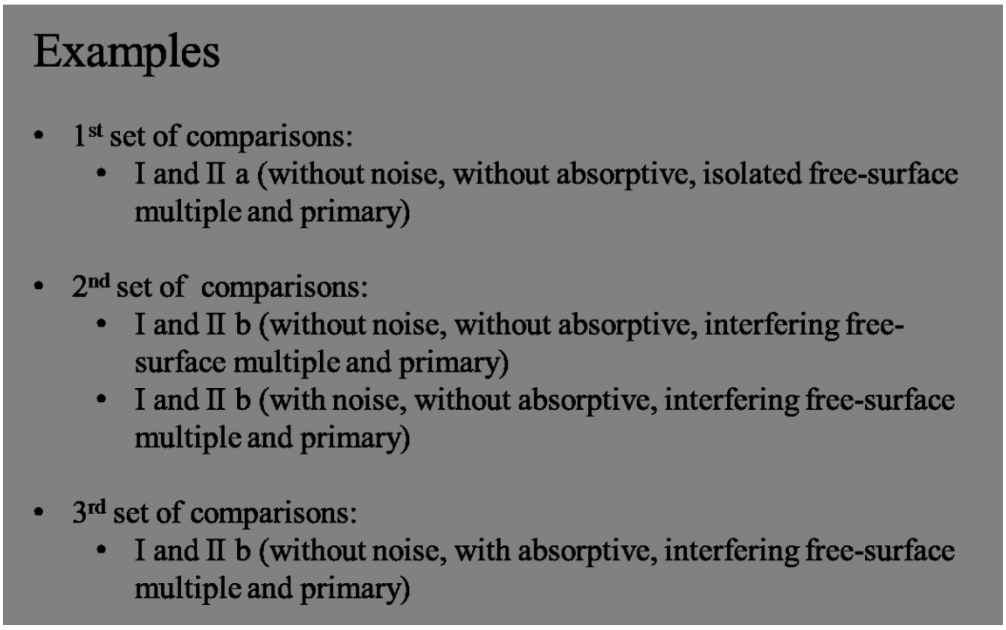

Three sets of comparisons between the ISS free-surface multiple prediction and SRME free-surface multiple prediction

202x125mm (300 x 300 DPI)

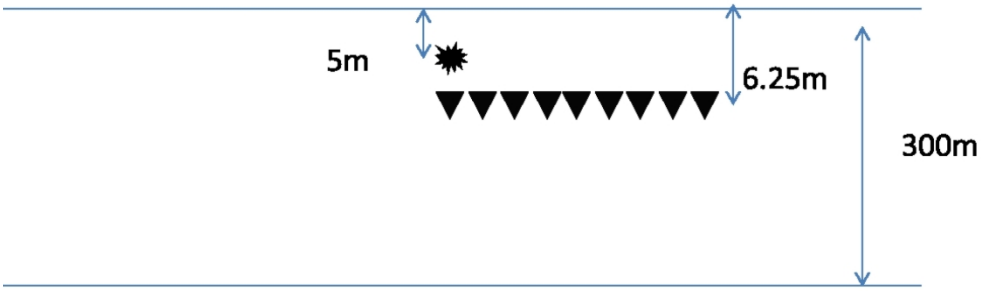

A 1D subsurface model with a horizontal reflector and a free-surface.

191x58mm (300 x 300 DPI)

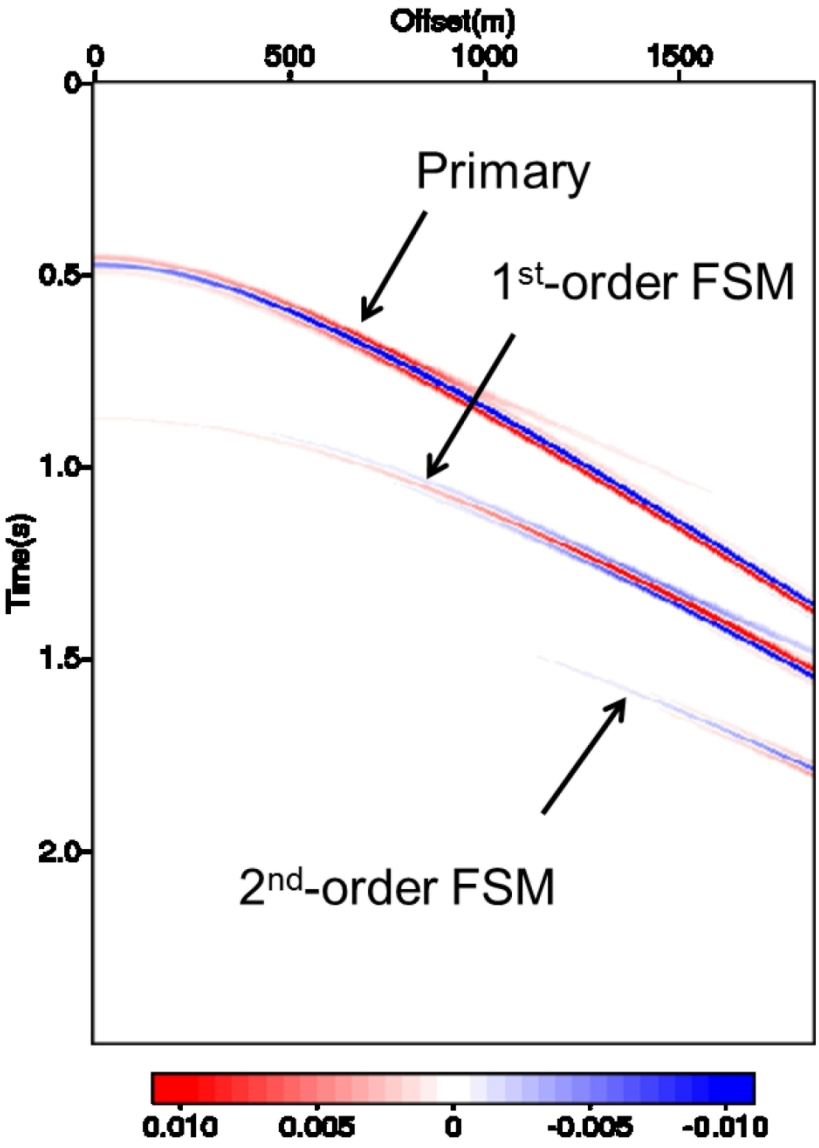

Input data for the ISS free-surface multiple prediction. Notice that, only primaries and free-surface multiples are generated for ISS FSME input.

124x152mm (300 x 300 DPI)

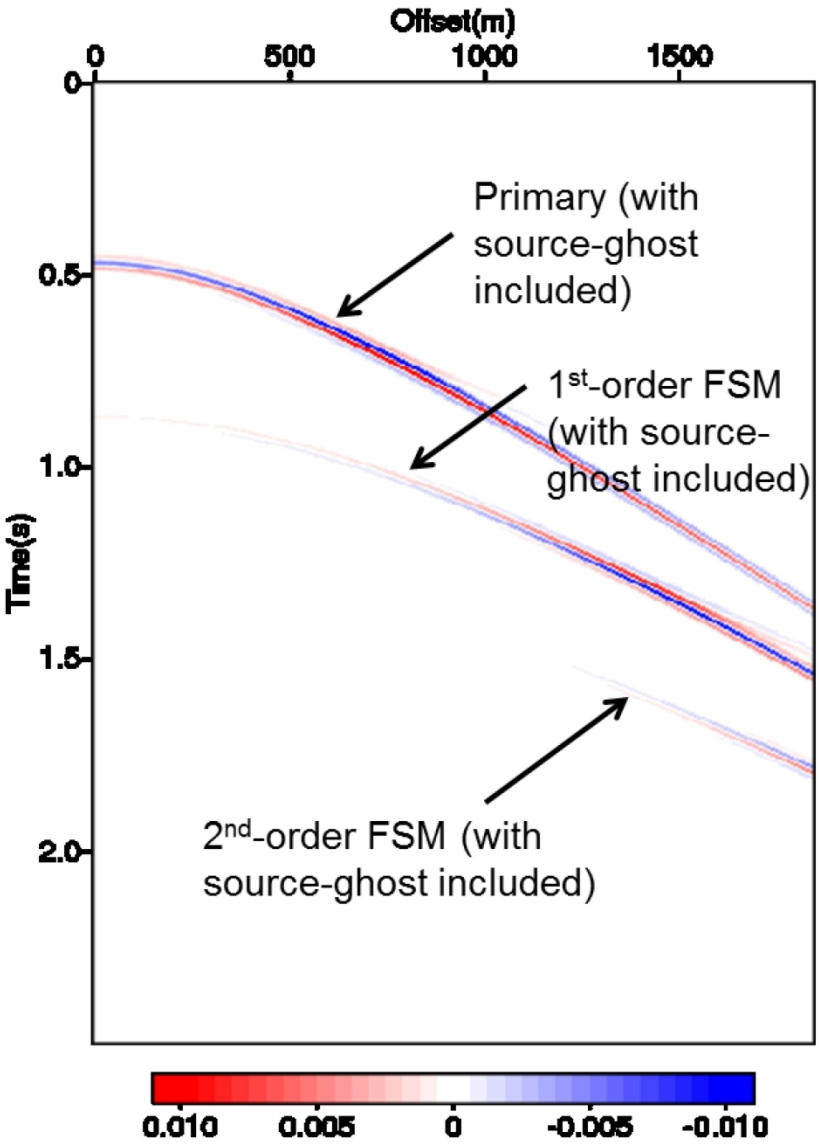

Input data for the SRME free-surface multiple prediction. Notice that, primaries and free-surface multiples and their source ghosts are generated for SRME input.

124x152mm (300 x 300 DPI)

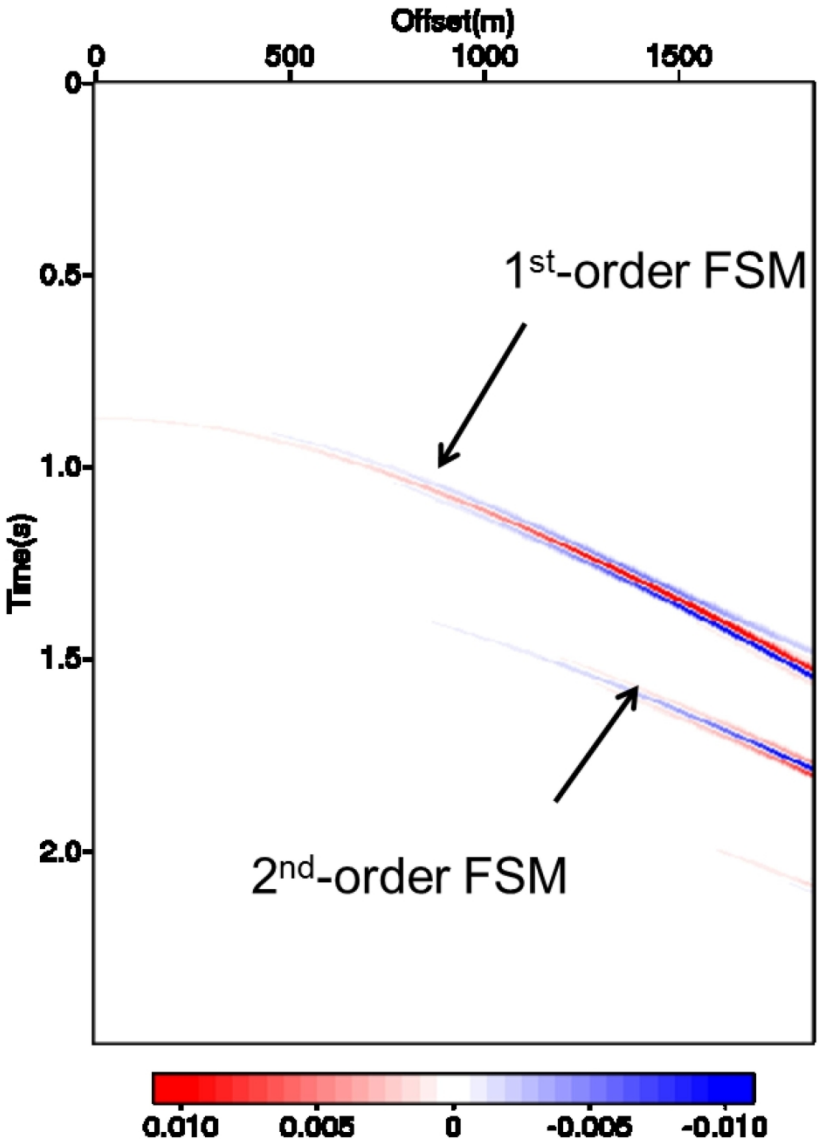

ISS free-surface multiple prediction (D_2' in equation 1) with the input in figure 5}.

124x152mm (300 x 300 DPI)

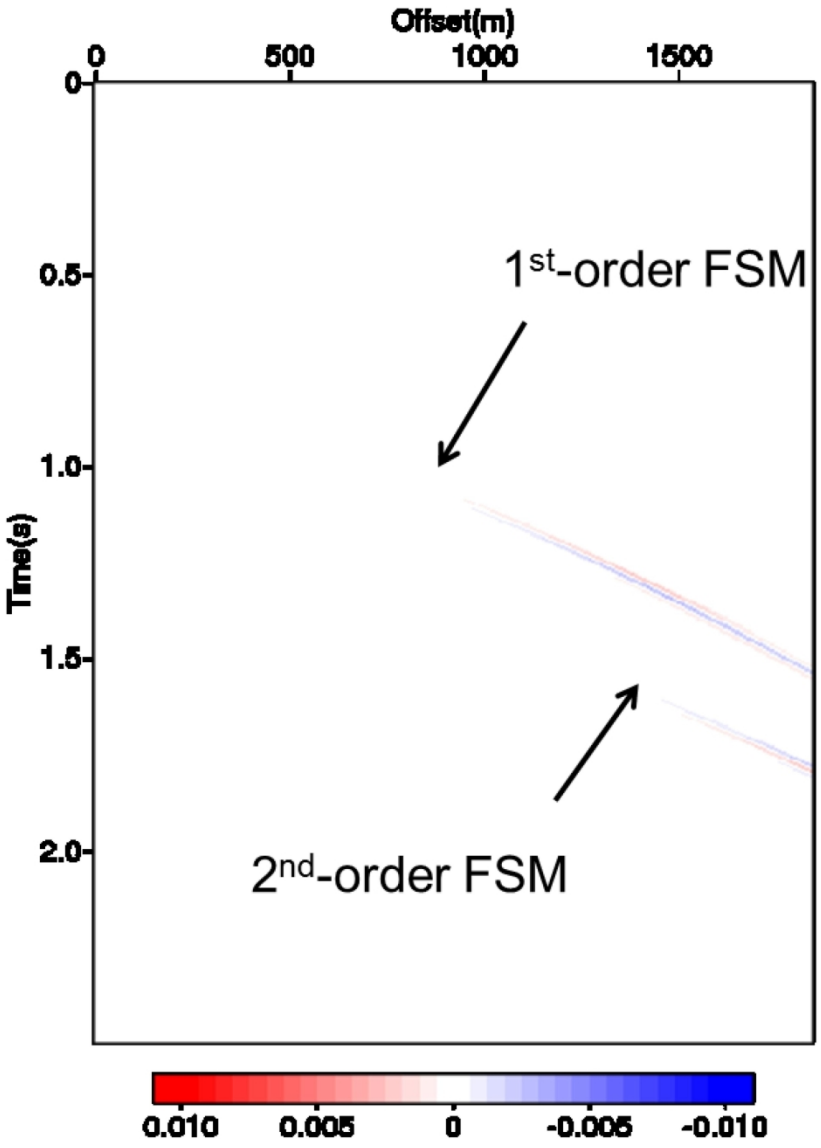

SRME free-surface multiple prediction (equation 3) with the input in figure 6.

124x152mm (300 x 300 DPI)

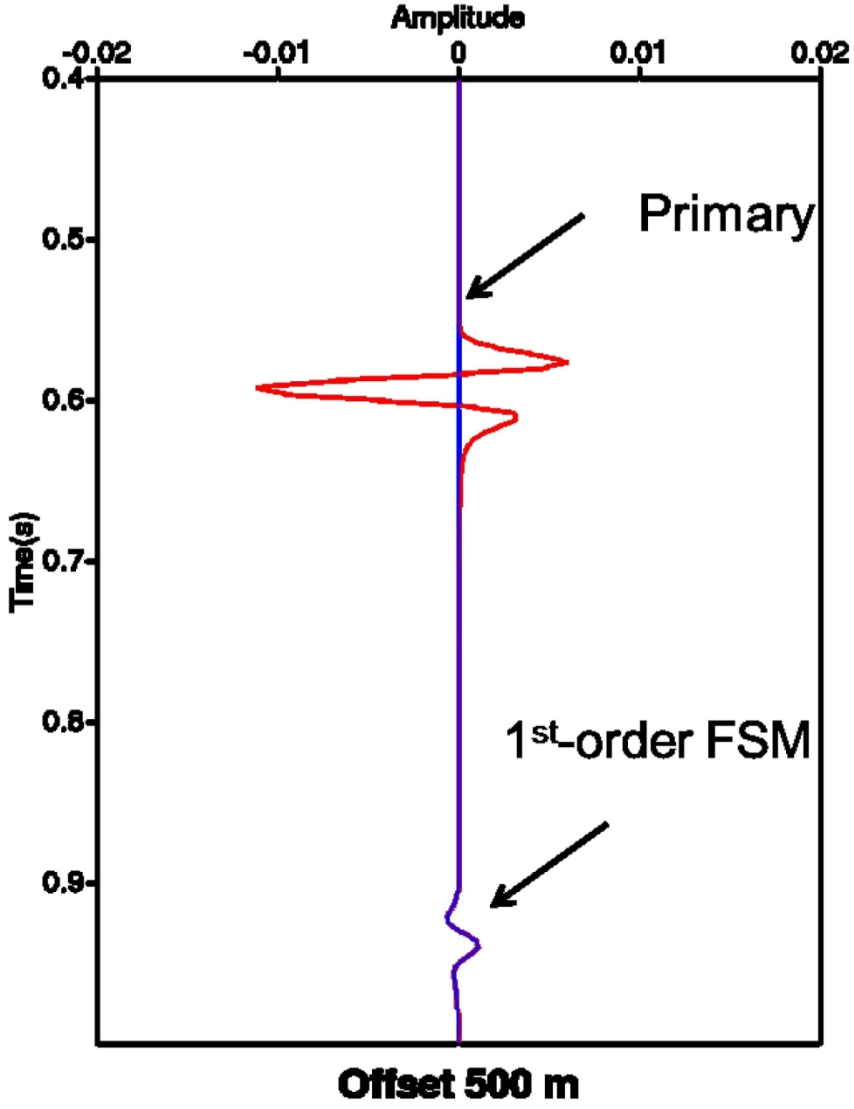

A trace comparison at 500m offset between the input of the ISS FSME and its prediction. The red and blue line represent input data to the ISS FSME and its prediction, respectively. We can see the ISS free-surface multiple prediction agrees with the actual free-surface multiple very well. Notice that, the predicted free-surface multiple has opposite sign compared with the actual free-surface multiple, we reverse the polarity of the prediction, then compare it with the actual data for easy comparison.

124x151mm (300 x 300 DPI)

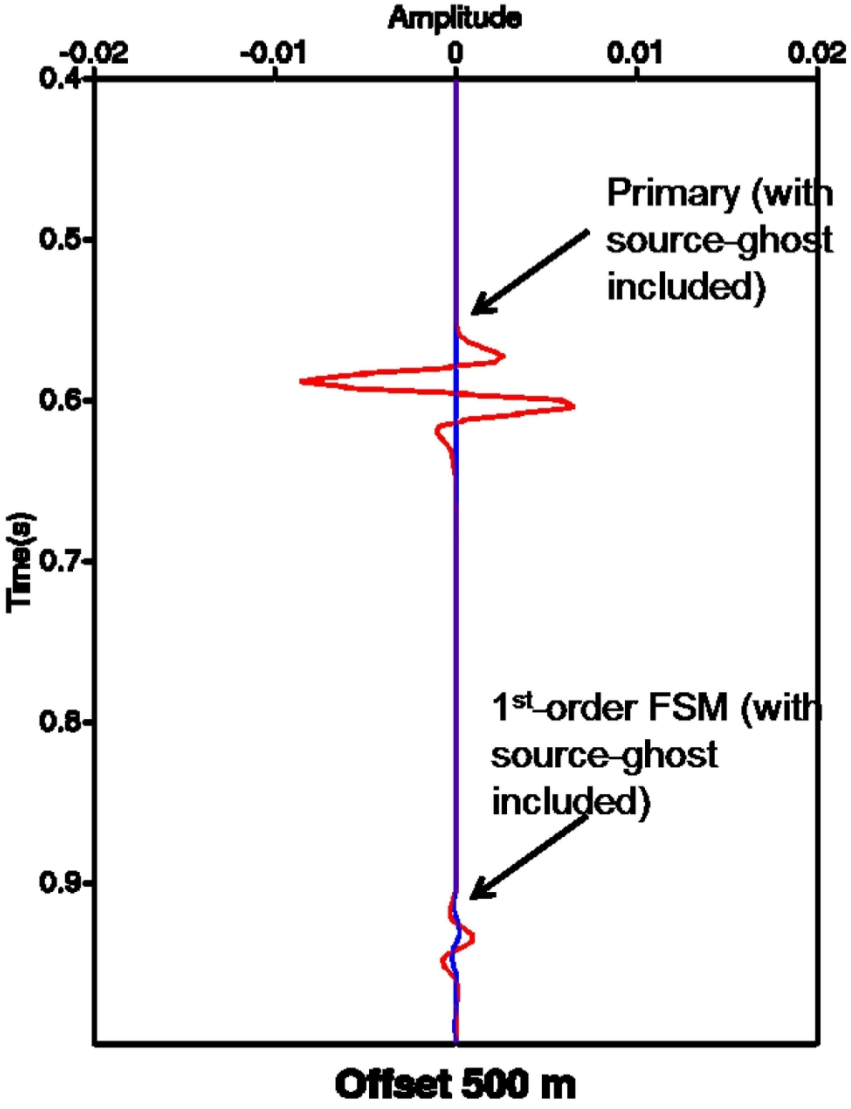

A trace comparison at 500m offset between the input of the SRME and its prediction. The red and blue represent the input data to the SRME and its prediction for free-surface multiples, respectively. We can see from this trace comparison, the SRME provides an approximate free-surface multiple prediction.

124x151mm (300 x 300 DPI)

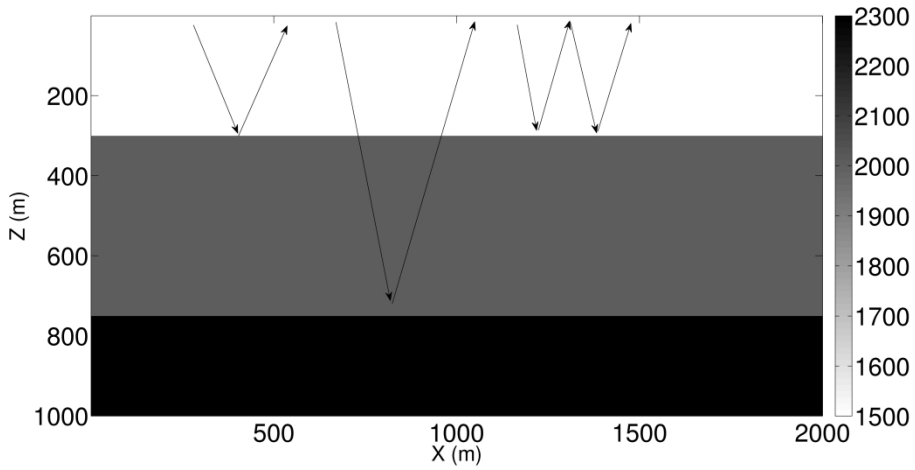

A 1D subsurface model with two primary events and one free-surface multiple event.

422x207mm (300 x 300 DPI)

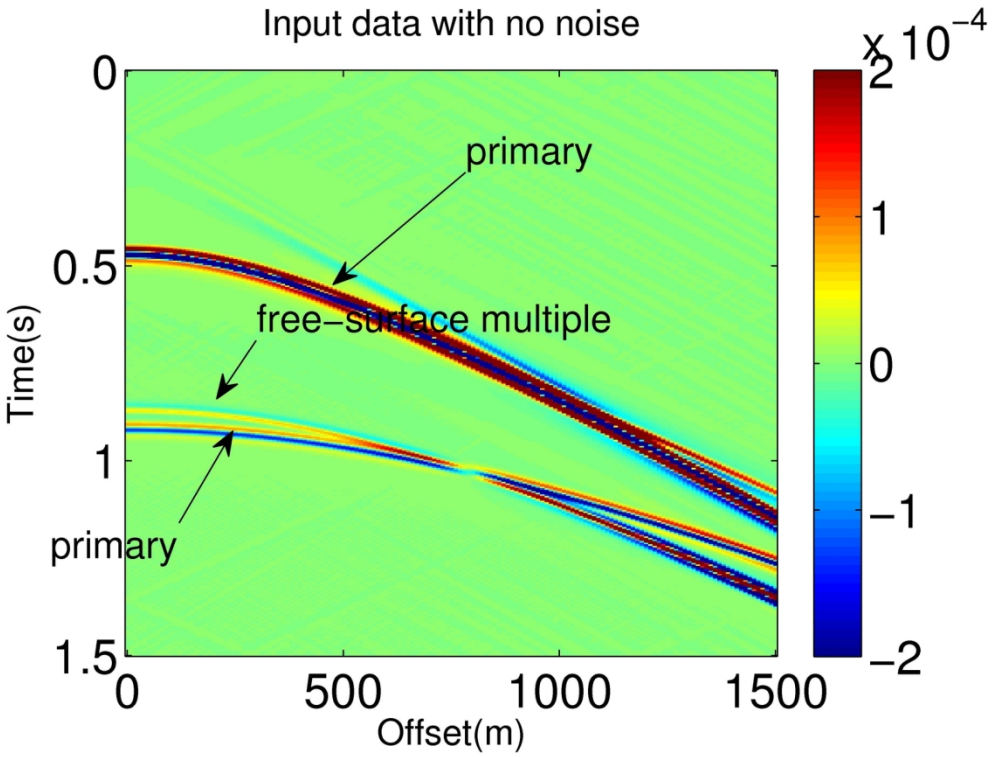

Input data generated based on the model shown in figure 11.

147x111mm (300 x 300 DPI)

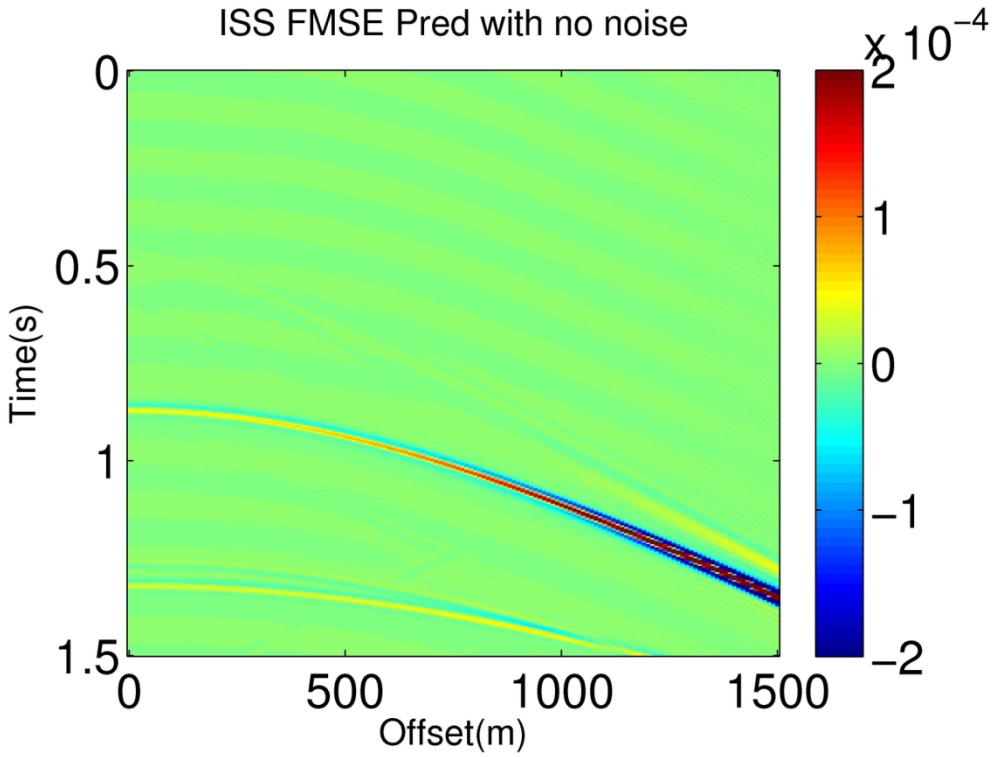

{Prediction of free-surface multiple by the ISS FSME (D_2' in equation 1) using the input data shown in figure 12.

148x111mm (300 x 300 DPI)

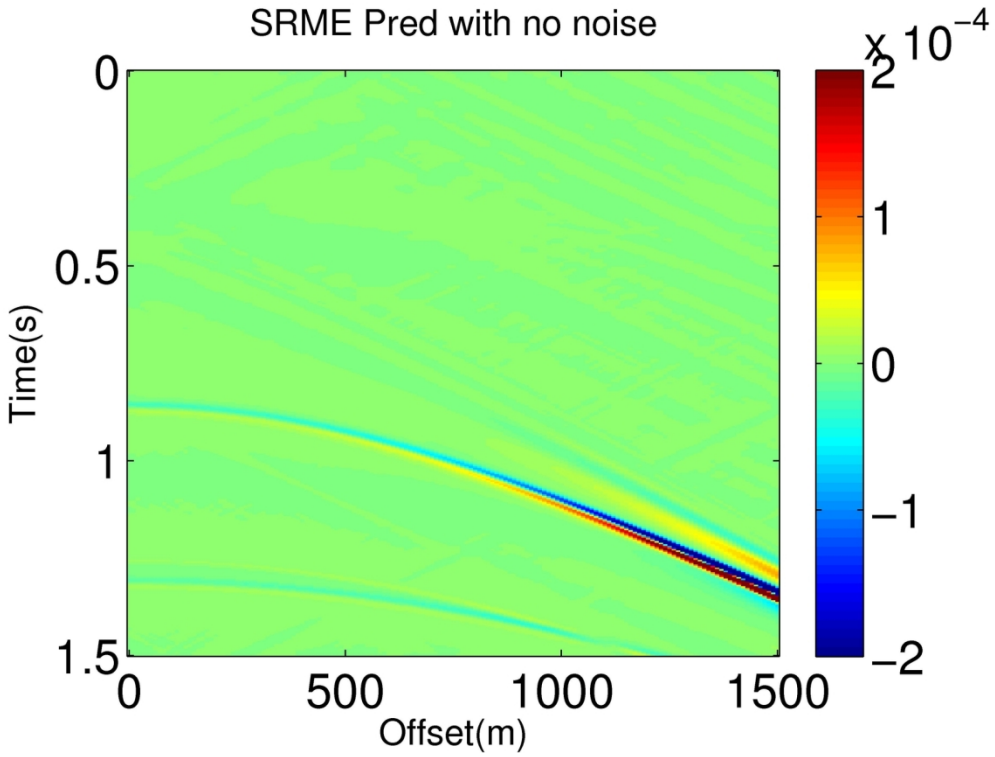

Prediction of free-surface multiple by the SRME using the input data shown in figure 12.

147x111mm (300 x 300 DPI)

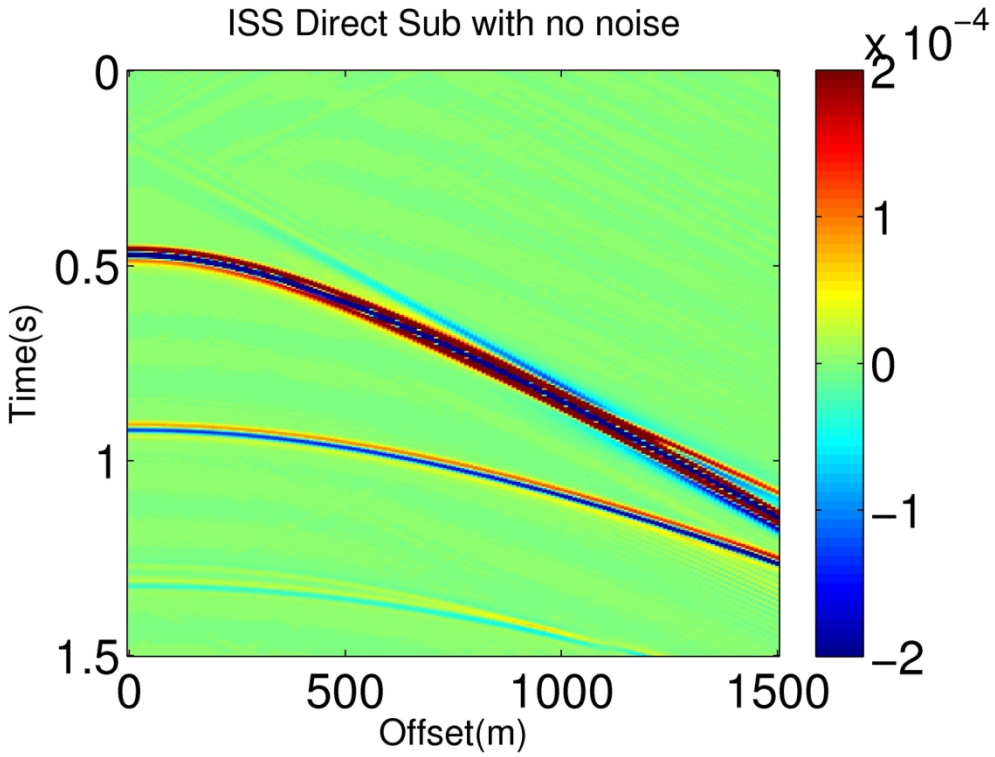

Free-surface multiple removal result after directly subtracting the ISS prediction result (figure 13) from the data (figure 12).

147x111mm (300 x 300 DPI)

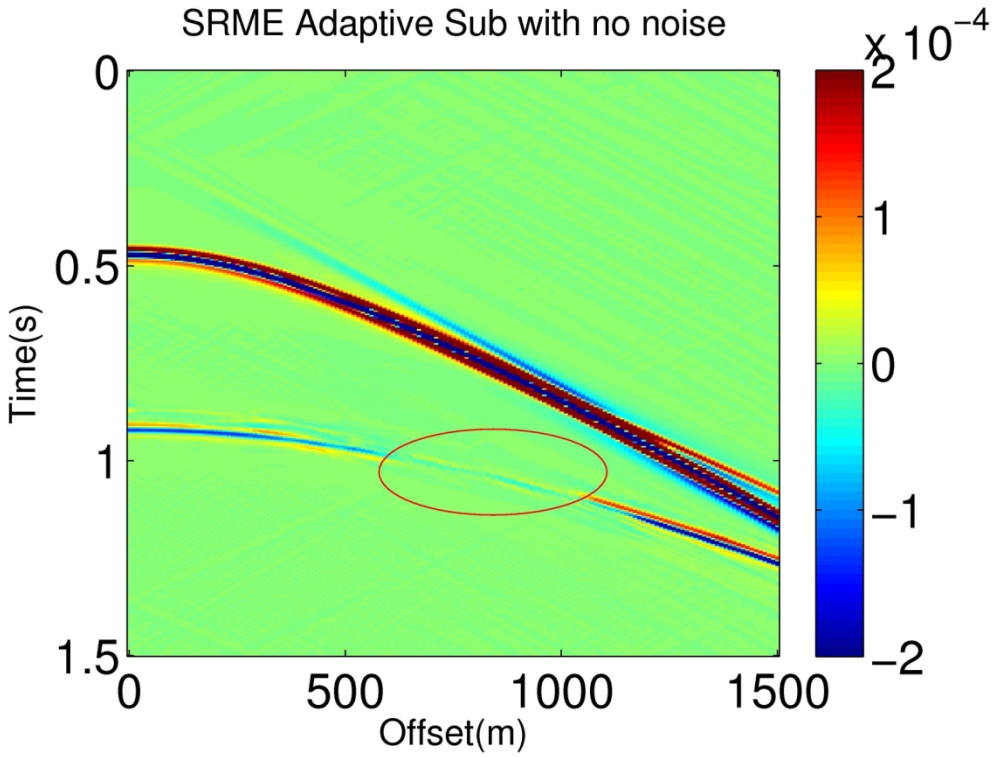

Free-surface multiple removal result by combing the SRME prediction (figure 14) and adaptive subtraction.

147x111mm (300 x 300 DPI)

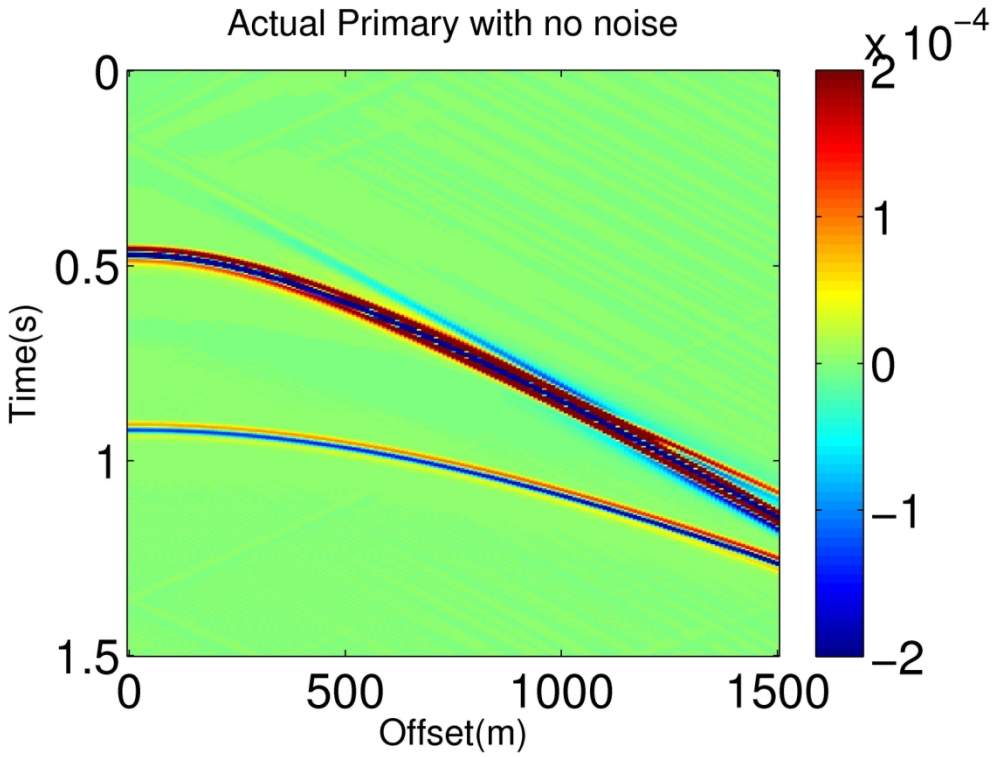

Actual primaries in the data shown in figure 12.

147x111mm (300 x 300 DPI)

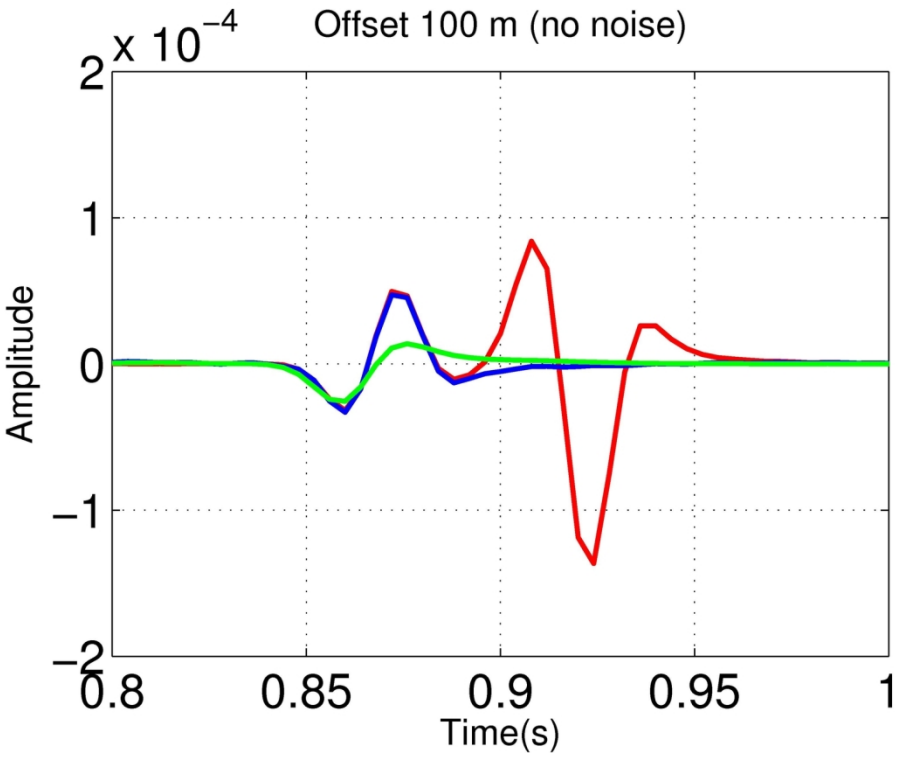

Trace comparison at Offset 100m. Red, blue and green line represent actual data, ISS free-surface multiple prediction and SRME prediction, respectively.

147x111mm (300 x 300 DPI)

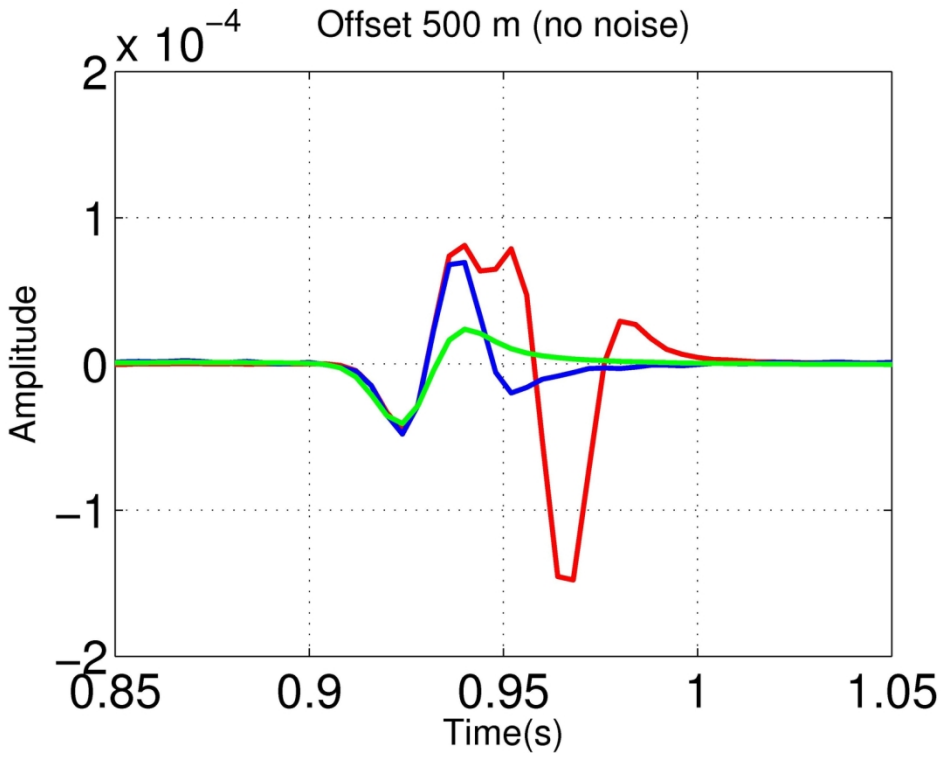

Trace comparison at Offset 500m. Red, blue and green line represent actual data, ISS free-surface multiple prediction and SRME prediction, respectively.

147x111mm (300 x 300 DPI)

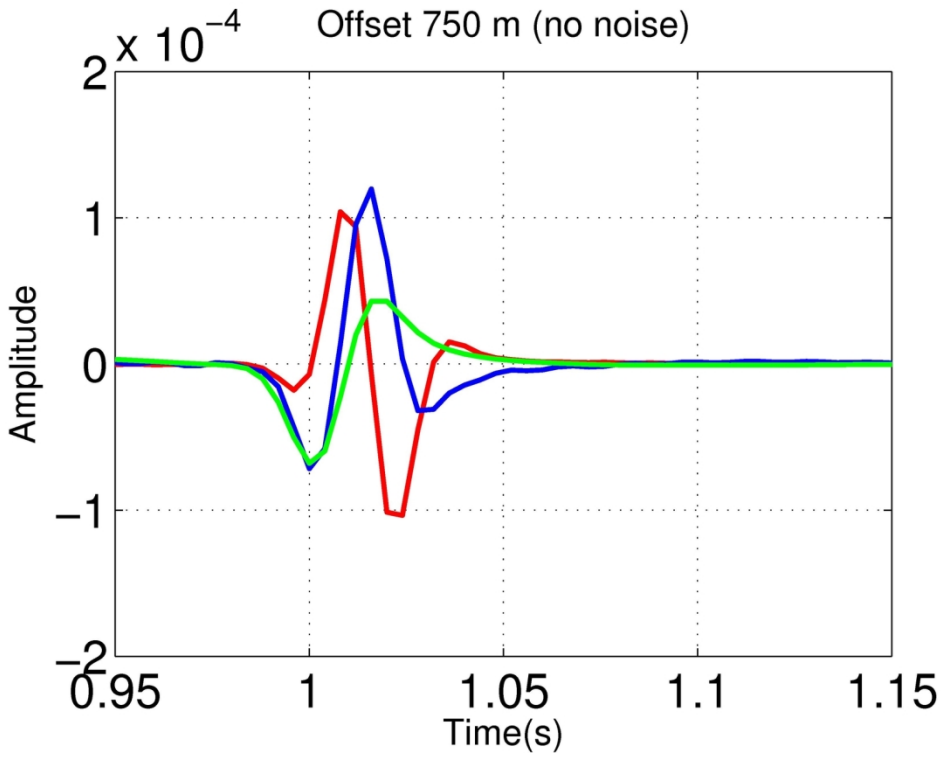

Trace comparison at Offset 750m. Red, blue and green line represent actual data, ISS free-surface multiple prediction and SRME prediction, respectively.

147x111mm (300 x 300 DPI)

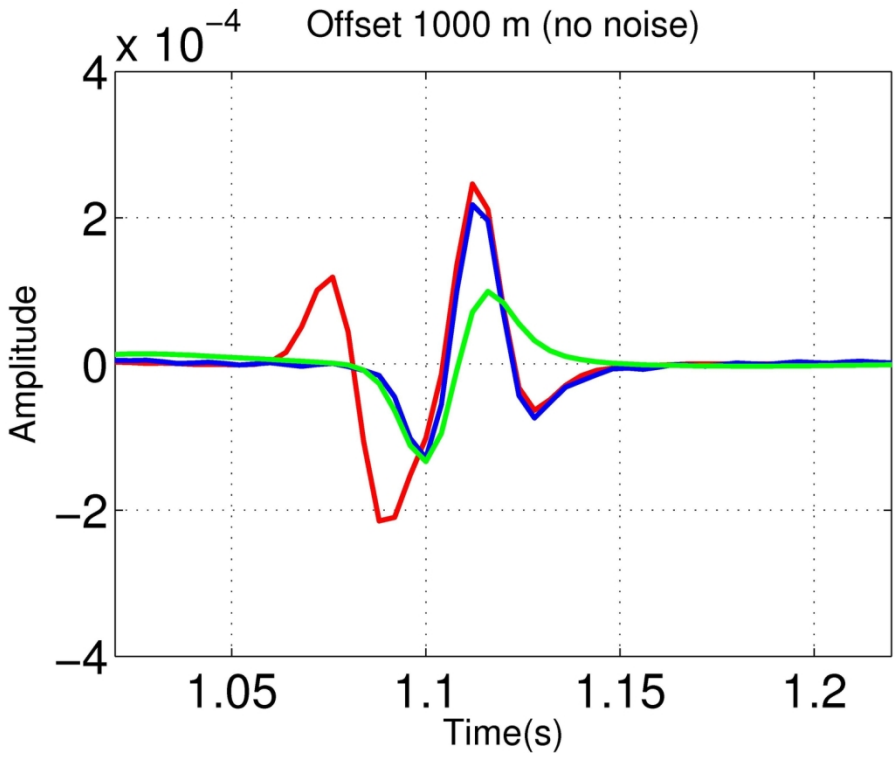

Trace comparison at Offset 1000m. Red, blue and green line represent actual data, ISS free-surface multiple prediction and SRME prediction, respectively.

147x111mm (300 x 300 DPI)

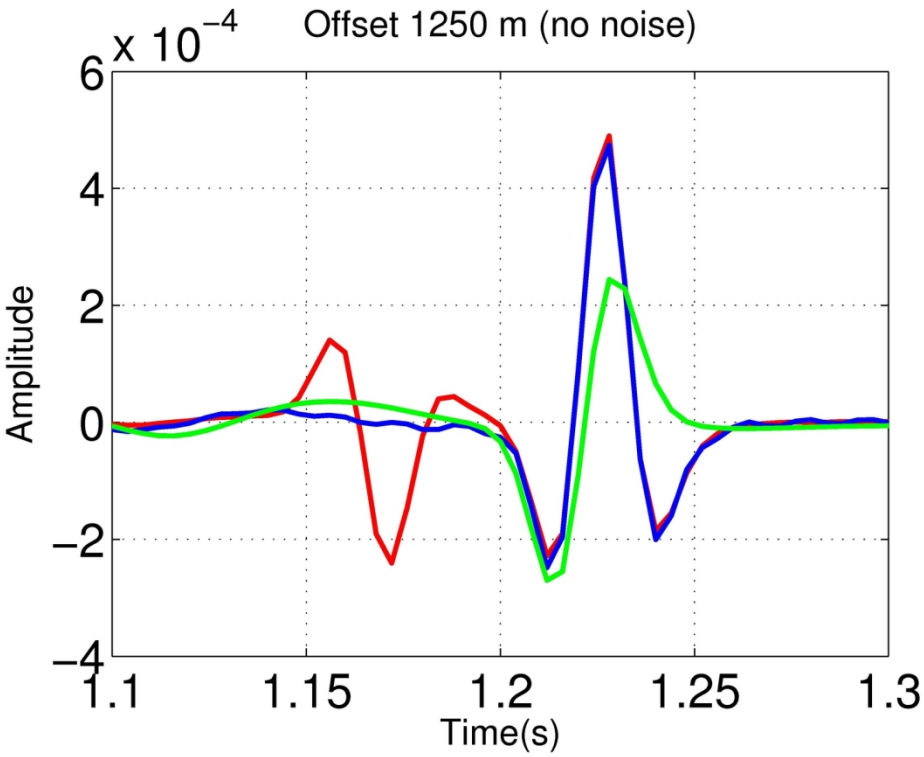

Trace comparison at Offset 1250m. Red, blue and green line represent actual data, ISS free-surface multiple prediction and SRME prediction, respectively.

147x111mm (300 x 300 DPI)

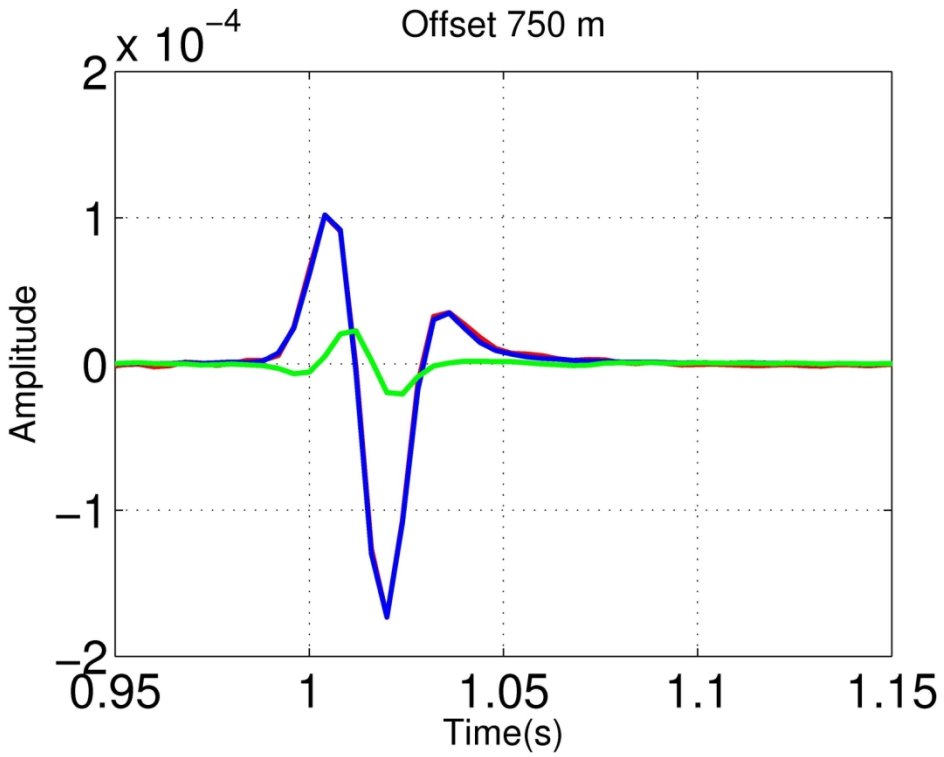

Trace comparison at Offset 750m. Red, blue and green represent the actual primary, result after ISS FSME and result after the SRME + adaptive, respectively.

147x111mm (300 x 300 DPI)

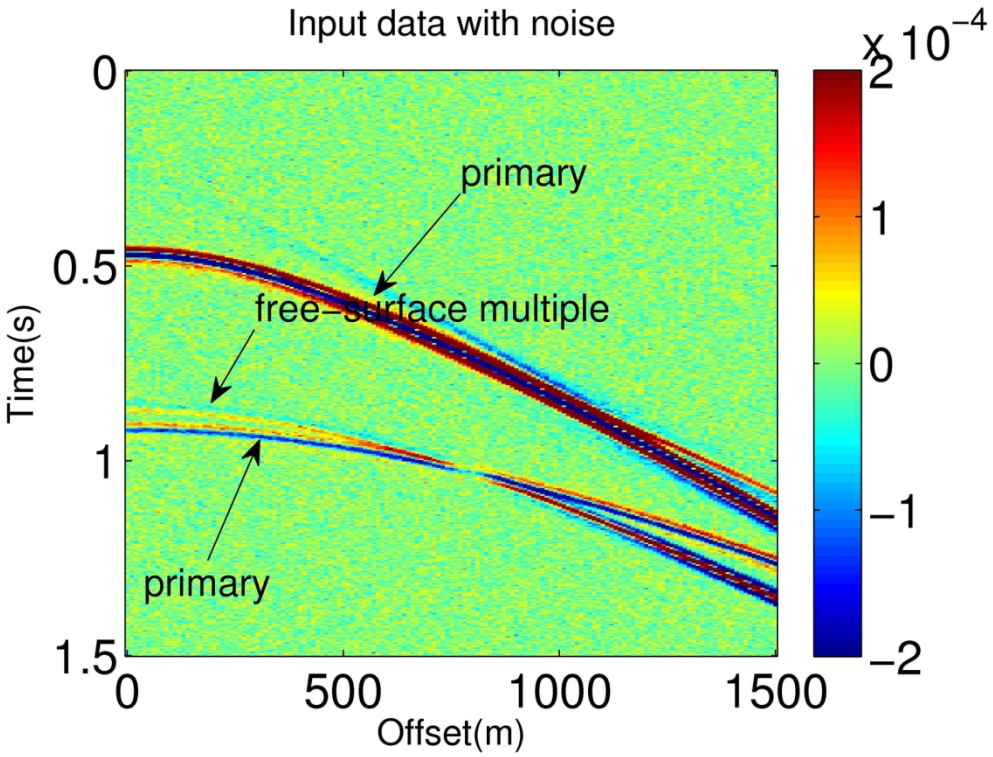

Input data with random noise added on the analytic data.

147x111mm (300 x 300 DPI)

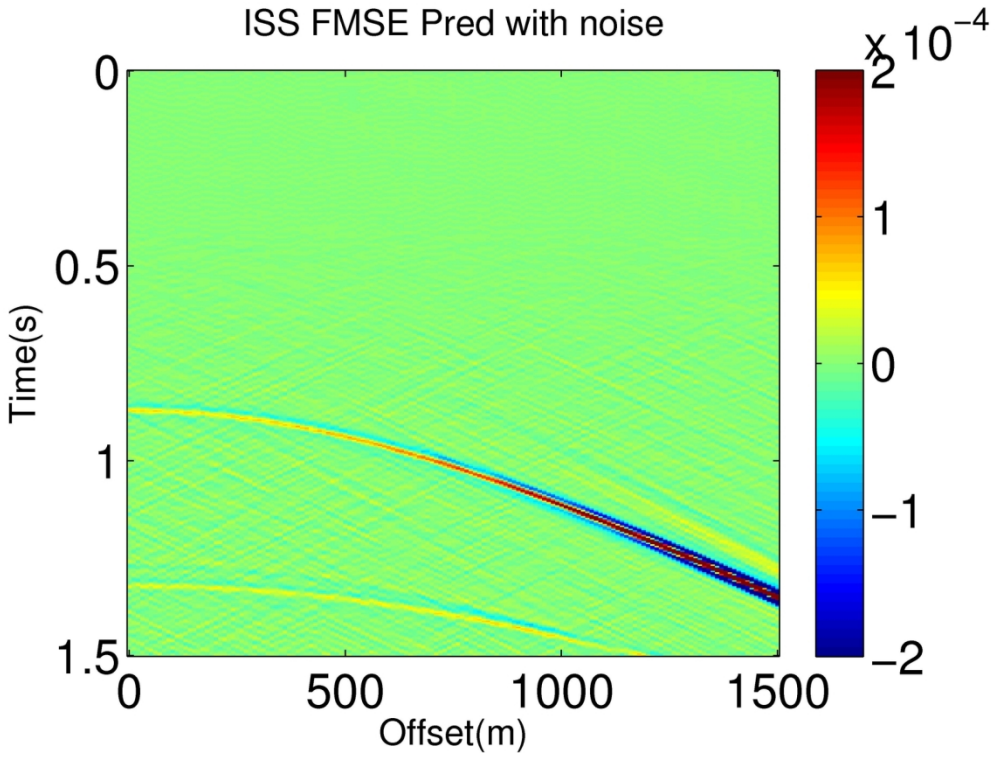

Prediction of free-surface multiple by the ISS FSME (D_2' in equation 1) using the input data shown in figure 24.

147x111mm (300 x 300 DPI)

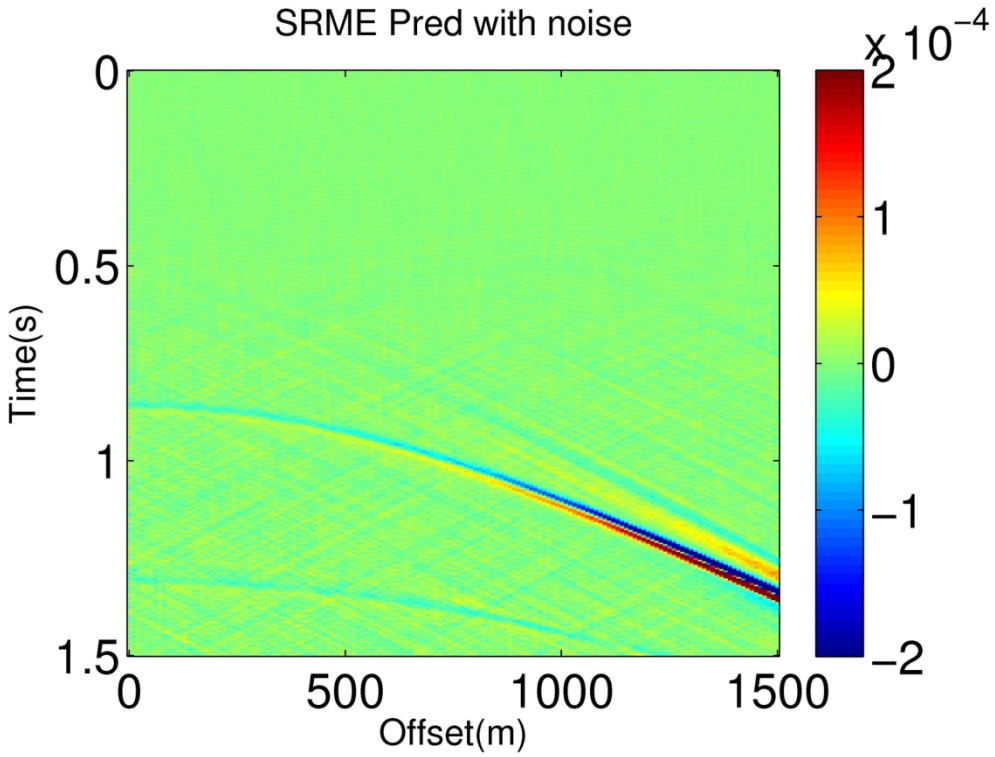

Prediction of free-surface multiple by the SRME using the input data shown in figure 24.

147x111mm (300 x 300 DPI)

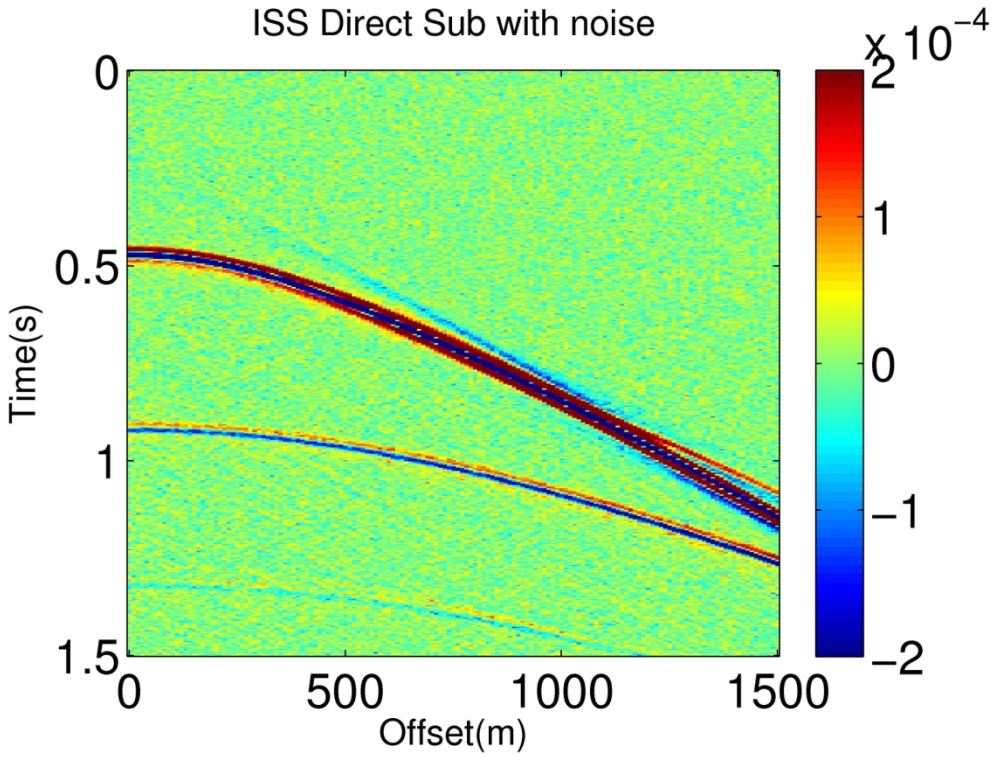

Free-surface multiple removal result after directly subtracting the ISS prediction result (figure 25) from the data (figure 24).

147x111mm (300 x 300 DPI)

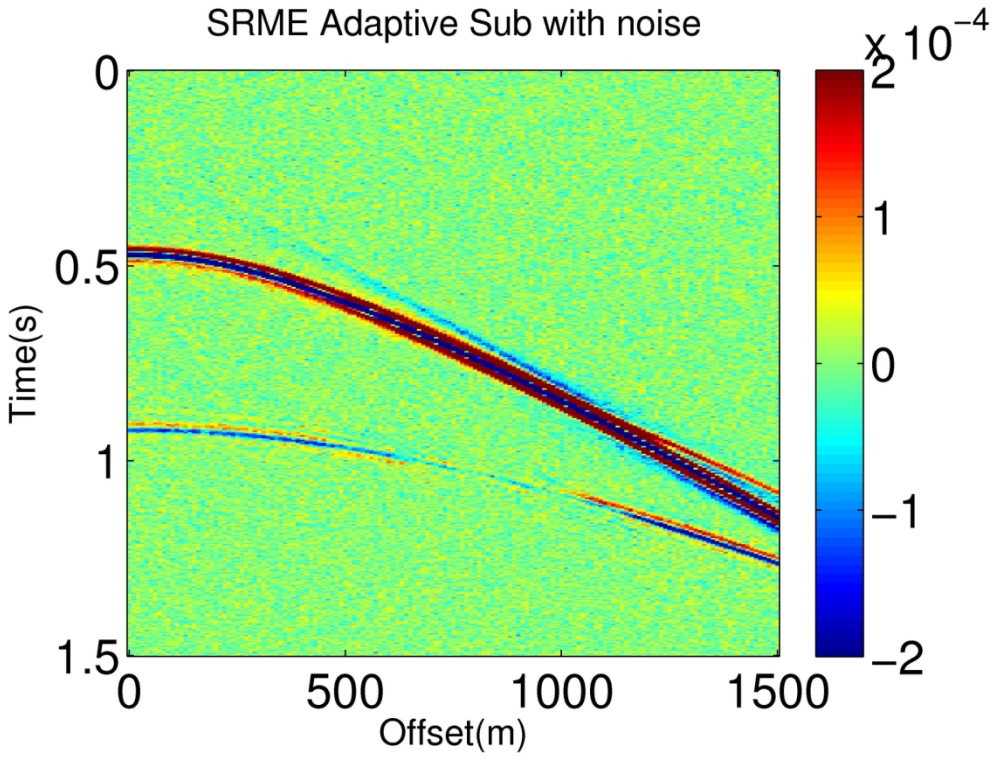

Free-surface multiple removal result by combing the SRME prediction (figure 26) and adaptive subtraction.

147x111mm (300 x 300 DPI)

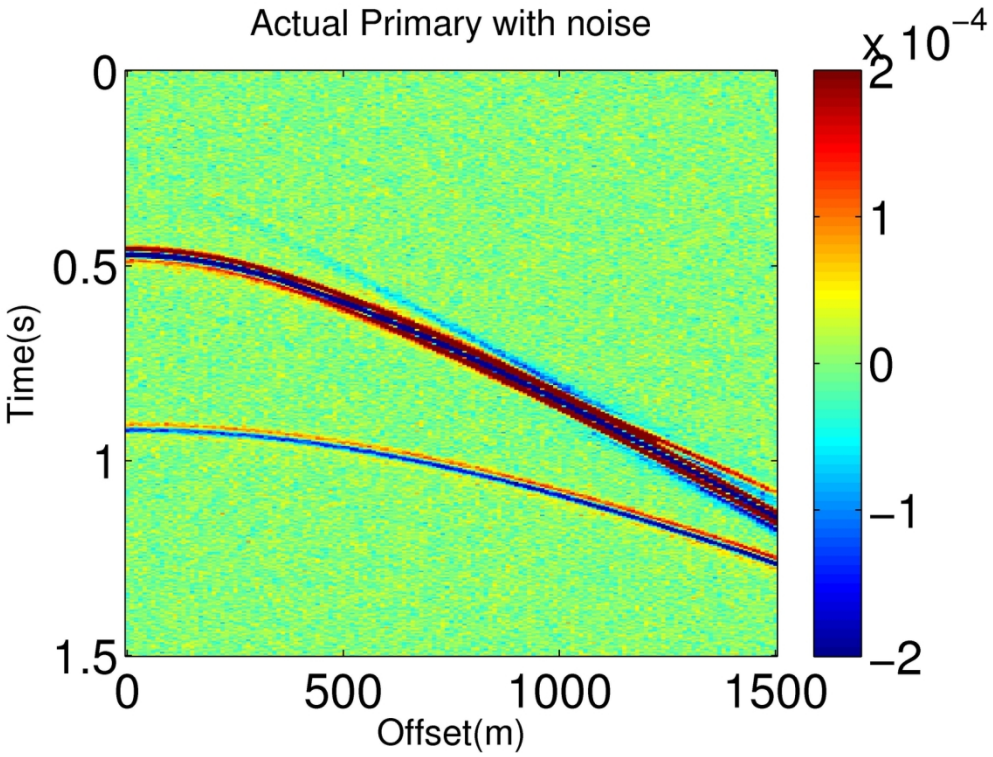

Actual primaries in the data shown in figure 24.

147x111mm (300 x 300 DPI)

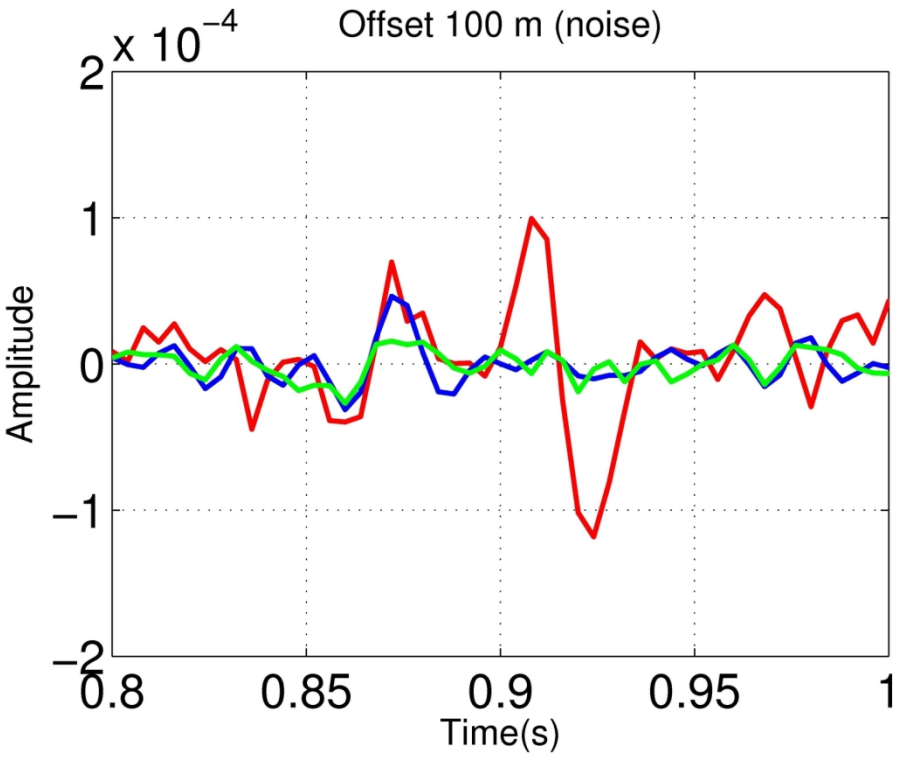

Trace comparison at Offset 100m. Red, blue and green line represent actual data, ISS free-surface multiple prediction and SRME prediction, respectively.

147x111mm (300 x 300 DPI)

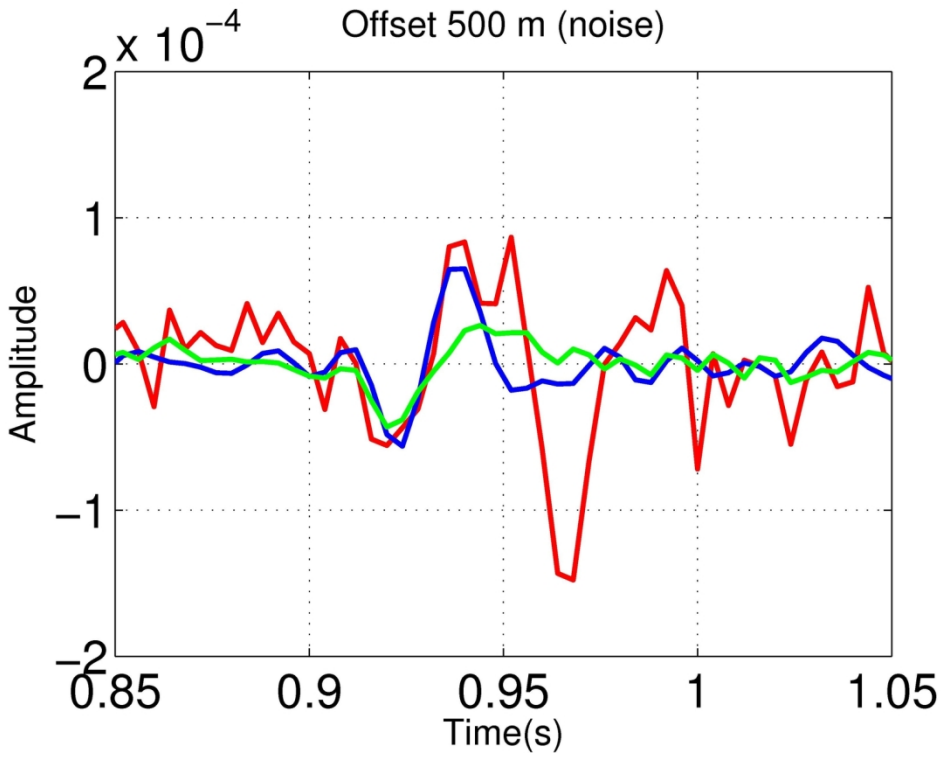

Trace comparison at Offset 500m. Red, blue and green line represent actual data, ISS free-surface multiple prediction and SRME prediction, respectively.

147x111mm (300 x 300 DPI)

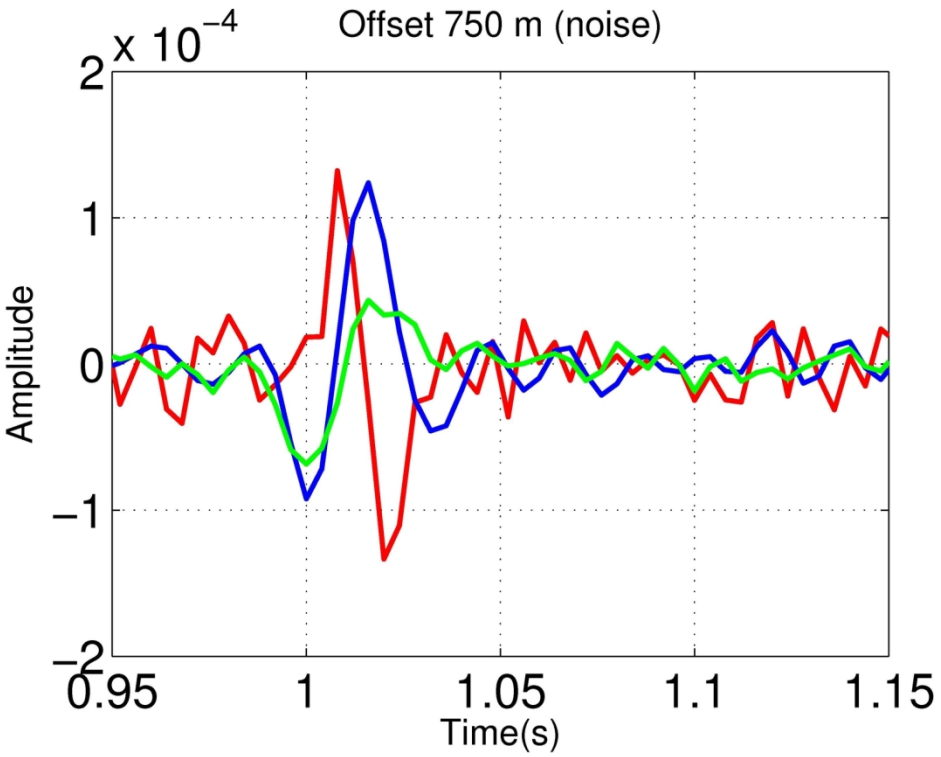

Trace comparison at Offset 750m. Red, blue and green line represent actual data, ISS free-surface multiple prediction and SRME prediction, respectively.

147x111mm (300 x 300 DPI)

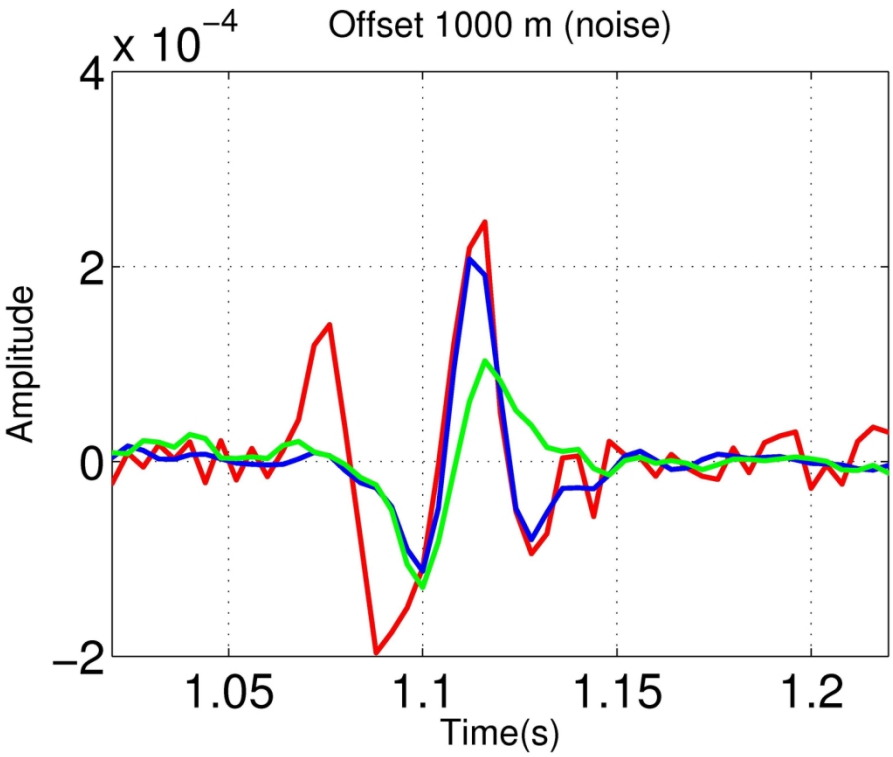

Trace comparison at Offset 1000m. Red, blue and green line represent actual data, ISS free-surface multiple prediction and SRME prediction, respectively.

147x111mm (300 x 300 DPI)

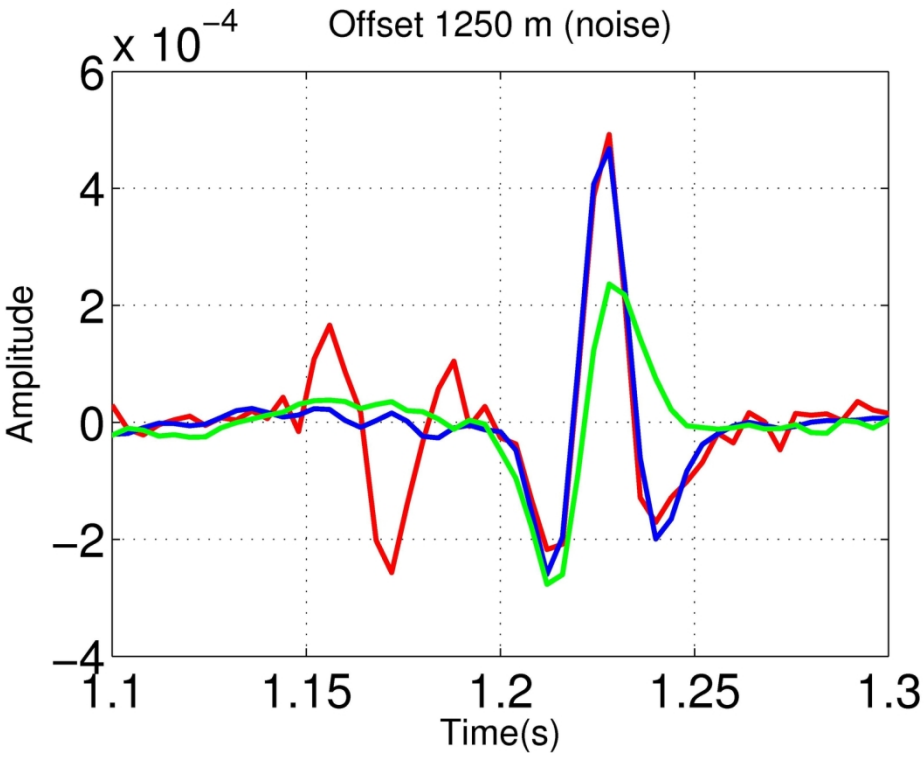

Trace comparison at Offset 1250m. Red, blue and green line represent actual data, ISS free-surface multiple prediction and SRME prediction, respectively.

147x111mm (300 x 300 DPI)

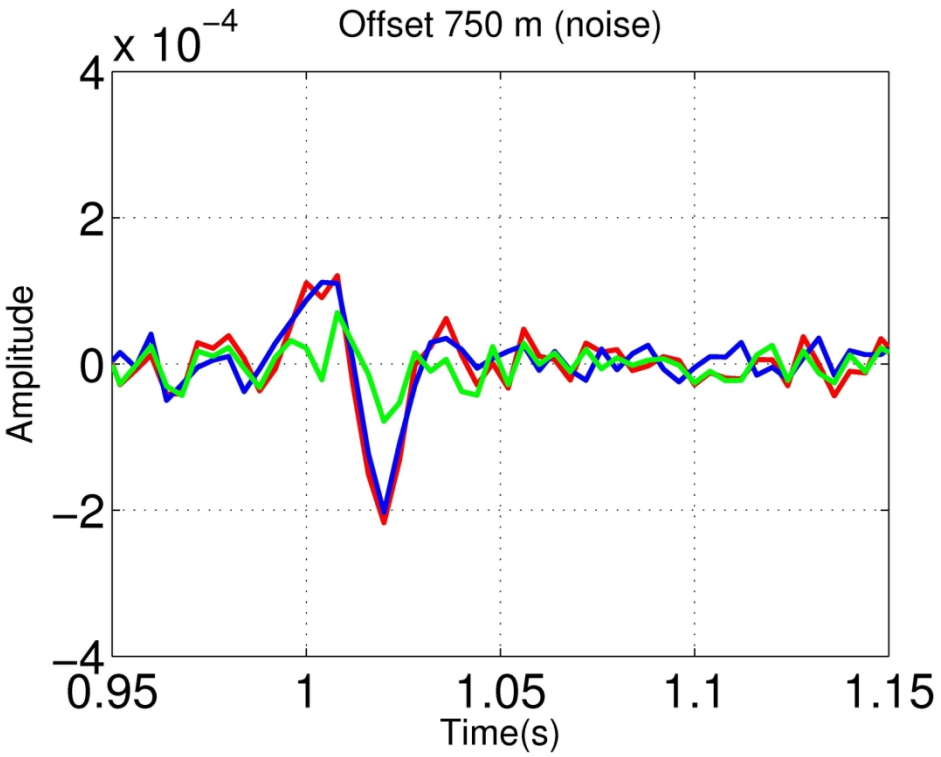

Trace comparison at Offset 750m. Red, blue and green represent the actual primary, result after ISS FSME and result after the SRME + adaptive, respectively.

147x111mm (300 x 300 DPI)

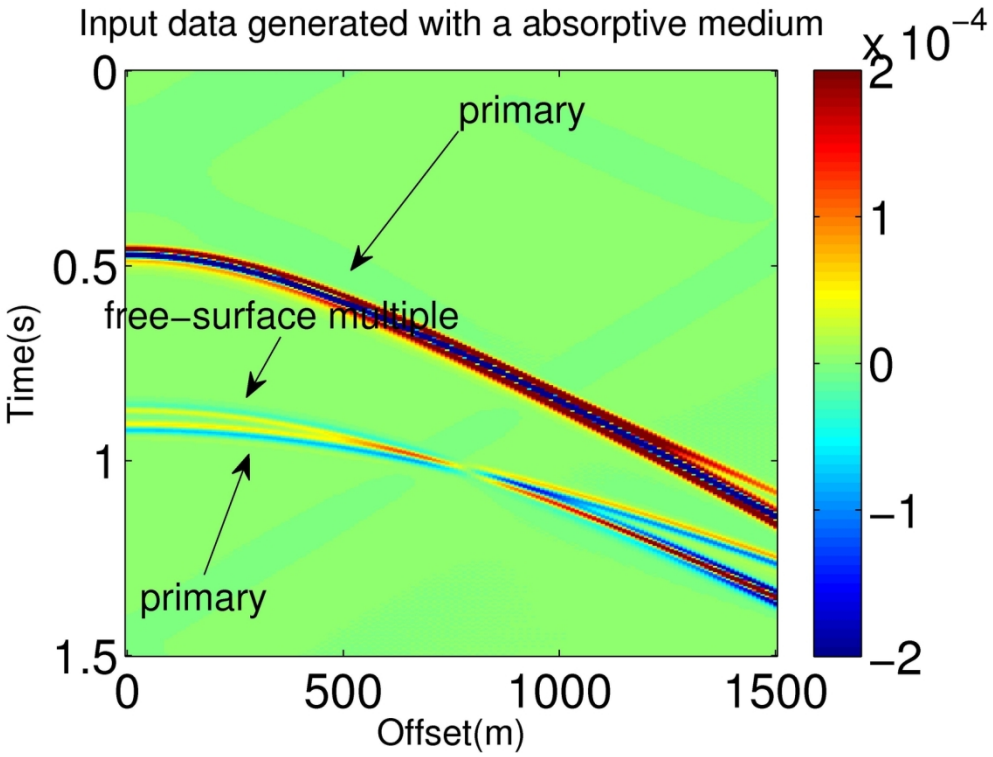

Input data generated from an absorptive medium.

147x111mm (300 x 300 DPI)

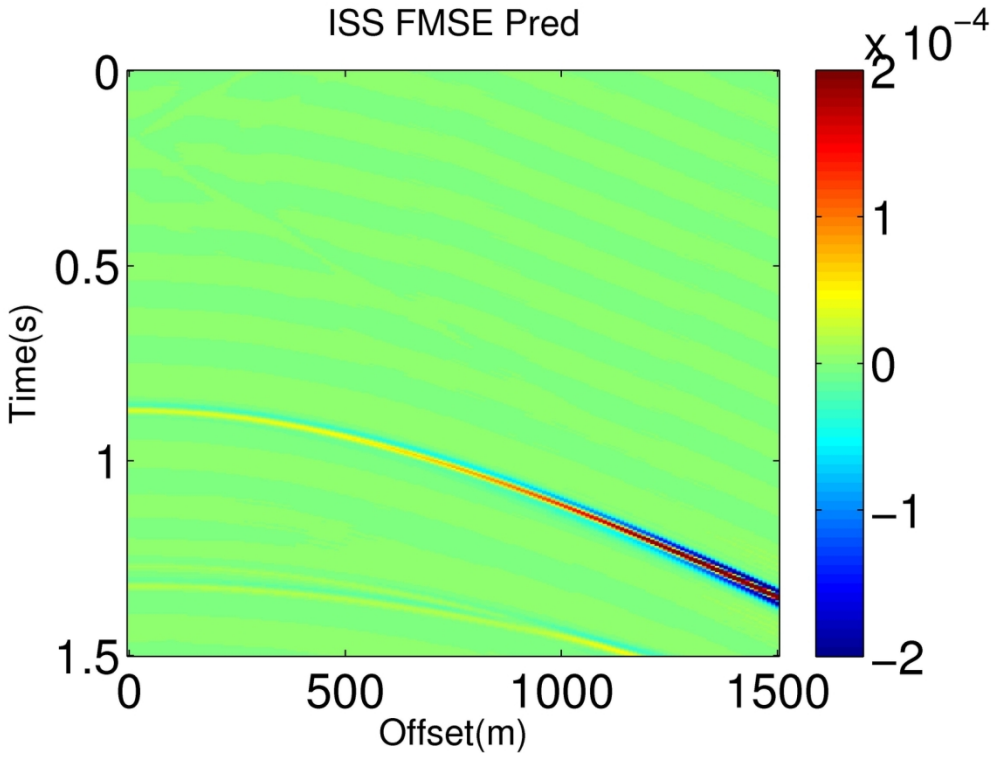

Prediction of free-surface multiple by the ISS FSME (D2' in equation 1) using the input data generated by an absorptive medium shown in figure 36.

147x111mm (300 x 300 DPI)

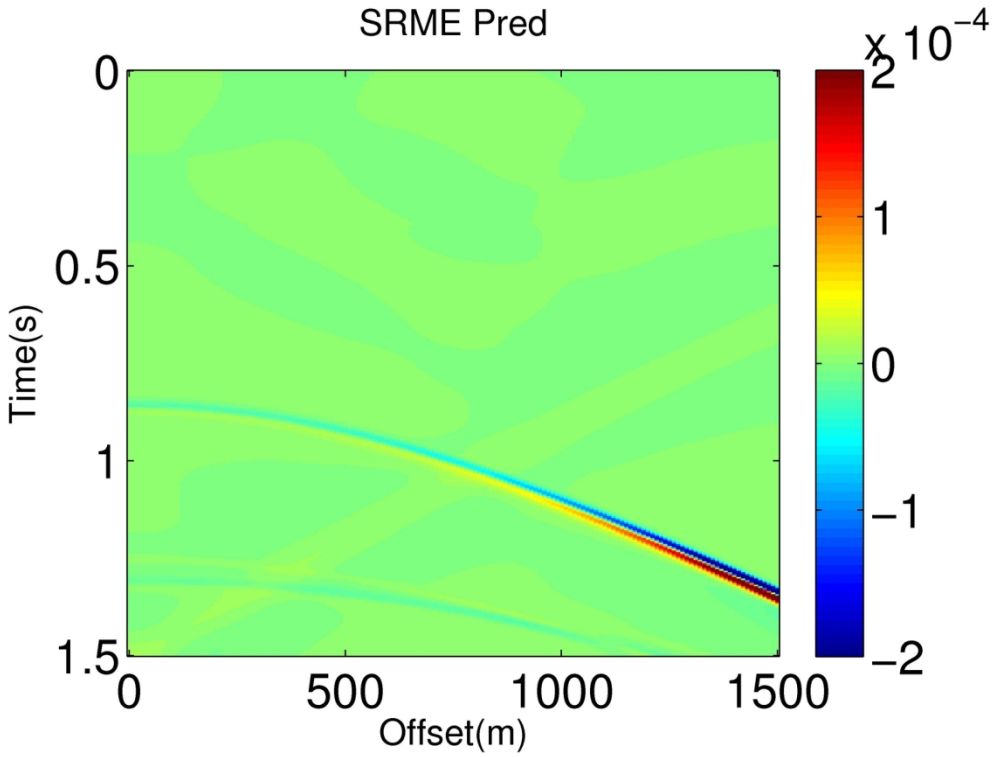

Prediction of free-surface multiple by the SRME using the input data generated by an absorptive medium shown in figure 36.

147x111mm (300 x 300 DPI)

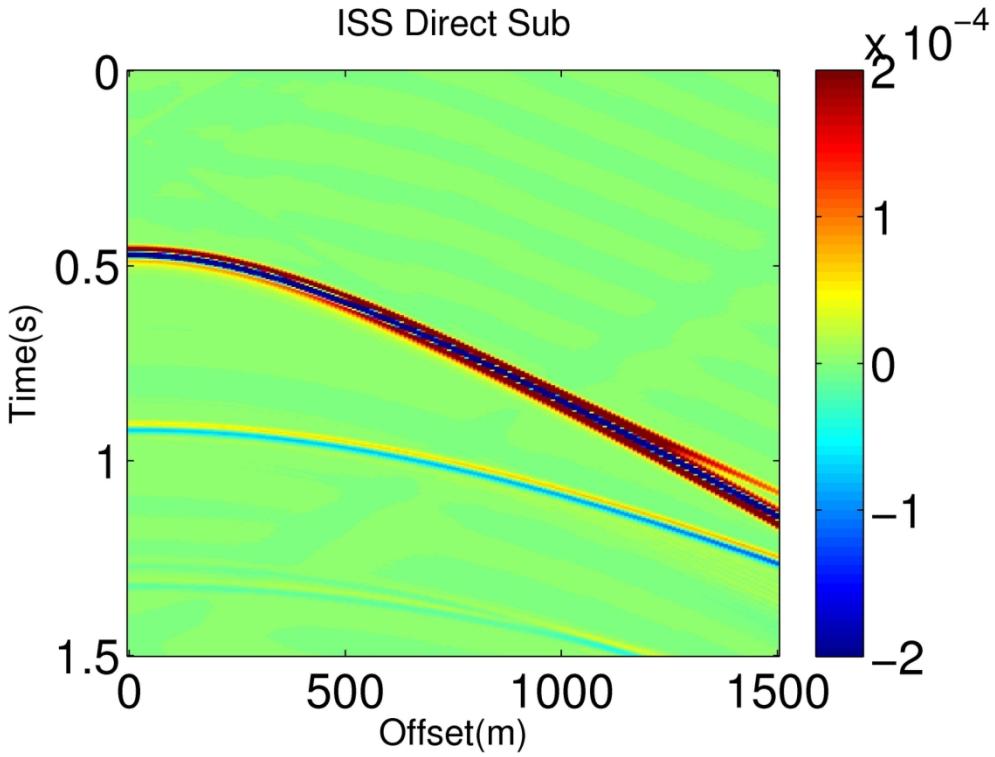

Free-surface multiple removal result after directly subtracting the ISS prediction result (figure 37) from the data (figure 36).

147x111mm (300 x 300 DPI)

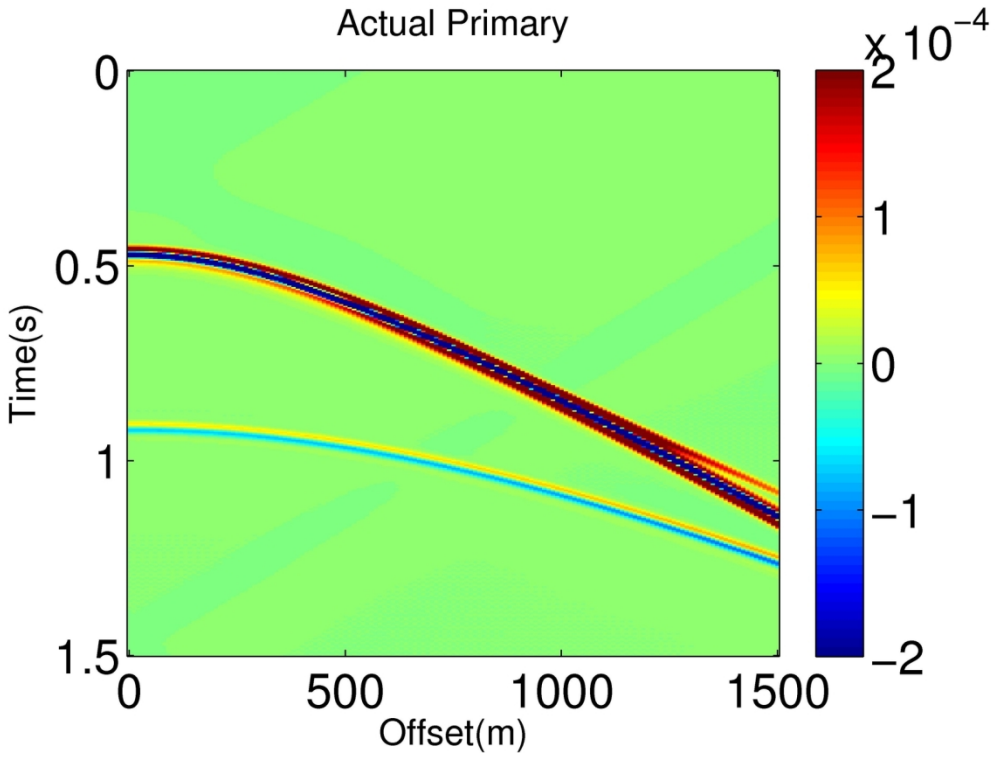

Free-surface multiple removal result by combing the SRME prediction (figure 38) and adaptive subtraction.

147x111mm (300 x 300 DPI)

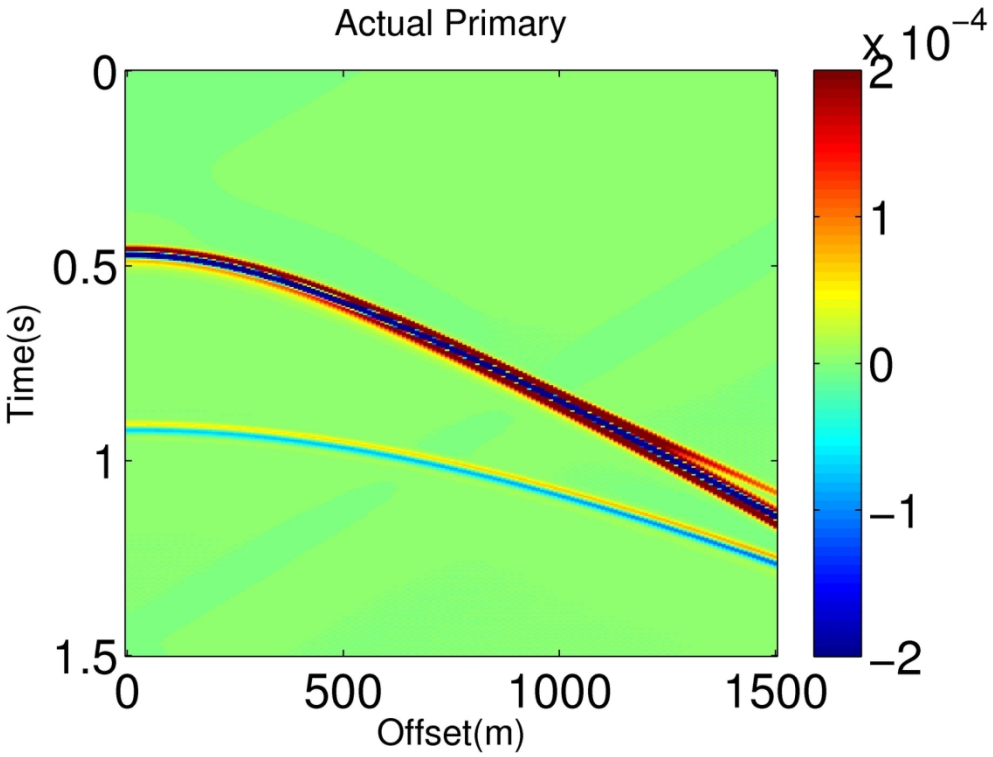

Actual primaries in the input data shown in figure 36.

147x111mm (300 x 300 DPI)

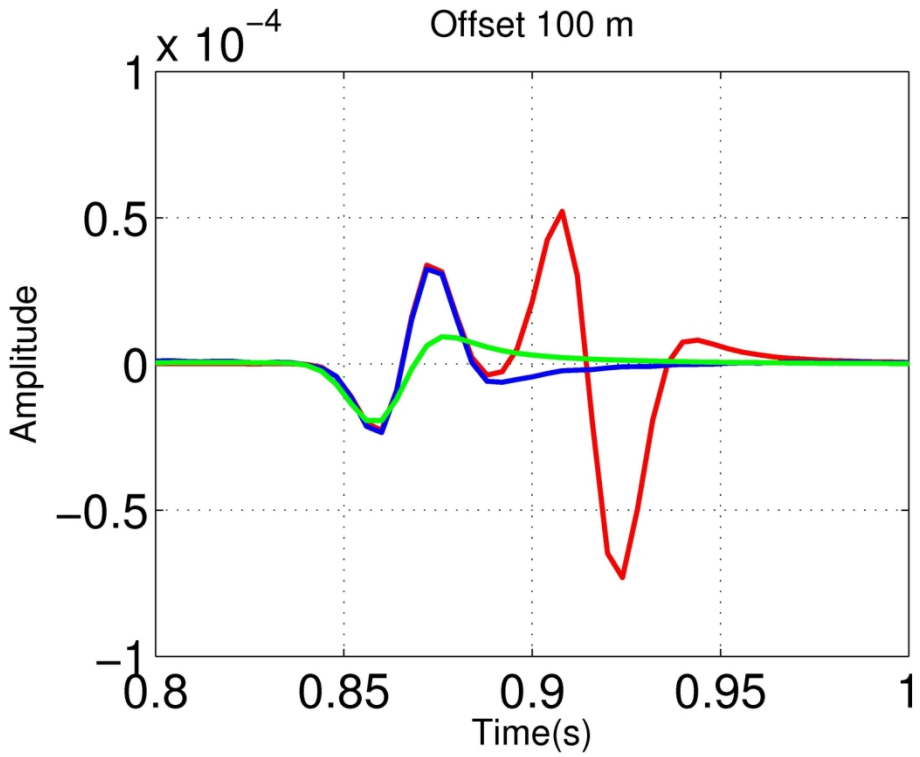

Trace comparison at Offset 100m. Red, blue and green line represent actual data, ISS free-surface multiple prediction and SRME prediction, respectively.

147x111mm (300 x 300 DPI)

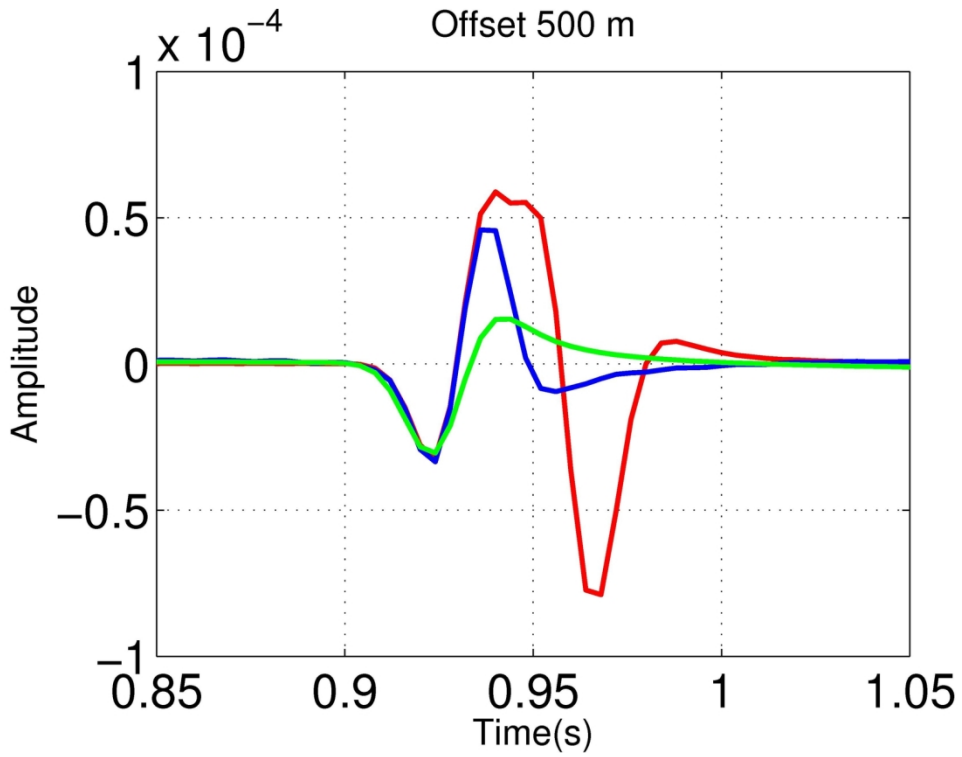

Trace comparison at Offset 500m. Red, blue and green line represent actual data, ISS free-surface multiple prediction and SRME prediction, respectively.

147x111mm (300 x 300 DPI)

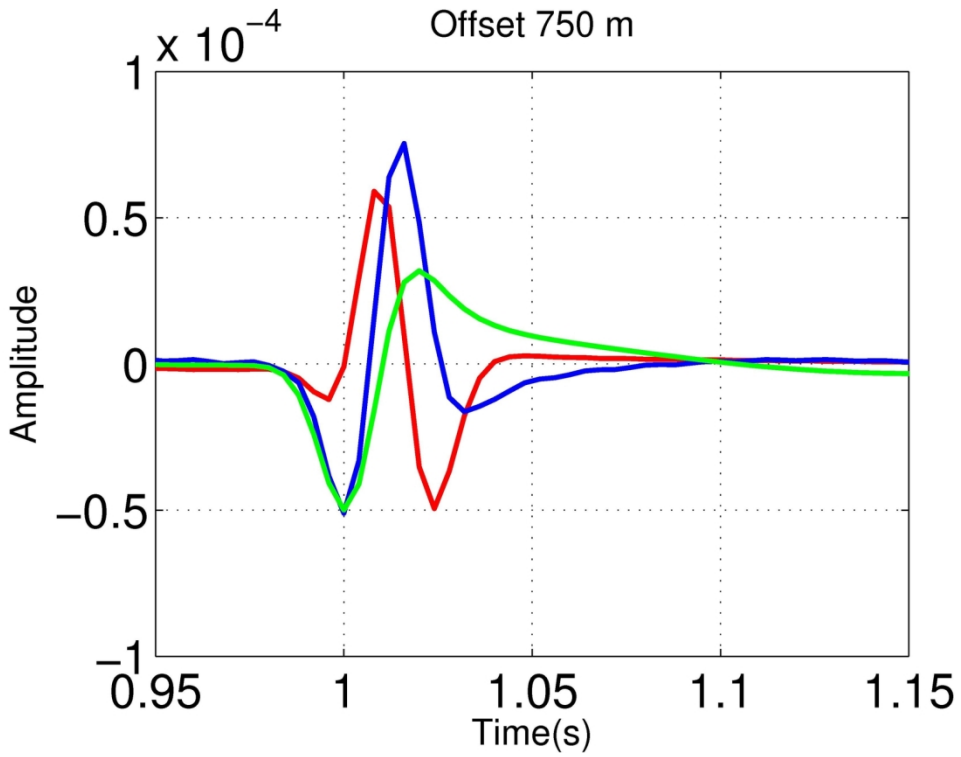

Trace comparison at Offset 750m. Red, blue and green line represent actual data, ISS free-surface multiple prediction and SRME prediction, respectively.

147x111mm (300 x 300 DPI)

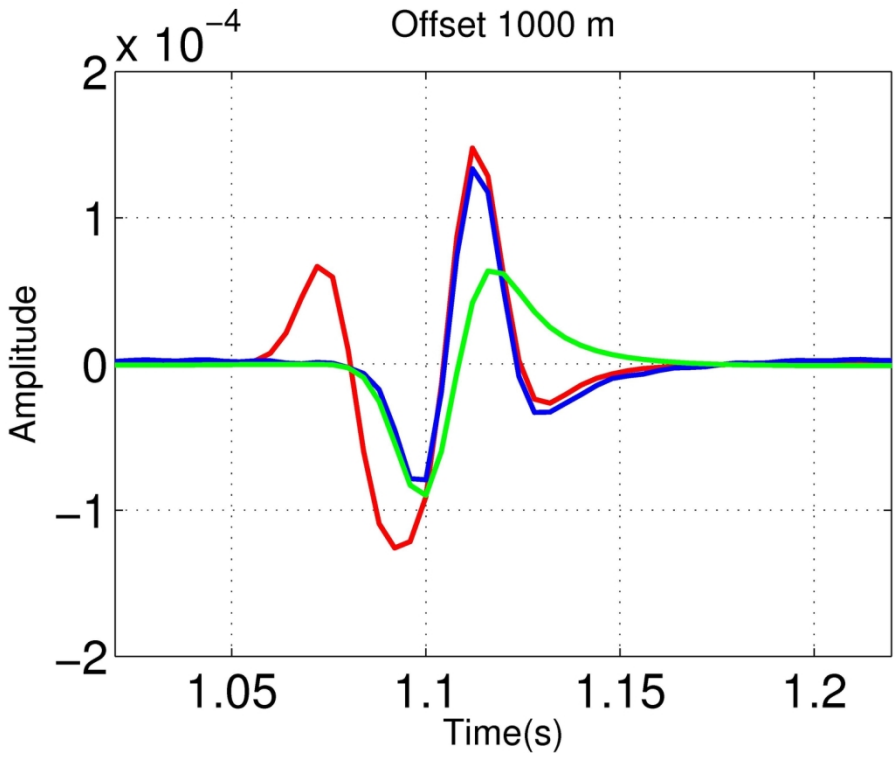

Trace comparison at Offset 1000m. Red, blue and green line represent actual data, ISS free-surface multiple prediction and SRME prediction, respectively.

147x111mm (300 x 300 DPI)

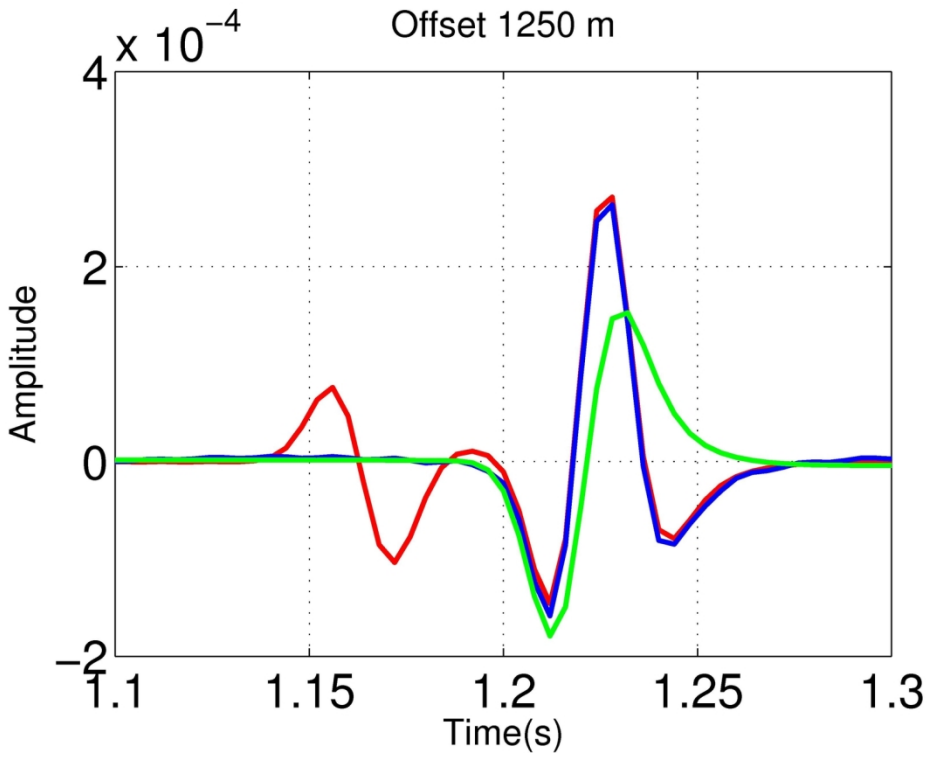

Trace comparison at Offset 1250m. Red, blue and green line represent actual data, ISS free-surface multiple prediction and SRME prediction, respectively.

147x111mm (300 x 300 DPI)

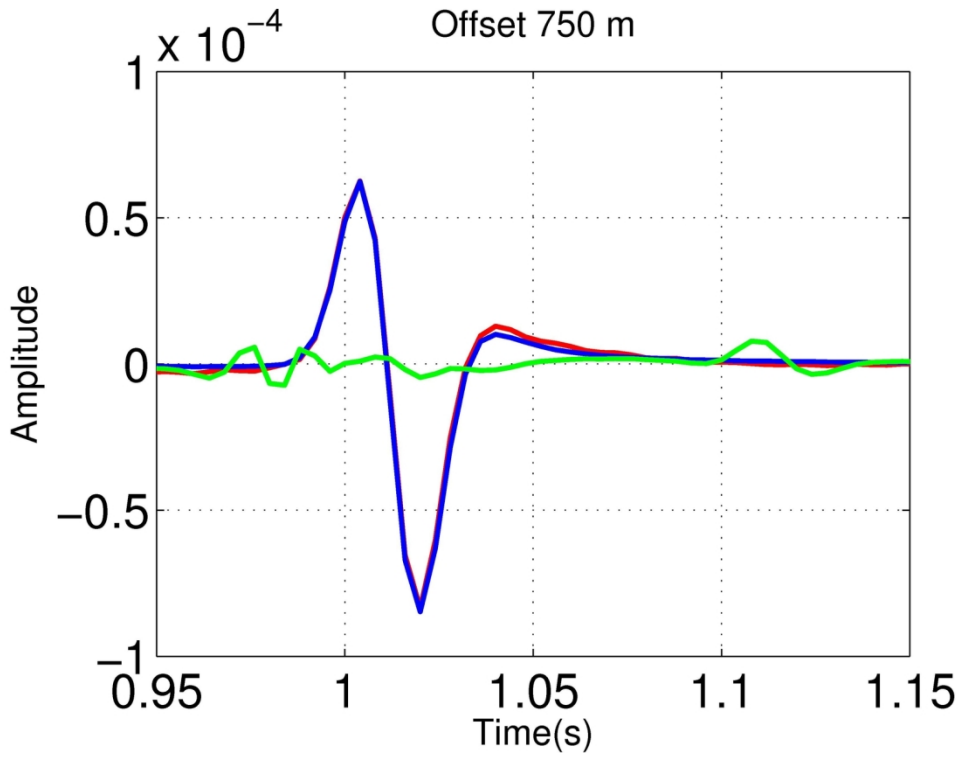

Trace comparison at Offset 750m. Red, blue and green represent the actual primary, result after ISS FSME and result after the SRME + adaptive, respectively.

147x111mm (300 x 300 DPI)

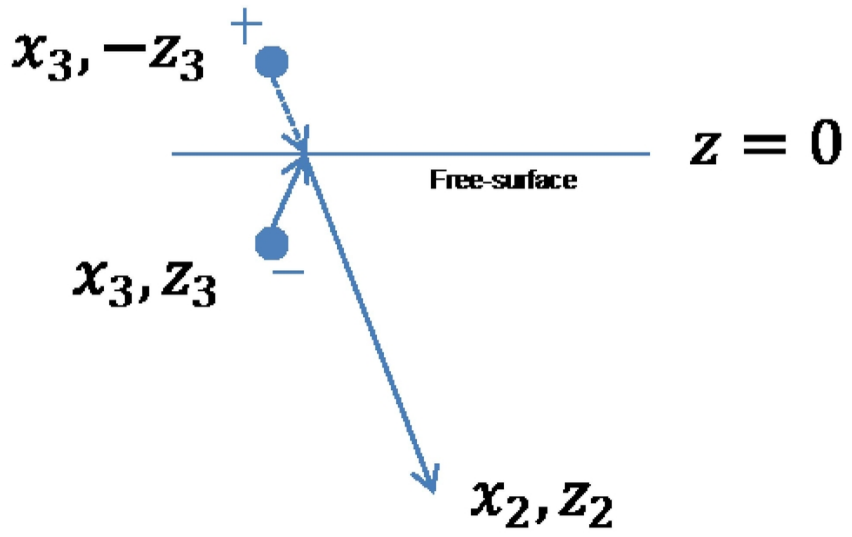

$$G_0{}^{fs}(x_2, z_2, x_3, z_3, \omega) = \frac{1}{2\pi}\int dk \frac{e^{ik(x_2 - x_3)} e^{iq|z_2 - (-z_3)|}}{2iq}$$

$$= \frac{1}{2\pi}\int dk \frac{e^{ik(x_2 - x_3)} e^{iq(z_2 + z_3)}}{2iq}$$

Green's function Gfs0 , travels up from the source to the free-surface and then down to the receiver.

97x108mm (300 x 300 DPI)

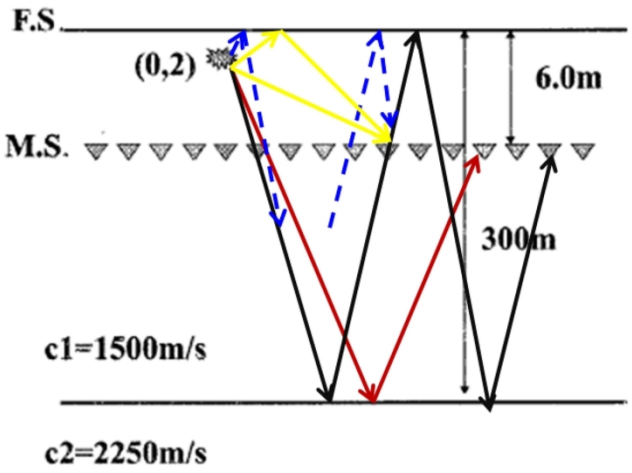

Model used to generated data in Zhang (2007) to test the ISS FSME.

171x94mm (300 x 300 DPI)

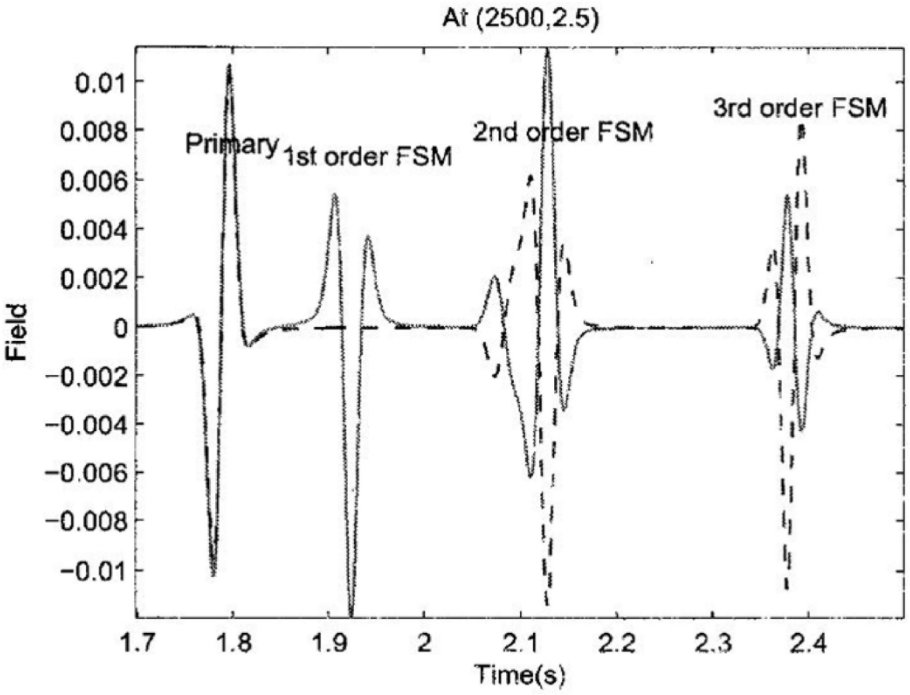

A trace comparison between the input data D1'(solid line) to the ISS FSME and output data D1'+ D2' after the ISS FSME. When D2' is added to D1', two things happen, the first-order free-surface multiple is eliminated, all higher-order free-surface multiples are altered, and prepared for their removal by D3';D4', etc.

140x105mm (300 x 300 DPI)

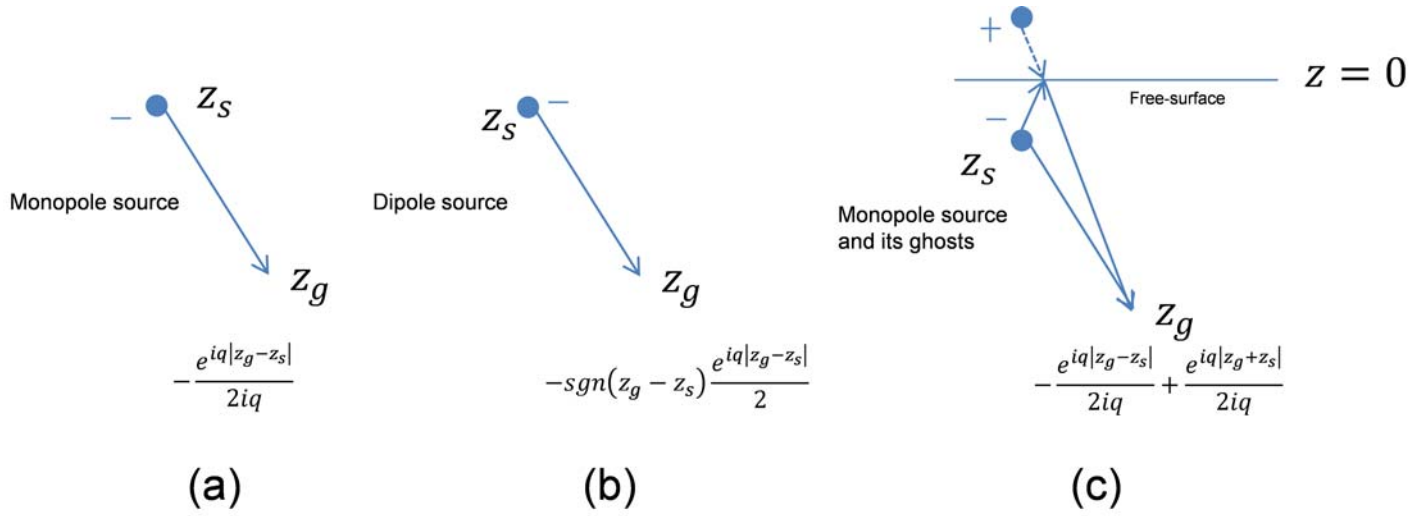
Monopole source
z_s
z_g
$-\frac{e^{iq|z_g-z_s|}}{2iq}$
(a)
Dipole source
z_s
z_g
$-sgn(z_g-z_s)\frac{e^{iq|z_g-z_s|}}{2}$
(b)
Free-surface
$z=0$
Monopole source
and its ghosts
z_s
z_g
$-\frac{e^{iq|z_g-z_s|}}{2iq}+\frac{e^{iq|z_g+z_s|}}{2iq}$
(c)